https://doi.org/10.5194/egusphere-2025-4114
Preprint. Discussion started: 5 September 2025
© Author(s) 2025. CC BY 4.0 License.

Lake hydrochemistry and aquatic plant diversity across permafrost landscapes of Yakutia, Eastern Siberia

Izabella Baisheva*[1,2,3§], Birgit Heim*[1§], Jorge García Molinos[4], Amelie Stieg[1,2], Hanno Meyer[1], Ramesh Glückler[1,2], Kathleen R. Stoof-Leichsenring[1], Antje Eulenburg[5], Pier Paul Overduin[5], Evgenii S. Zakharov[3], Aital V. Egorov[3], Paraskovya V. Davydova[3], Lena A. Ushnitskaya[3], Sardana N. Levina[3], Ruslan M. Gorodnichev[3], Robert Jackisch[6], Antonie Haas[7], Stefan Kruse[1], Luidmila A. Pestryakova[3], Ulrike Herzschuh[1,2,8]

[1]Polar Terrestrial Environmental Systems, Alfred Wegener Institute Helmholtz Centre for Polar and Marine Research, 14473 Potsdam, Germany
[2]Institute for Environmental Science and Geography, University of Potsdam, 14476 Potsdam, Germany
[3]Institute of Natural Sciences, North-Eastern Federal University of Yakutsk, 677007 Yakutsk, Russia
[4]Arctic Research Center, Hokkaido University, 001-0021 Sapporo, Japan
[5]Section of Permafrost Research, Alfred Wegener Institute Helmholtz Centre for Polar and Marine Research, 14473 Potsdam, Germany
[6]Institute of Landscape Architecture and Environmental Planning, Technical University Berlin, 10623 Berlin, Germany
[7]Computing and Data Centre, Alfred Wegener Institute Helmholtz Centre for Polar and Marine Research, 27570 Bremerhaven, Germany
[8]Institute for Biochemistry and Biology, University of Potsdam, 14476 Potsdam, Germany

* *Equal contributions:* Izabella Baisheva and Birgit Heim
§ *Correspondence to*: Izabella Baisheva (izabaiant@gmail.com) and Birgit Heim (birgit.heim@awi.de)

Abstract. Freshwater ecosystems are a major feature of the northern landscapes that are expected to experience significant future changes due to climate change and land-use alterations. In Central Yakutia, abundant lakes in topographic permafrost-thaw depressions, named 'alaas', define the traditional cultural landscape that is home to the indigenous Sakha people, with critical ecosystem services like freshwater supply, meadows for cattle breeding, as well as fishing and hunting grounds. In contrast, lakes in the Verkhoyansk mountain region east of Central Yakutia are of glacial origin or developed on glacial moraines and represent deeper and more oligotrophic lake systems much less used as human resources.

Here, we analyse the hydrochemistry, sedimentary DNA (sedDNA)-derived aquatic plant diversity, geomorphology, and adjacent land cover of sixty-six lakes across the Central Yakutian lowland permafrost landscape and the Verkhoyansk Oymyakon high mountain plateau to understand their characteristics and environmental drivers. Our hydrochemical analysis reveals a clear distinction between the low-mineralised mountain lakes and the highly variable hydrochemistry of the lowland thermokarst lakes. The lake developmental stage within the thermokarst lake sequence seems to be a key driver of lake hydrochemistry in the lakes of the Central Yakutian lowland. Specifically, the lake's developmental stage is reflected by dissolved organic carbon (DOC), pH, its stable isotopic composition, and the hydrochemical facies of alkali and earth alkali elements. New thermokarst lakes have a depleted stable isotopic composition, possibly due to contributions from meltwater of adjacent permafrost ground-ice. This thermokarst lake stage is typically located within forest and has the highest DOC. In contrast, the hydrologically open thermokarst lake systems, typically located in large connected alaas systems with settlements and managed land use, have lower DOC and fewer mineralisation than recently formed thermokarst lakes or old alaas lakes. The dilution in the hydrologically connected alaas lakes occurs due to flushing, mainly during high discharge events such as the regular snowmelt. Old alaas lakes show an enriched oxygen isotope composition and have high salinity and mineral content, suggesting processes of evaporation and highlighting their vulnerability to future warming. However, low chloride together with an enriched isotopic composition and elevated fluoride characterise several of the sampled high-salinity lakes. This points to an additional process beyond the current evaporation, such as fluoride leakage from lacustrine sediments or salt deposits.

SedDNA-derived macrophyte diversity reflects lake types and reveals the dominance of brackish water-tolerant cosmopolitan submerged macrophytes, particularly *Stuckenia* and *Potamogeton*, across all lake types. The macrophytes *Myriophyllum* and

https://doi.org/10.5194/egusphere-2025-4114
Preprint. Discussion started: 5 September 2025
© Author(s) 2025. CC BY 4.0 License.

M. verticillatum are exclusively found in freshwater lakes in the lowlands and the mountain regions, supporting their indicator value for freshwater conditions. Our results provide a detailed examination of lake systems in modern conditions within highly climate-sensitive lowland and mountain permafrost landscapes.

Keywords:
Lakes, ion hydrochemistry, sedDNA, macrophytes, stable isotopes, alaas, thermokarst lakes, land cover, permafrost

https://doi.org/10.5194/egusphere-2025-4114
Preprint. Discussion started: 5 September 2025
© Author(s) 2025. CC BY 4.0 License.

1 Introduction

Climate change is occurring at an accelerated rate particularly at high latitudes (Bekryaev et al., 2010; Serreze and Barry, 2011; Walsh, 2014; IPCC, 2022; Rantanen et al., 2022). Global warming has profound consequences, including the rapid warming and degradation of permafrost (Romanovsky et al., 2010; Nitze et al., 2018; Biskaborn et al., 2019; Smith et al., 2022; Miner et al., 2022), especially in areas with sedimentary Yedoma deposits rich in ground-ice, which are particularly vulnerable to permafrost degradation in the future (Strauss et al., 2017; Nitzbon et al., 2020). In this context, boreal forests and permafrost are recognised as critical tipping elements in the planetary climate system (Wang et al., 2023; Rockström et al., 2024), potentially acting as environmental drivers of change in high-latitude surface waters. The Conservation of Arctic Flora and Fauna (CAFF) working group of the Arctic Council has already reported changes in freshwater chemistry across the Northern Hemisphere with a major data gap located in Eastern Siberia (Lento et al., 2019, 2022; Huser et al., 2020; Aronsson et al., 2021). In the Republic of Sakha (Yakutia) in Eastern Siberia, lakes are a dominant landscape form; there are over 700,000 lakes (Rumyantsev et al., 2012) and a population of less than a million unevenly distributed over a vast territory of 3.084 million km^2 (Sukneva, 2021). Access to running water and sewage services is limited (Dudarev, 2018), also in the most populated Central Yakutia region. Lakes are traditionally used for agriculture but are also the main source of drinking water for humans and livestock, and provide other resources such as fishing (Crate, Ulrich, Habeck et al., 2017; Zakharova et al., 2018; Naumov et al., 2020; Desyatkin et al., 2021). Future changes in lake hydrochemistry, lake and lake catchment geomorphology, and surrounding ecosystems are therefore expected to have a large impact on the local population, making it crucial to understand the current state and drivers of these high-latitude lake systems that are expected to undergo significant changes in response to climate change.

The unique landscape of the central Yakutian lowland was formed by intense thermokarst processes in ice-rich permafrost starting during the Holocene warming (12–11 calibrated thousand years before present (cal ka BP)), which subsequently developed into an alaas landscape during the Holocene Thermal Maximum (8.2–5 cal ka BP) (Katamura et al., 2006; Biskaborn et al., 2012; Pestryakova et al., 2012). Deciduous needleleaf boreal forests – the dominant land cover across the Eastern Siberian boreal region – enhance the ion content and alkalinity input into the lowland lakes (Herzschuh et al., 2013), which are predominantly shallow and eutrophic (Pestryakova et al., 2012). The lakes in this unique alaas landscape can be classified according to the thermokarst lake chronosequence (Bosikov, 1991; Soloviev, 1959; Fig. A17). The first stage called "byllar" (in Sakha language Быллар) starts with the formation of small depressions and ponds due to the thawing of the ground-ice and subsequent ground subsidence. Eventually, the system moves into the next stage where several ponds form a "dyede" lake (in Sakha language Дүөдэ); a semi-rounded shallow lake with an ice-wedge derived polygonal pattern on the bottom and steep banks (Soloviev, 1959). The next lake stage, "tympy" lake (in Sakha language Тымпы) occurs when the water bodies enlarge due to ground-ice melt, resulting in further basin subsidence and increasing water volume (Bosikov, 1991). More recently, new thermokarst lakes are forming much more rapidly, in just a few decades, initiated by human land use or fire disturbance, (Fedorov et al., 2014; Ulrich et al., 2017b), and after agricultural land has been abandoned or in settlement areas (Lytkin et al., 2021; Zhirkov et al., 2023; Suleymanov et al., 2023). In this study, we refer to these lakes as ‘new thermokarst lakes’. The hydrochemical properties of newly forming thermokarst lakes remain largely uncharacterised in the literature. Consequently, their potential to develop into viable habitats or resource bases for the Yakut people is not yet understood.

Continuing with the thermokarst lake chronosequence, a mature “alaas” (in Sakha language Алаас) lake stage develops when evaporation or draining causes the lake to recede, resulting in residual lakes at the lowest point of topographic depressions (Soloviev, 1959; Desyatkin, 2008; Ulrich et al., 2019). Alaas landscapes developed in Eastern Siberia during the Holocene Thermal Maximum, and since then, alaas lakes have undergone subsequent development stages with notable lake-level changes and the deposition of sedimentary sequences covering several millennia (Ulrich et al., 2017a,b). These residual alaas lakes are usually very shallow (<1 m water depth), although they may reach depths of several metres, and are referred to hereafter as ‘old alaas lakes’.

https://doi.org/10.5194/egusphere-2025-4114
Preprint. Discussion started: 5 September 2025
© Author(s) 2025. CC BY 4.0 License.

In strongly degraded and interconnected alaas systems, lakes can become hydrologically connected, eventually only during high discharge events when water levels are high, such as during the annually occurring snow melt. These lakes are generally larger in area and often more elongated and deeper (up to 10 m) (Ulrich et al., 2017a; Hughes-Allen et al., 2023) and are named in this study 'connected alaas lakes'. Previous studies have categorised lowland lakes in Yakutia by their lake history, finding high variability in inorganic lake hydrochemistry, but do not link the hydrochemistry to lake type, with the notable exception of the less mineralised sand-dune lakes (Kumke et al., 2007, Pestryakova et al., 2012). In contrast to the Central Yakutian thermokarst lowland lakes, lakes towards the east in the Verkhoyansk Mountain region represent aquatic ecosystems under even more extreme climate conditions, although with minimal human impact. These lakes are characterised by cold and deep water bodies with very low nutrient and mineral content, which we refer to here as 'mountain lakes'.

In this study, we examine a comprehensive dataset of lake hydrochemistry and aquatic plant diversity derived from sedimentary DNA (sedDNA) from lake surface-sediments across two contrasting permafrost landscapes: the eastern Central Yakutian lowland (hereafter Central Yakutia) and the Verkhoyansk Oymyakon high mountain plateau (hereafter Verkhoyansk mountain region). Inorganic and organic hydrochemistry (e.g., concentrations of major and minor ions and dissolved organic carbon (DOC)) can be a diagnostic tool for natural or anthropogenic processes in lakes such as land cover and human practices (Hu et al., 2020, Du et al., 2023). SedDNA as well as environmental DNA can be powerful tools for biodiversity monitoring, enabling the reconstruction and contemporary detection of fish, diatoms, macrophytes, and a wide range of other aquatic and terrestrial organisms (Thomsen et al., 2015; Taberlet et al., 2018; and for reconstruction studies specifically from macrophyte metabarcoding Stoof-Leichsenring et al., 2022; Baisheva et al., 2023; Revéret et al., 2023a,b; Li et al. 2024). In this study, we analyse lake macrophytes, as they are linked to the hydrochemical and morphological diversity of lakes (Różańska-Boczula and Sender, 2025). For example, the Directive 2000/60/EC of the European Parliament (2000) proposes macrophyte composition, particularly submerged macrophytes, as an indicator of water quality. Furthermore, aquatic plant diversity, including richness and composition, can indicate lake trophic status (Bennion et al., 2000). Baisheva et al. (2023) describe the sequential formation of an alaas lake through turnover of macrophytes and diatoms in Lake Satagay in the southwestern Central Yakutian lowland. Stoof-Leichsenring et al. (2022) identify lake depth, conductivity, and July temperature as the main environmental drivers of macrophyte diversity, as captured by the plant sedaDNA proxy in their extensive high-latitude lake surface-sediment dataset from Eastern Siberia and the high Tibetan Plateau. However, the spatial patterns and complex interactions between hydrochemistry and lake vegetation in lakes in Central Yakutia and mountainous areas remain understudied.

Our objectives are to (i) assess the inorganic, organic, and isotopic lake hydrochemistry and sedDNA-derived aquatic plant diversity in mountain lakes in the Verkhoyansk mountain region and in lowland thermokarst lakes of Central Yakutia, (ii) evaluate if there is an impact of land cover and land use in the surroundings of the lakes on lake hydrochemistry, and (iii) identify the potential environmental drivers of lake hydrochemistry and lake-specific aquatic plant diversity, with a particular focus on the role of land cover and the thermokarst lake sequence.

2 Data and methods

2.1 Study area

The study area spans a substantial region of over 700 km from west to east, extending from eastern Central Yakutia between the Lena, Aldan, and Amga rivers to the Oymyakon high mountain plateau in the Yakutian Verkhoyansk mountain region (Fig. 1B,C). Central Yakutia is characterised by an extreme subarctic continental climate, with long, cold, and dry winters (mean monthly temperature in January −40 °C) and warm summers (mean monthly temperature in July +20 °C). The lowlands feature a unique, lake-rich alaas landscape with a relatively high population density and land-use management contributing to

https://doi.org/10.5194/egusphere-2025-4114
Preprint. Discussion started: 5 September 2025
© Author(s) 2025. CC BY 4.0 License.

a predominance of grassland around lakes within the alaas systems. The main settlements east of the Lena River include Nizhny Bestyakh, Maya, Churapcha, and Ytyk-Kyuyel (Fig. 1D).

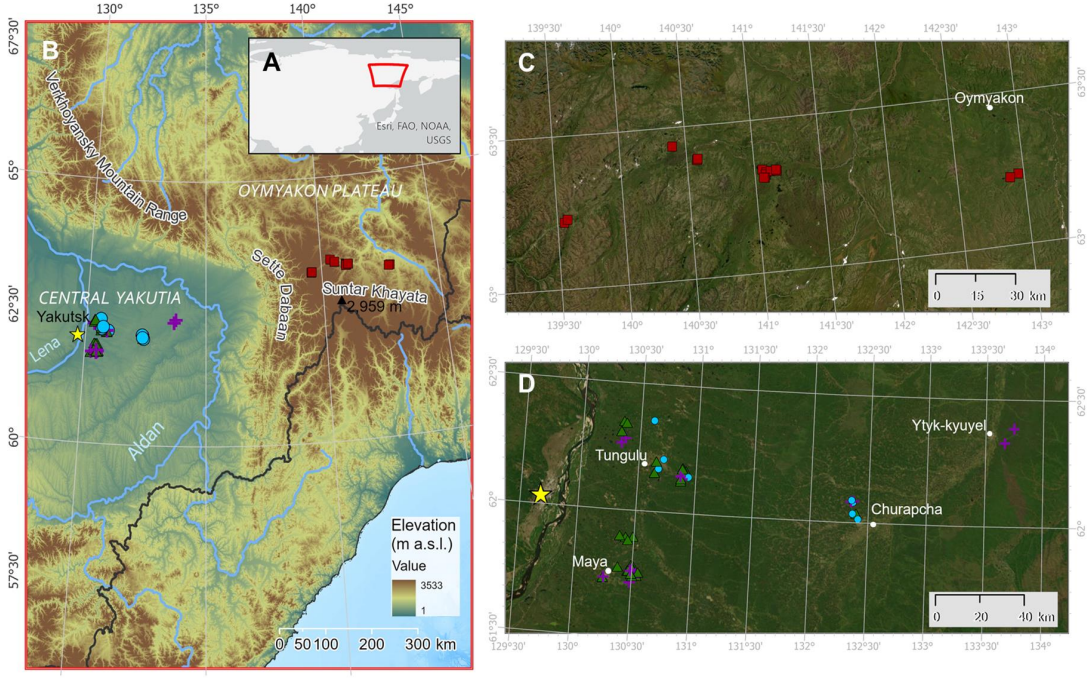

Figure 1: (A) Yakutian study area in Eastern Siberia. (B) Map overview on the 66 sampled lakes of the 2021 expedition covering the eastern Central Yakutian lowland (blue colours) and the Oymyakon high mountain plateau in the Verkhoyansk mountain range (red colours), Eastern Siberia. The yellow star shows Yakutsk, the capital of the Republic of Sakha. Background topography is the colour-coded GEBCO Elevation Grid-2021. (C) Overview of the sampled Verkhoyansk mountain lakes (red squares), and the settlement Oymyakon (white circle). (D) Overview of the sampled lakes in Central Yakutia with connected alaas lakes (blue circles), old alaas lakes (green triangles), and new thermokarst lakes (purple crosses). The settlements Maya, Tungulu, Churapcha and Ytyk-Kyuyel are marked with white circles. The yellow star marks the city Yakutsk. Background images ©ESRI World Imagery (C,D).

Central Yakutia is characterised by extensive larch forests, transitioning from pure larch stands in the east, into mixed forests with evergreen needleleaf tree species westward towards the sandy banks of the Lena River (Troeva et al., 2010).

The sampled lowland lakes are distributed across four Pleistocene terraces, from the younger and lower terraces in the west to the older and higher terraces in the east. These Eastern Yakutian Pleistocene Lena terraces are described in detail in Soloviev (1959) and Zakharova et al. (2018). From west to east, the Bestyakh terrace, a non-dated terrace with alluvial sand and gravel covered by aeolian sand located along the eastern bank of the Lena River, gives place to the Tungulu terrace (22–14 cal ka BP), with loamy sand/loess and loam of lacustrine/bog origin, while the Abalakh terrace (56–45 cal ka BP) with cryogenic lacustrine silt/loam, gives place to the Magan terrace with the highest elevation (Middle Pleistocene to Holocene) and a stratigraphy of loam over alluvial gravel (Ulrich et al., 2017a; Zakharova et al., 2018). The Tungulu and Abalakh terraces' loamy deposits are characterised by sedimentary Yedoma deposits with a high concentration of ground-ice with a high degradation potential (Zakharova et al., 2018).

The Verkhoyansk mountain range rises east from Central Yakutia (Fig. 1B), as part of the western segment of the Verkhoyansk fold-and-thrust belt (Khudoley and Prokopiev, 2007), and composed of terrigenous and carbonate sedimentary rock from the Riphean, Palaeozoic, and Mesozoic eras (Shahgedanova, 2003). The Suntar Khayata mountain range (Stauch and Lehmkuhl, 2010), with Muus-Khaya ("Ice Mountain" in Sakha) as its highest peak (2,959 m a.s.l.), and the Oymyakon high mountain plateau (around 1,200 m a.s.l) are located within the southernmost part of the Verkhoyansk mountain range. The Oymyakon high mountain plateau is also known as the 'cold pole of the Earth' because of its extreme continentality, with extremely low

https://doi.org/10.5194/egusphere-2025-4114
Preprint. Discussion started: 5 September 2025
© Author(s) 2025. CC BY 4.0 License.

minimum winter temperatures (-67.7 °C) due to the permanent position of the Siberian High, which is further exacerbated by strong topographic temperature inversions in winter (Shahgedanova, 2003).

The landscapes of the Oymyakon high mountain plateau are characterised by wide braided river valleys punctuated by small lakes, while a high number of lakes are also located in mountainous terrain on rock or in glacial moraine belts. These mountain slopes are covered by open larch forests, which give way to mountain tundra as elevation increases, at around 2000 m a.s.l. The lakes in this region remain ice-covered for most of the year, representing oligotrophic aquatic ecosystems, and are largely unaffected by human activity apart from sparse settlements and occasional fishing and hunting.

2.2 Fieldwork

Sixty-six lakes in Central and Eastern Yakutia were sampled during a joint German-Russian expedition conducted in 2021 from 6th August to 2nd September (Fig. 1). We assigned lake codes (EN21401 to EN21467) according to the temporal order of the sampling as the majority of the smaller sampled lakes have no officially recognised names, (Table A1). Of these sampled lakes, 15 (EN21401 to EN21415) are located within the Verkhoyansk mountain range at elevations ranging from 789 m to 1310 m, primarily on the Oymyakon high mountain plateau (Fig. 1B,C; Table A1); and 51 lakes are located in Central Yakutia at elevations between 115 m and 307 m (Fig. 1B,D; Table A1). These 51 lakes are thermokarst lakes in various stages of development.

The fieldwork and sampling methods are described in detail in Morgenstern et al. (2023). For this study, we measured lake-water depth, transparency, pH, and specific electrical conductivity (EC), and collected water and surface-sediment samples for each lake (Fig. A1). From an inflatable boat, lake depth was measured across the lakes using a handheld Echo-Sounder (Hondex PS-7) and lake transparency with a Secchi disk that was lowered on the shady side of the boat until the white part of the disk was no longer visible to the observer. Physical parameters, such as EC and pH, were measured directly in the upper water layer using a Multi-340i device (WTW, Germany) in the Verkhoyansk mountain range. In the Central Yakutian part, EC and pH were measured at the camp field laboratory on the same day of water sampling. All sampling locations in the lakes were recorded with a GPS device (Garmin, GPSMAP67i).

The water samples were collected from the upper water layer at a sampling depth of 0.5 m into 2 L sample containers (Whirl-Pak®). The fieldwork treatment of water samples for anions and cations involved a filtration step using 0.45 µm pore-size pre-syringe cellulose-acetate filters. Filtrated anion samples were directly stored in 8 mL wide-mouth bottles (Nalgene), while filtrated cation samples were placed in 15 mL tubes (Falcon) and preserved by adding 65% HNO_3. Water samples for DOC and coloured dissolved organic matter (cDOM) were filtered through 0.7 µm pore-size pre-syringe glass fibre filters and stored in 20 mL glass vials (Scientific Fischer) and 50 mL brown glass bottles, respectively. A 30% HCl solution was added to DOC samples for preservation, but avoided for cDOM so as to maintain the aquatic optical properties.

Water samples for isotope analysis were collected either directly from the lake or transferred as soon as possible from the water sample container into 30 mL narrow-mouth polyethylene bottles, which were filled to the top and sealed tightly. Additionally, a single rain event (22 August 2021) was sampled for isotope measurement at the Tungulu campsite in Central Yakutia. Except for isotopic samples (with 2–3 bottles) all water samples were collected once. Lake surface-sediment was collected with sterile spoons for sedDNA from a HYDRO-BIOS grabber. The sediment samples for DNA analysis were stored in 250 mL bottles (Nalgene). All samples were stored and transported in cool and dark conditions until analysis.

2.3 Laboratory analysis

Inorganic and organic hydrochemistry

The ionic composition of surface water and DOC was measured at the Hydrochemistry Laboratory of the Alfred Wegener Institute Helmholtz Centre for Polar and Marine Research, Potsdam, Germany (AWI). Major cations (magnesium (Mg^{2+}), calcium (Ca^{2+}), sodium (Na^{+}), potassium (K^{+})) were measured using inductively coupled plasma optical emission spectrometry

https://doi.org/10.5194/egusphere-2025-4114
Preprint. Discussion started: 5 September 2025
© Author(s) 2025. CC BY 4.0 License.

(ICP-OES; Perkin-Elmer, Optima 8300 DV); major anions (chloride (Cl^-), fluoride (F^-), sulfate (SO_4^{2-})) using ion chromatography (ICS; Thermo Scientific, Dionex ICS-2100). Hydrogen carbonate content (HCO_3^-) was analysed by potentiometric pH endpoint titration up to pH 4.3 (potentiometric pH endpoint titration (HCO_3^-/alkalinity), 794 Basic Titrino, Metrohm). Total dissolved solids (TDS) were calculated using the sum of major cations and major anions. Minor ion measurements included barium (Ba^{2+}) and strontium (Sr^{2+}). Metals measured were aluminium (Al), iron (Fe), manganese (Mn), and bromide (Br^-) using an ICP-OES (Perkin-Elmer, Optima 8300 DV). DOC was measured as Non Purgeable Organic Carbon (NPOC) using a TOC-VCPH 2.00 device with an uncertainty of 10% and a detection limit of 0.25 mg L^{-1} (Shimadzu, Japan). The adopted measurement method involved a catalytic combustion process at 680°C, leveraging a Non-Dispersive Infrared (NDIR) detector with a catalyst used of standard sensitivity.

Stable water isotopes (δ18O, δD)

Oxygen ($\delta^{18}O$) and hydrogen (δD) stable water isotopes were measured at the ISOLAB Facility at AWI, with a Finnigan MAT Delta-S mass-spectrometer following the equilibration method (details in Meyer et al., 2000). The compositions of hydrogen and oxygen isotopes are represented using the δ notation of $\delta^{18}O$ and δD in per mille (‰) versus Vienna Standard Mean Ocean Water (V-SMOW) as the standard. The standard deviation includes all measurements of the three samples per lake, which is generally better than the external error of long-term standard measurements of ±0.8‰ for δD and ±0.10‰ for $\delta^{18}O$ (Meyer et al., 2000). Deuterium excess (d) was calculated as $d = \delta D - 8 * \delta^{18}O$, using the mean values, according to Dansgaard (1964). The linear relationship between hydrogen and oxygen isotopes for water samples that have not undergone evaporation is represented by the global meteoric water line (GMWL; Craig, 1961). Local evaporation lines (LELs) were calculated by fitting a linear regression to the $\delta^{18}O$ and δD values of the lake water samples for all lowland lakes as $Yak21_{Lowland}$, and separately by lake types as $Yak21_{CAL}$, $Yak21_{OAL}$, $Yak21_{NTL}$, and $Yak21_{ML}$. The slopes of the LELs were compared to the GMWL, and the Local Meteoric Water Line for Yakutsk in Central Yakutia based on precipitation measurements in Yakutsk (LMWL, Kloss, 2008) and to an existing LEL of Yakutian lakes from 2008 (Wetterich et al., 2008) to characterise the isotopic signature of the lake waters and assess the effect of evaporation.

Sedimentary DNA from aquatic and terrestrial plants

SedDNA extraction to polymerase chain reaction (PCR) set-up steps was conducted for 64 lake surface-sediment samples in the palaeogenetic laboratories at AWI under a cleaned and UV-irradiated working hood (Biosan, Latvia). DNA extractions were performed using the Dneasy PowerSoil Max DNA Isolation Kit (Qiagen, Germany) with about 5–8 g sediment input, following established protocols (Epp et al., 2019). Sediments were added to 15 mL of PowerBeadPro tubes with 1.2 mL of C1 buffer (VWR International, Germany), 0.4 mL of Proteinase K (VWR International, Germany) and 0.1 mL of 5M dithiothreitol solution (VWR International, Germany) and vortexed for 30 s, on the highest speed. Samples were homogenised using FastPrep-24 bead beating grinder (Biomedicals, USA) for 50 s and in an incubator with a rotating system at 56°C overnight. For each extraction batch, one extraction blank and No Template Controls for PCR preparation step were added to control for potential chemical contamination during the DNA extraction and PCR setup following the protocol of Zimmermann et al. (2017). Extracted sedDNA was combined and concentrated with the GeneJet PCR purification Kit (Thermo Scientific, USA). The concentrated DNA was quantified with a broad-range sedDNA Assay Qubit Fluorometer (Invitrogen, USA) with DNA diluted to 3 ng μL^{-1} for initial input into the PCR reactions. For PCR set-up we followed the protocol described in Baisheva et al. (2023). We used standard primers targeting the chloroplast trnL P6 loop amplification of vascular plant DNA metabarcoding (Taberlet et al., 2007). The APMG-60 pool of PCR samples were prepared by Fasteris (Genesupport, Fasteris SA, Switzerland) into a PCR-free library (using the metafast protocol) and sequenced in paired-end mode on a NextSeq Illumina sequencing device with the NextSeq Mid kit (Illumina).

https://doi.org/10.5194/egusphere-2025-4114
Preprint. Discussion started: 5 September 2025
© Author(s) 2025. CC BY 4.0 License.

DNA amplicon sequencing and taxonomic assignment

After Illumina sequencing, datasets of the sequenced plants were processed using OBITools3 (https://git.metabarcoding.org/obitools/obitools3) following the bioinformatic pipeline after Boyer et al. (2016). Data were combined using the "*obi alignpairedend*" command to align forward and reverse reads and "*obi grep*" was used to remove unpaired reads. To allocate reads to the corresponding combinations of primer tags the command "*obi ngsfilter*" was used. Grouping and counting of identical sequences was performed using "*obi uniq*". Denoising data using "*obi annotate*" removed sequences with <10 counts and <10 length. The taxonomic assignment was conducted by using the new, customised database for Siberian plants "SibAla" (Courtin et al., 2025). Output data separation into terrestrial and aquatic plants followed Baisheva et al. (2024). No sedDNA counts were amplified from only one lake (EN21436), one sample with only two counts (EN21432) and two samples with no counts (EN21440, 431) were discarded from the terrestrial plant dataset. The final data consists of more than 8,606,990 counts, of which 6,729,397 are aquatic plants (78 %) and 1,877,639 are terrestrial plants (22 %). We then divided macrophytes into four functional groups as floating, submerged, submerged-emergent, and emergent macrophyte types (following Stoof-Leichsenring et al., 2022, Baisheva et al., 2023, 2024; Różańska-Boczula and Sender, 2025). Emergent plants include all plants which typically occur in marshlands, wetlands, bogs, and wet, boggy soils. Terrestrial plants are divided into three main functional groups: trees, shrubs (including subshrubs), and graminoids and forbs comprising one group (following Baisheva et al. 2024), including bryophytes (following Herzschuh et al., 2025).

2.4 Lake type classification

Multiple unoccupied Aerial Vehicle (UAV) transects were flown at the 2021 expedition to map the lakes and the landscape. A Yellowscan Mapper LiDAR (Light detection and ranging) sensor employed on a DJI M300 RTK UAV scanned detailed 3D point clouds of forest canopy, understory and the subground morphology. In addition, multispectral drone images were acquired specifically along lake shorelines and their vegetation using the consumer-grade, lightweight DJI Phantom-4 quadcopter. For small to medium lakes, we completely mapped the lake along the full shorelines, for large lakes we could only map representative sections of the lake shores. The multispectral imaging system included five spectral channels (Blue, Green, Red, Red-edge and Near-infrared (NIR)). The LiDAR data was processed using proprietary software (Yelloscan, Saint-Clément-De-Rivière, France) to derive digital surface and elevation models of resolutions at 5-10 cm per pixel. The multispectral drone overflights for each lake were mosaiced together from flight-corrected flightstripes in the lake-specific area-true Universal-Transverse-Mercator (UTM) projection using Agisoft Metashape Professional and are published as orthomosaics (Stieg et al., 2023a,b). Using QGIS Geographic Information System 3.22.3 we manually delineated the lake shorelines for each lake using the NIR image with the high contrast between water and the land surface.

In cases (13 of the 66 lakes) where lakes could not be surveyed due to poor visibility or if the lake shore was only partly mapped because of the large lake size, we manually digitised the lake shores on an ESRI high-resolution background image. Using the digitised lake outlines in their respective area-true UTM zones (UTM N52, N53, and N54), we calculated lake morphology variables such as area, length, and width. We further assigned lake shapes using the formula [C=lake length / lake width] after Grigoriev (1959) resulting in four categories: 'round' (C>1.5), 'close to round' (C=1.5–3.0), 'close to oval' (C=3.0–5.0), and 'oval-elongated' (C=5.0–7.0). We then classified the lakes according to their lake morphology and geographical setting. At the first hierarchical level, we separated the mountain lakes that include two large deep glacial lakes (Fig. A2.A) and 13 smaller lakes (Fig. A2.B), and the lowland lakes (in general shallow lakes, Fig. A2.C–H).

We then separated the lowland lakes according to their specific stage of thermokarst lake development (Soloviev, 1959; Bosikov, 1991; Desyatkin et al., 2009; Fedorov et al., 2014) classifying them into the three lake types based on the visual inspection of field photos (Fig. A2), our field knowledge, the drone images (Stieg et al., 2023a,b), on the morphological settings from UAV LiDAR digital surface models (Fig. 2) and high-resolution ESRI background images.

https://doi.org/10.5194/egusphere-2025-4114
Preprint. Discussion started: 5 September 2025
© Author(s) 2025. CC BY 4.0 License.

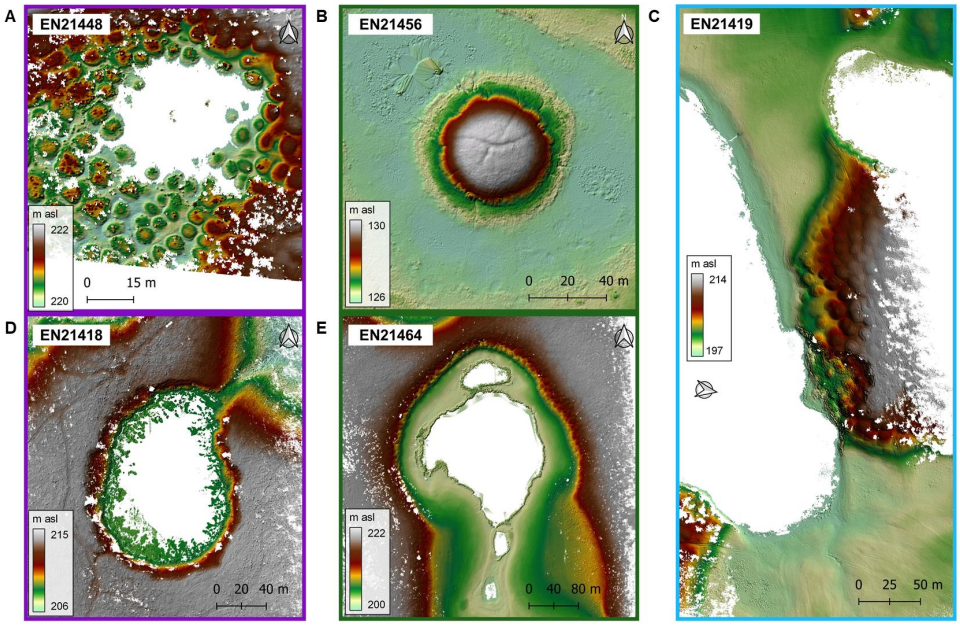

Figure 2: (A-E) Figurative examples from UAV-LiDAR derived surface models (with trees and understorey vegetation removed and water surface masked in white with exception for lake EN21456) of the three thermokarst lake types (connected alaas lakes, new thermokarst lakes and old alaas lakes). (A,D) Two examples of new thermokarst lakes are EN21418 and EN21448 (purple outlines) which show the steep slopes with up to 6 m height difference to the top of the Yedoma plateau and EN21448 (A) showing the baydzharakh permafrost degradation features. (B,E) Two examples of old alaas lakes are EN21456 and EN21464 (green outlines). EN21456 (B) is one example with a nearly circular developed 'ice-hill' (pingo) of around 4 m height and 55 m diameter within an old alaas lake (in this case surface water not masked as white). (C) Lake EN21419 (blue outline) is of the connected alaas lake type showing a typical elongated shape.

Table A1, Figures A2, 2 and 3 visualise our resulting lake classification scheme of the 66 sampled lakes into mountain lakes, old alaas lakes, new thermokarst lakes, and connected alaas lakes.

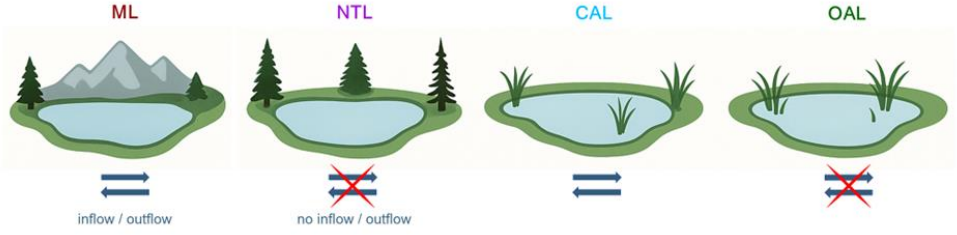

Figure 3: Scheme of our classified lake types in this study: new thermokarst lakes (NTL) and old alaas lakes (OAL) show no in- and outflows in contrast to mountain lakes (ML) and connected alaas lakes (CAL). The lake types in this figure were generated using Perplexity AI.

2.5 Environmental data processing

Satellite-derived land cover

We used the 10 m resolution European Space Agency (ESA) World Cover 2021 land cover product (derived from Sentinel-1 and Sentinel-2; Zanaga et al., 2022) to extract the dominant land cover around the lakes. Due to the very flat yet locally complex (e.g., braided rivers, ponds and other lakes close by) geomorphological relief in Central Yakutia, a robust lake catchment delineation for each of the lakes from Digital Elevation Model data could not be carried out. Instead, we created 50-m buffer zones extending landward from the shoreline around each lake for a consistent extraction of the surrounding land

https://doi.org/10.5194/egusphere-2025-4114
Preprint. Discussion started: 5 September 2025
© Author(s) 2025. CC BY 4.0 License.

cover. We also created a wider buffer zone of 360 m according to the relevant source area of pollen areas in Central Yakutia (Geng et al., 2022).

The ESA World Cover 2021 land cover in WGS84 geographic projection was reprojected to the respective UTM zones (N52, N53, or N54) using QGIS before extracting the land cover for each buffer zone in area-true projection. Up to seven ESA World Cover 2021 land-cover classes (tree cover, shrubland, grassland, built-up, bare/sparse vegetation, permanent water bodies, moss/lichen) occurred within the buffer zones of the mountain region lakes. Built-up and bare/sparse classes were subsequently merged into a single 'barren' class while the moss/lichen class was renamed to 'tundra' for descriptive purposes. The Central Yakutian lakes included up to nine land-cover classes (tree cover, shrubland, grassland, cropland, built-up, bare/sparse vegetation, permanent water bodies, wetland, moss/lichen). Here, the classes 'grassland' and 'cropland' were merged into the single class 'grassland'. As 'moss/lichen' does not occur as true land cover in the lowlands but represents sparsely vegetated areas in settlement and on agricultural land we further merged this class into the 'barren' class (i.e., built-up and bare/spare vegetation) for the lowland region. As a result, for the final analyses, we used five land-cover classes for the mountain region (forest, grassland, tundra, wetland, barren) and four land-cover classes for the lowland region (forest, grassland, wetland, barren).

Climate data

We used contemporary climatologies at a high resolution of 1 km for the Earth's land surface areas (CHELSA) v.2.1 (Karger et al., 2017, 2023; last accessed on May, 2024) to derive three temperature-related and three precipitation-related bioclimatic variables representing the mean conditions for the period 1981–2010 (Table A2). The bioclimatic variables corresponding to the CHELSA grid cell at each lake centre coordinate were extracted using the R platform (R Core Team, 2025) using the packages 'sf' (Pebesma and Bivand, 2023), 'raster' (Hijmans, 2025), 'devtools' (Wickham et al., 2022), and 'climatedata' (https://github.com/MirzaCengic/climatedata; last accessed on July, 2025). For the visualisation of the extracted data, we used the packages 'raster' (Hijmans, 2025) and 'maps' Becker et al. (2025).

Statistical processing and data visualisation

We used a range of complementary statistical analyses and data visualisations for processing the data using R (R Core Team, 2025) except for the Piper diagram. We applied the Piper diagram analyses (Piper, 1944) to delineate the hydrochemical facies of the sampled lakes from the concentrations of major cations and anions and to identify the water composition. The Piper calculations were done using macros developed in Microsoft Excel-2019 by the United States Geological Survey, USGS (https://halfordhydrology.com/piper-and-stiff; last accessed September, 2024), transforming concentrations in milligrams per litre (mg L^{-1}) and calculating total dissolved solids (TDS) and charge balances by the concentration of major ions. Two samples were excluded from the Piper analyses because of exceeding 50% major ion imbalance (EN21426-2) and missing HCO_3^- (EN21457).

Clustering analysis was undertaken using the package 'stats' (R Core Team, 2025) on the lake data of major ions, DOC, TDS, and isotopes. Data were first standardised and then scaled by the Euclidean method. The hierarchical clustering matrix was generated with the method 'ward.D2'. Figures of isotopes and land cover referenced against HCO_3^- are plotted as basic x, y plots (R Core Team, 2025). We used Principal Component Analysis (PCA) to determine the main variations and dependencies in the datasets within lake types. We performed PCA for the hydrochemical variables using the package 'factoextra' (Kassambara and Mundt, 2020) with the function 'prcomp'. Plot visualisations were done in R using 'ggfortify' (Tang et al. 2016), 'ggrepel' (Slowikowski, 2024), and 'ggplot2' (Wickham, 2025). Similarly to the Piper analyses, we excluded two lakes (EN21426-2, EN21457) from the PCA using the hydrochemistry as input, and an additional lake (EN21403) was missing sedDNA data for the multivariable PCA and multi-level statistics. To further understand the hydrochemical components of the

https://doi.org/10.5194/egusphere-2025-4114
Preprint. Discussion started: 5 September 2025
© Author(s) 2025. CC BY 4.0 License.

lakes and potential sources of the dominating major ions, we applied the Gibbs diagram (Gibbs, 1970) in which the ratio of dominant cations $(Na^+)/(Na^+ + Ca^{2+})$ is referenced against TDS on a log-scale from 1 to 10000.

SedDNA data are visualised as Bubble charts, Chord diagrams, and a stratigram (R Core Team, 2025). Relative abundances of macrophytes and terrestrial plants were calculated for each lake using the package 'vegan' (Oksanen et al., 2022). Bubble charts were created using the package 'reshape2' (Wickham, 2007) to transform the data from wide format to long format by lake type with the function "melt", and with the 'ggplot2' package (Wickham, 2025) for visualisation. Data manipulation for Chord diagram filtering, grouping, and summarising was done using the package 'dplyr' (Wickham et al. 2023). To create circular plots of Chord diagrams, we used the package 'circlize' (Gu et al. 2014). Stratigraphic plots are visualised using the package 'rioja' (Juggins, 2022) with the function "strat.plot".

To examine relationships between environmental variables, we conducted a pairwise Pearson correlation analysis. The analysis was performed on the combined environmental dataset (n = 28), using the function "corr.test" from the package 'psych' (Revelle, 2025). Pairwise complete observations were used to handle missing data, and no adjustment for multiple testing was applied. The resulting correlation coefficients and corresponding p-values were visualised using the 'corrplot' package (Wei et al., 2024). A colour gradient was applied to reflect the strength and direction of correlations, and significance levels were overlaid using yellow labelled asterisks ($*p < 0.05$, $**p < 0.01$, $***p < 0.001$). We applied multi-level pattern analyses (MPA) to see the associations and patterns between our environmental and hydrochemical data for the different lake types using the package 'indispecies' (De Cáceres et al., 2025) with the function 'multipatt'. To compare land cover distribution across lake types, we created boxpolts using the function 'ggboxplot' from package 'ggpubr' (Kassambara, 2025), highlighting medians, interquartile ranges, whiskers and outliers without hypothesis testing. Scatterplots were created using the function 'ggscatter' from package 'ggpubr' (Kassambara, 2025).

3 Results

3.1 Summary of the morphological, physico-chemical and isotopic lake characteristics

Our collection of lake data forms a large dataset across a wide (> 700 km) west to east gradient encompassing two contrasting groups of lakes: thermokarst lowland lakes (n = 51) and mountain lakes (n = 15). In terms of lake morphology, most of the sampled mountain lakes (n = 13) are characterised by a relatively small surface water area with a median of 0.05 km² (range 0.008–0.44 km²) and a median water depth of 7.4 m (with standard deviation of ±3.8 m) (Table 1). However, a characteristic of the Verkhoyansk mountain range is the existence of large glacial lakes. We were able to sample two deep glacial lakes, Lake Uluu (EN21401) and lake EN21405 with an area of 7.46 km² and 0.87 km² and maximum lake depth measured during our expedition of 43 m and 33.8 m, respectively. The surface area of the sampled lowland lakes show wide variability both among and within lake types, ranging overall between 0.0012 km² and 7.34 km² (Table 1). The group of connected alaas lakes (n=8) have the largest surface area with a high variability, ranging from 0.09 km² to 7.34 km² with a median of 1.06 km², compared to the group of old alaas lakes (n = 28; 0.0012 km² to 2.97 km² with 0.07 km² median), and the smallest lake type of the new thermokarst lakes (n = 15; 0.0016 km² to 1.97 km² with a median of 0.02 km²).

The limnological variables and lake hydrochemistry are shown in tables 1 and A3 and published in Baisheva et al. 2022, Stieg et al. 2022). Mountain lakes are characterised by a median neutral pH of 7.6. Contrastingly, the lowland lakes display more neutral (~7) to strongly alkaline (~9) pH with a median pH of 8.8. Large differences between mountain and lowland lakes are also shown by the EC (median and range) in the lowland lakes being over an order of magnitude greater than the very low conductivity values of the mountain lakes. In accordance, TDS of mountain lakes are low with a median of 49 mg L^{-1}, compared to lowland lakes with a median of 812 mg L^{-1} in connected alaas lakes, 870 mg L^{-1} in new thermokarst lakes, and 1645 mg L^{-1} in old alaas lakes. Similarly, the lowland lakes have very high concentrations of DOC, which is highest in the new thermokarst lakes with a median of 106.1 mg L^{-1}, in contrast to the very low DOC in mountain lakes with 13.3 mg L^{-1}.

https://doi.org/10.5194/egusphere-2025-4114
Preprint. Discussion started: 5 September 2025
© Author(s) 2025. CC BY 4.0 License.

Table 1: Major physical and hydrochemical parameters of the different lake types. Values are shown as the median across all lakes per category. In this table, we do not incorporate the two large mountain lakes with outstanding properties (e.g., maximum water depth > 30 m). The values of the two deep mountain lakes are shown in supplementary table (*Table S1*) in the appendix. EC = electrical conductivity; TDS = total dissolved solids; DOC = dissolved organic carbon. Not Available (NA) and Not Determined (ND) refer to lakes per category with no data available, or not applicable, respectively; dl and bdl refer to detection limit and below detection limit, respectively.

Lake type	**Mountain lakes**	**New thermokarst lakes**	**Old alaas lakes**	**Connected alaas lakes**
Number	13	15	28	8
Variable	median min-max	median min-max	median min-max	median min-max
Elevation (m a.s.l.)	**1036** 789-1310	**202** 126-307	**173** 115-246	**166** 134-299.6
Lake area (km^2)	**0.05** 0.008-0.44	**0.02** 0.002-1.9	**0.07** 0.001-2.9	**1.05** 0.09-7.3
Lake depth (m)	**7.84** 3-14.3	**3.2** 1-19.1	**1.9** 0.5-8.4	**2.4** 1.7-6.9
Secchi depth (m)	**2.56** 1.35-5.39	**1.3** 0.2-2	**0.5** 0.2-1.9	**0.4** 0.2-0.8
pH	**7.6** 6.6-8.6	**8.6** 7-9.2	**8.9** 8-9.4	**9** 8.1-9.4
EC (µS cm^{-1})	**83.2** 14-194	**999** 274-3140	**1619** 487-6010	**894** 379-1238
TDS (mg L^{-1}	**61** 8-115	**870** 238-3294	**1553** 460-5276	**812** 336-1248
DOC (mg L^{-1})	**14** 4.53-23.9	**106** 4.57-417	**80** 52-279	**69** 34-117
Ca^{2+} (mg L^{-1})	**10.6** 1.61-18.6	**32.7** 9.78-64.8	**18.9** 2.7-46.8	**28** 15.3-39.7
Mg^{2+} (mg L^{-1})	**4.21** 0.59-7.98	**111.6** 16.8-388	**118.5** 29.5-274	**87.3** 33.7-139
Na^{+} (mg L^{-1})	**0.94** 0.21-2.08	**78.1** 7.32-401	**209.4** 46.7-1222	**80.5** 13.5-122
K^{+} (mg L^{-1})	**0.66** 0.32-0.95	**4.9** 0.32-0.95	**12.1** 5.44-105	**11** 5.37-20.1
HCO_3^- (mg L^{-1})	**32.6** 5.2-82.5	**607.4** 179.9-2153.8	**835.9** (ND=1) 320.3-2791.4	**581.9** 250.92-924.2
Cl^- (mg L^{-1}) dl - 0.1 mg L^{-1}	**NA** (bdl=13)	**30.8** 0.9-258	**89.2** 5.7-697	**32** 2.5-58.2
SO_4^{2-}(mg L^{-1}) dl - 0.1 mg L^{-1}	**1.74** (bdl=2) 0.12-20.5	**7.7** (bdl=5) 1.38-507	**33.9** (bdl=4) 0.28-947	**1** (bdl=2) 0.15-15.9
F^- (µg L^{-1}) dl - 0.1 mg L^{-1}	**NA** (bdl=13) 0.13-0.15	**0.43** 0.14-1.3	**0.29** (bdl=2) 0.15-1.42	**0.43** 0.28-0.48
$\delta^{18}O$ (‰ V-SMOW)	**-17.67** -19.6 to -14.07	**-9.1** -14.7 to -7.3	**-7.7** (ND=1) -11.3 to -5.2	**-8.9** -10.1 to -6.3
δD (‰ V-SMOW)	**-148.9** -159.3 to -135.91	**-112.9** -142.1 to -96.5	**-99.8** (ND=1) -121.3 to -85.1	**-105.1** -111.6 to -84.9
d.excess (‰)	**-10.1** -23.3 to 4.5	**-34.06** -41.2 to -24.9	**-39.8** (ND=1) -46.5 to -30.1	**-35.6** -40.8 to -30.5

The dominant hydrochemical facies of the majority of lakes is of the $CaMgHCO_3$ type as shown by the Piper analyses (Fig. 4) indicative of calcium and magnesium carbonate weathering. Weak acids exceed the strong acids (CO_3^-+HCO_3^-)>(SO_4^{2-}+Cl^-), and alkaline earths exceed alkalis (Ca^{2+}+Mg^{2+})>(Na^++K^+) for a large majority of the lakes (n = 60), corresponding to the bicarbonate type in the anion triangle. Lake cations most frequently correspond to the magnesium type (n = 32), while calcium type is encountered in 13 mountain lakes (EN21401 to 409, EN21412 to 415) and one new thermokarst lake (EN21423). In Central Yakutia, eight lakes (EN21420, 426, 428, 430, 431, 436, 440, 444) are of the sodium type. One highly saline lake EN21426 is of the NaCl type, while two other high saline lakes (EN21430, 436) are of the $NaHCO_3$ alkali carbonate type. For brackish Central Yakutian lakes, alkalis often exceed alkaline earths (Na^++K^+)>(Ca^{2+}+Mg^{2+}) (n = 9, EN21420, 426, 428, 431, 436, 438, 440, 444, 449) and extreme hydrochemical facies characterise four of the sampled lakes (EN21426, 448, 456, 465) with strong acids exceeding weak acids (SO_4^{2-}+Cl^-)>(CO_3^-+HCO_3^-).

https://doi.org/10.5194/egusphere-2025-4114
Preprint. Discussion started: 5 September 2025
© Author(s) 2025. CC BY 4.0 License.

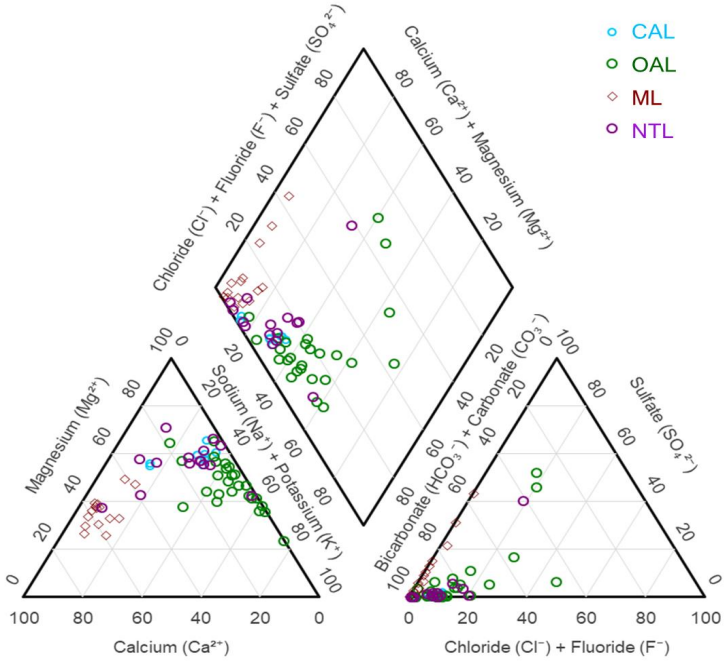

Figure 4: Piper diagram showing the hydro-chemical facies of the different lake types: connected alaas lakes (CAL), old alaas lakes (OAL), mountain lakes (ML), new thermokarst lakes (NL).

The hierarchical clustering of the lakes according to major ion hydrochemistry confirms the clustering in the Piper hydrochemical facies, with the lakes grouping according to the concentration of salts into three main clusters (Fig. A3). Brackish lowland lakes with high ion content (Clusters 1, 2; n = 26) are clearly separated from the freshwater lakes from mountain and lowland areas (Cluster 3, n = 38), with the exception of three brackish lakes (EN21418, 453, 462). Cluster 1 specifically envelops three lowland old alaas lakes (EN21430, 436, 440) characterised by very high TDS at 4006 mg L^{-1}, 3324 mg L^{-1}, and 5276 mg L^{-1}, respectively. Cluster 2 includes 23 lowland lakes of different lake types with brackish waters. Similarly, the brackish lakes are also grouped by multilevel pattern analyses (Table 2). The freshwater lakes in Cluster 3 include 38 lakes of which 15 are mountain lakes, forming a separate subcluster together with one new thermokarst lake (EN21445) and 23 lowland freshwater lakes of different lake types. TDS for three lakes in this subcluster (EN21418, 453, 462) are moderately high at 1357, 1001, and 1192 mg L^{-1}, respectively.

The Gibbs diagram (Fig. A4) partitions the mountain lakes into precipitation and groundwater/runoff dominated systems while the majority of lowland lakes, specifically of the old alaas lake type, are clustered in the sector assigned to evaporation as the dominating process, although several of the new thermokarst lakes and connected alaas lakes are also located in the sector that characterises more diluted waters commonly associated with groundwater or runoff influenced systems.

The isotopic composition of the sampled lake waters across the 700-km transect clearly separates the lakes into two groups (Fig. 5), the lowland lakes ($Yak21_{Lowland}$) with a steep slope of the local evaporation line (6.14, n = 50), and the mountain lakes ($Yak21_{ML}$), with a more gentle slope (3.71, n = 15). All evaporation lines stretch away from the GMWL and the LMWL, indicating evaporative effects. The high-elevation mountain lakes show a widespread low isotopic value range apart from the two most eastern lakes on the Oymyakon Plateau (EN21410, 411). The evaporation line of $Yak21_{Lowland}$ intercepts the LMWL at -30‰ $\delta^{18}O$ (V-SMOW) indicating an isotopically depleted lake-water source such as snowmelt and no relevant influence of isotopically enriched summer precipitation, as occurred in August 2021 (see single rain event). This is in contrast to the $Yak21_{ML}$, where the isotopic composition intercepts the LMWL at -20‰ $\delta^{18}O$ (V-SMOW) indicating an isotopically enriched source signal.

https://doi.org/10.5194/egusphere-2025-4114
Preprint. Discussion started: 5 September 2025
© Author(s) 2025. CC BY 4.0 License.

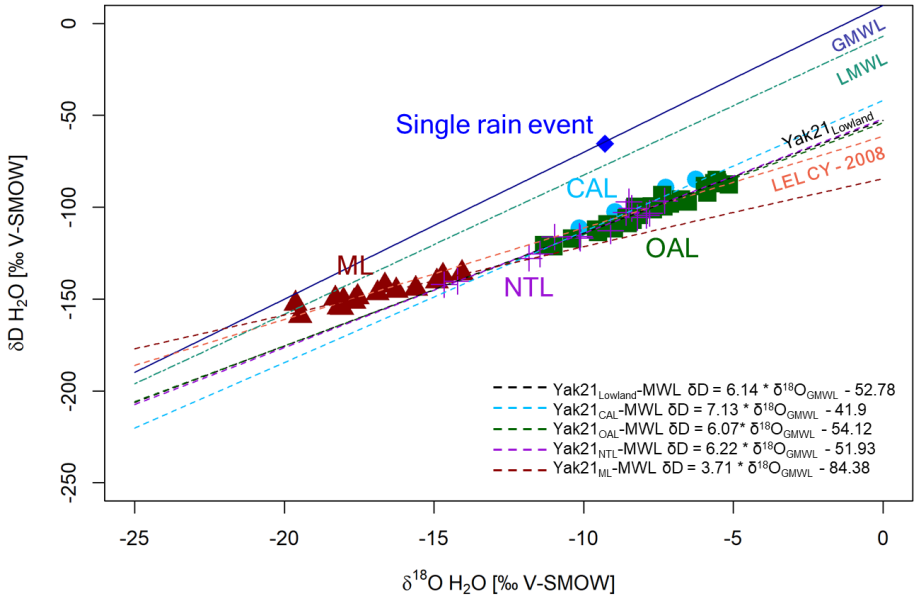

Figure 5: Stable isotopes ($\delta^{18}O$ and δD) from lake surface-water and from one summer precipitation sample (August 2021) along a 700 km west to east transect from Central Yakutia (old alaas lakes (OAL), connected alaas lakes (CAL), new thermokarst lakes (NTL)) to the Oymyakon High mountain plateau in the east (mountain lakes (ML)). Displayed are the Global Meteoric Water Line (in solid blue), GMWL: $\delta D = 8*\delta^{18}O + 10$ (Craig 1961), the Local Meteoric Water Line (in dashed green) LMWL: $\delta D = 7.57*\delta^{18}O\_GMWL - 6.86$ (Kloss, 2008), and a local evaporation line from Central Yakutia (in dashed orange), LEL CY (lake sampled in 2008): $\delta D = 4.99*\delta^{18}O\_GMWL - 61.41$ (Wetterich et al. 2008), and our local evaporation lines based on the different lake types ($Yak21_{Lowland}$, $Yak21_{CAL}$, $Yak21_{OAL}$, $Yak21_{NTL}$, and $Yak21_{ML}$).

The relationship between chloride (Cl^-) concentrations and $\delta^{18}O$ specifically for the lowland lakes, exhibits significant scatter (Fig. A5), suggesting that contemporary evaporation processes are not the primary drivers of the observed $\delta^{18}O$ variability. Notably, although some of the highly saline lakes show enriched $\delta^{18}O$ values, at the same time they show low to moderate Cl^- concentrations but elevated fluoride (F^-) concentrations.

The first two PCs explain a good proportion (69.53 %) of the total variance in hydrochemistry parameters among all lakes showing a strong separation of the mountain and lowland lakes (Fig. 6). While the mountain lakes form a distinct cluster, the lowland lakes are more scattered across PC1 and PC2 without a clear distinction between the different lake types. Relevant lake hydrochemistry variables, such as DOC, Mg^{2+}, HCO_3^-, TDS, EC, and K^+ show the strongest negative loadings along the PC1 axis for all lakes. However, a PCA considering the group of lowland lakes only (Fig. A6), HCO_3^-, TDS, EC, and Mg^{2+} show strong positive loadings on PC1, potentially separating the lake types, whereas DOC and SO_4^{2-} show less variance for the lowland lakes only. The major ions Ca^{2+} and Si^+ and the minor ions Sr^{2+} and Ba^{2+} are mainly expressed along the positive PC2 axis when analysing all lakes (Fig. 6), but when analysing only the lowland lakes the minor ions Ba^{2+} and Sr^{2+} align along the negative axis of PC2 (Fig. A6).

https://doi.org/10.5194/egusphere-2025-4114
Preprint. Discussion started: 5 September 2025
© Author(s) 2025. CC BY 4.0 License.

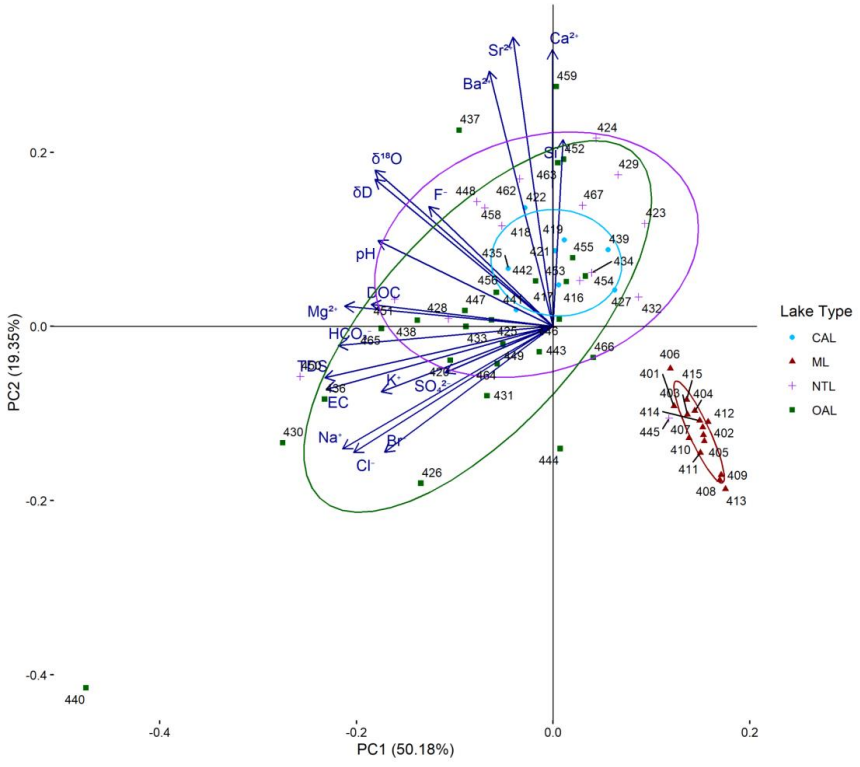

Figure 6: Principal component (PC)1-2 biplot of hydrochemical variables (minor and major ions, hydrophysics, isotopes) from all lakes with ellipses outlining the lake types with mountain lakes (ML) forming a separate cluster, but overlapping for all lowland thermokarst lakes: new thermokarst lakes (NTL), old alaas lakes (OAL), and connected alaas lakes (CAL). The length of the vectors expresses the loadings of the hydrochemical variables in the PC1 to PC2 space.

3.2 Aquatic plants per lake type

Total macrophyte sedDNA richness for all lake types is 87 amplicon sequence variants (ASVs), with the highest diversity in emergent (65 ASVs), followed by submerged (13 ASVs), floating (7 ASVs), and submerged-emergent (2 ASVs) macrophyte taxa (Fig. 7, A8). Most counts are from submerged macrophytes (74 %), with the three other functional groups accounting for only a quarter of the total counts with emergent 17 %, floating 5 %, and submerged-emergent 4 %. Macrophyte composition varies by lake type, with certain taxa associated with specific lake types (Fig. 7A; Table A4). However, submerged macrophytes consistently dominate across all lakes, comprising a median of 94 % in connected alaas lakes, 82 % in old alaas lakes, 63 % in mountain lakes, and 46 % in new thermokarst lakes.

Emergent macrophytes are well represented in old alaas lakes (median of 13 % of total share). Submerged-emergent macrophytes are the least diverse group (only two *Hippuris* ASVs), yet relatively frequent in ten mountain lakes, with a median of 40 % of the macrophyte total share per lake. The dominant submerged macrophytes are *Potamogeton*-1, (with a median of 32 %) across all lake types, and *Stuckenia pectinata* in connected alaas lakes (with a median of 31 %) and old alaas lakes (with a median of 13 %). Two submerged macrophytes *Myriophyllum* and *M. verticillatum* occur only in freshwater lakes, as does the submerged-emergent *Hippuris*, except for one brackish new thermokarst lake (EN21451).

https://doi.org/10.5194/egusphere-2025-4114
Preprint. Discussion started: 5 September 2025
© Author(s) 2025. CC BY 4.0 License.

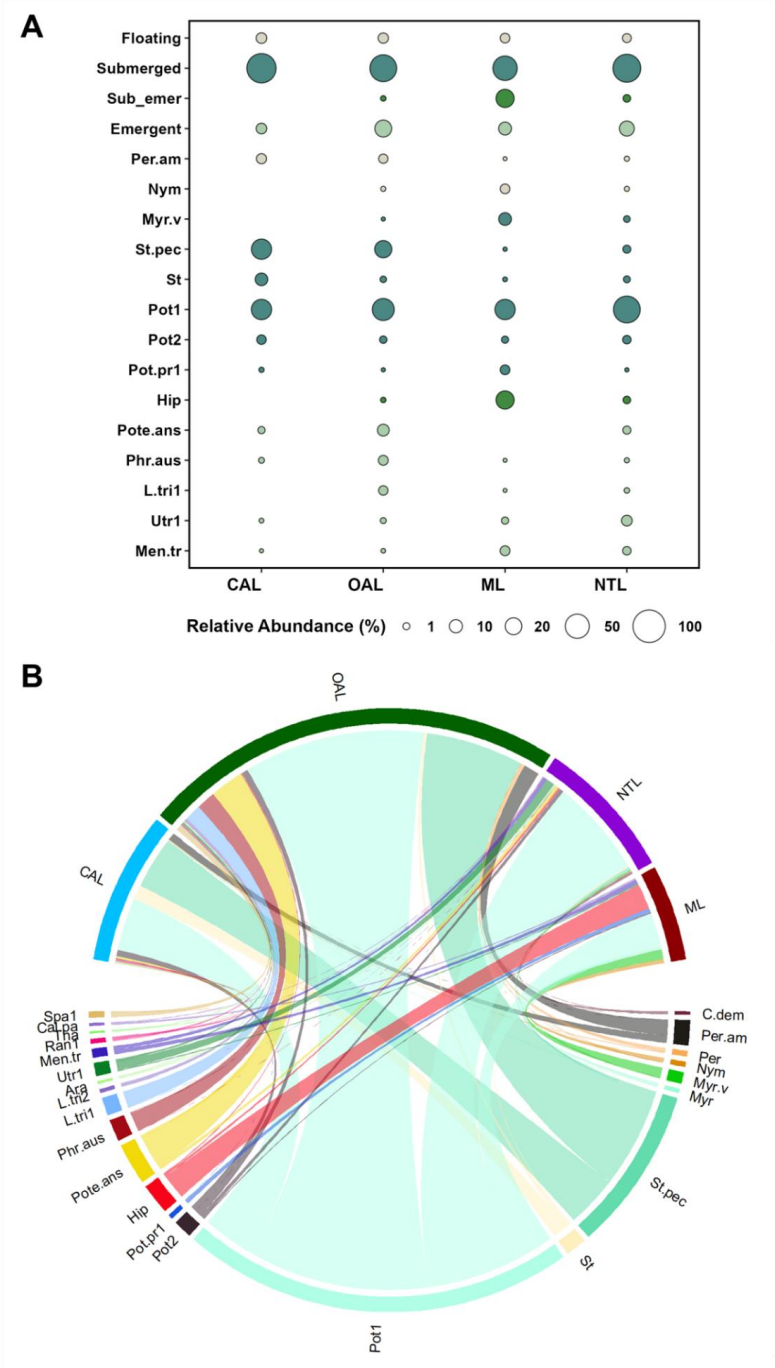

Figure 7: (A) Bubble-chart illustrating the relative abundance of macrophytes in four lake types: mountain lakes (ML), old alaas lakes (OAL), connected alaas lakes (CAL), and new thermokarst lakes (NTL). Relative abundance of plant types is displayed as the total share per lake type. A subset of plants with >4 % occurrence is also shown. (B) Chord-diagram showing the most abundant taxa within the four lake types and their relationship to lake type. Short names of taxa refer as follows: Spa1-*Sparganium1*, Cal.pa-*Caltha palustris*, Tha-*Thalictrum*, Ran1-*Ranunculus1*, Men.tr-*Menyanthes trifoliata*, Utr1-*Utricularia1*, Ara-Aracaceae, L.tri1-*Lemna triscula1*, Phr.aus-*Phragmites australis*, Pote.ans-*Potentilla anserina*, Hip-*Hippuris*, Pot.pr1-*Potamogeton praelongus1*, Pot2-*Potamogeton2*,Pot1-*Potamogeton1*, St-*Stuckenia*, St.pec-*Stuckenia pectinata*, Myr-*Myriophyllum*, Myr.v-*Myriophyllum verticillatum*, Nym-Nymphaeaceae, Per-*Persicaria*, Per.am-*Persicaria amphibia*, C.dem-*Ceratophyllum demersum*.

https://doi.org/10.5194/egusphere-2025-4114
Preprint. Discussion started: 5 September 2025
© Author(s) 2025. CC BY 4.0 License.

3.3 Land cover and terrestrial vegetation

Terrestrial vegetation richness derived from sedDNA (total 116 ASVs) is highest for grasses and herbs (83 ASVs), with lower richness for shrubs (16 ASVs), trees (9 ASVs), and mosses (8 ASVs) (Fig. A7, A9). The most count-contributing terrestrial plants are trees (54 %) followed by grasses and herbs (39 %), shrubs (8 %), and mosses (only 0.1 %). Taxonomic richness and relative abundance vary with lake type (Fig. A7, A9; Table A5), with new thermokarst lakes exhibiting the highest median richness (17 taxa), followed by connected alaas lakes (14 taxa), old alaas lakes (12 taxa), and mountain lakes (11 taxa). Grasses and herbs are the most taxonomically diverse group deposited in lowland lakes, with median richness ranging from 9 to 9.5 taxa. These taxa are also dominant in the surface sediments in connected alaas lakes (75 %) and old alaas lakes (74 %), while contributing less in new thermokarst lakes (25 %). SedDNA counts of trees and shrubs are around a quarter in old alaas lakes (24 %) and in connected alaas lakes (25 %). In contrast, trees and shrubs represent the dominant sedDNA-derived material in new thermokarst lakes (75 %) and mountain lakes (93 %), with the latter showing the highest tree richness (median of 4 taxa per lake). Prominent woody taxa include Salicaceae, *Larix*, and *Betula*, particularly in mountain lakes and new thermokarst lakes, while old alaas lakes and connected alaas lakes have a more evenly distributed taxonomic occurrence of grasses and herbs (Fig. A7).

Results of sedDNA-derived terrestrial plant assemblages agree with the satellite-derived land-cover composition surrounding the lakes. Forest land cover has a significant ($p \leq 0.001$) positive correlation ($R = 0.40$) with the proportion of trees from sedDNA samples, while grassland correlates ($R = 0.43$) significantly ($p \leq 0.001$) with proportions of grasses and forbs.

Land cover differs according to lake type within the 50 m and 360 m buffer zones (Fig. A10, A11). Grasslands are the most abundant class within the 50 m buffer zone around the old alaas lakes (60 % median proportion) and connected alaas lakes (55 % median proportion) (Fig. A10), comprising cultivated grasses for hay and grain production, although forest becomes the dominant class when extending the buffer zone to 360 m for old alaas lakes (70 % median proportion) and connected alaas lakes (54 % median proportion) (Fig. A11). Old alaas lakes and connected alaas lakes also have the highest proportions of wetlands around them, compared to mountain and new thermokarst lakes although the proportion is rather small (up to 4 % median proportion). Most mountain lake environments are dominated by forest (83 % median proportion), while only two of our sampled mountain lakes (EN21412 and 413) are surrounded by tundra (with a 64 % and 44 % of total share, respectively). Similarly, forest is the dominant land cover around new thermokarst lakes (83 % median proportion). Land-cover dominance and relative proportions remain mostly unchanged for both mountain lakes and new thermokarst lakes under both buffer widths (Fig. A10; A11). Seven lakes (EN21421, 427, 439, 440, 441, 458, 459) occur within settlement areas (one in Churapcha, one in the summer settlement Aryylaakh, three in Tungulu, and two in Maya, respectively).

3.4 Combined environmental analyses

The CHELSA-derived mean annual temperature (MAT) spatial distribution is characterised by a west-to-east decreasing gradient with MAT ranging from a maximum value of -8.9 °C in the westernmost region (around the settlement Maya), to -10.3 °C eastwards in the Tattinsky district, and a minimum of -13°C in the Verkhoyansky mountain region to the east (Fig. A12). Conversely, mean annual precipitation (MAP) shows a west-to-east increasing gradient in the lowland with the lowest MAP of 291.3 mm in the west, and 300.3 mm in the Tattinsky district to the east. MAP is higher in the mountain areas, with the highest value of 365 mm reached in the Tomponsky district (Fig. A13).

Land cover with DOC and HCO_3^- generally displays positive and negative relationships for forest (Fig. A10, A11, A14) with a negative relationship observed between tundra and HCO_3^- for mountain lakes in the 360 m buffer zone. A positive relationship is observed between wetlands and DOC for old alaas lakes. The highest percentage of forest occurs together with relatively higher DOC concentrations than for other land-cover types, for both mountain and lowland lake types. Specifically, new thermokarsts lakes that are characterised by a high percentage of forest in the immediate 50 m buffer show highest DOC concentrations. The land cover assigned hydrochemical facies in the Piper diagram visualisation (Fig. A15) shows that the

https://doi.org/10.5194/egusphere-2025-4114
Preprint. Discussion started: 5 September 2025
© Author(s) 2025. CC BY 4.0 License.

settlement and grassland-linked lakes are widespread along the chloride and fluoride and the potassium and sodium ranges, and forest-linked lakes are mostly located in the lower mineralised range.

The first two principal components of the PCA performed on hydrochemical data from lakes (major and minor ions, TDS, EC, pH) with all environmental variables (lake type, elevation, hydrochemical clusters, climate variables, shares of land cover classes within 50 m buffer zone, terrestrial vegetation functional type and aquatic plants explain 83 % of the variability in lake hydrochemical facies (Fig. A16). An examination of the active variables, the ions and position and lengths of the vectors reveals that the strongest direction of hydrochemistry variability along PC1 occurs linked to forest and tundra land-cover classes together with trees and shrubs derived from sedDNA associated with mountain lakes, while the sedDNA group of grasses and land-cover class grass are associated with lowland lakes. The clear distinction between the lowland and the mountain lakes seems specifically related to the highly soluble alkali Ca^{2+} versus HCO_3^-, TDS, EC, freshwater, and its associated Cluster 3 versus brackish and the associated major ions of Cluster 2. Freshwater lakes are associated with Sr^{2+} and Ca^{2+}. HCO_3^- also has a strong negative loading on PC1, grouping the brackish old alaas lakes into a separate cluster along with EC and TDS. Connected alaas lakes occur across the brackish to freshwater gradients shared between PC1 and PC2, whereas the old alaas lake type is specifically spread along the negative PC1, close to brackish waters.

The climate variables precipitation of the driest month (Pdry), mean annual air temperature (MAT), and mean maximum air temperature of the warmest month (Tmax) show strong negative PC1 loadings, separating the lowland lakes from the mountain lakes. In contrast, precipitation of the wettest month (Pwet) and elevation (Elev) are linked to the distribution of the mountain lakes along the positive PC1 axis. Clear distinction between sedDNA-derived aquatic plant types occurs in mountain lakes associating with sub-emergent plants, and floating plants next to the connected alaas lakes.

Table 2: Results from the multi-level pattern analysis showing the list of statistically significant associations of environmental variables with the different lake types: connected alaas lakes (CAL), old alaas lakes (OAL), new thermokarst lakes (NTL), mountain lakes (ML). Significance level coding: * ≤ 0.001, ** ≤ 0.01, * ≤ 0.05.**

Lake type	Associated variables	Short names	*p*-value
OAL	Major ion Cluster	C2	0.0122 *
ML	Elevation	Elev	0.0001 ***
	Precipitation of the wettest month	Pwet	0.0001 ***
	SedDNA submerged-emergent macrophytes	subemergent	0.0002 ***
	Land cover Tundra	TUNDRA	0.0003 ***
	Minimum annual temperature of the coldest month	Tmin	0.0030 **
	SedDNA-derived shrubs	shrubs	0.0061 **
Group: CAL + OAL	Land cover Grass	GRASS	0.0001 ***
	SedDNA-derived grasses and forbs	grasses	0.0001 ***
	Land cover Wetland	WETLAND	0.0095 **
Group: CAL + ML	Freshwater	freshwater	0.0021 **
Group: NTL + OAL	Positively charged sodium ions	Na^+	0.0015 **
	Negatively charged chloride ions	Cl^-	0.0023 **
	Brackish water	brackish	0.0019 **
	SedDNA-derived emergent macrophytes	emergent	0.0422 *
	Negatively charged bromide ions	Br^-	0.0149 *
Group: ML + NTL	Land cover Forest	FOREST	1e-04 ***
	SedDNA-derived trees and shrubs	trees	8e-04 ***
Group: CAL + ML + NTL	Major ion Cluster 3	C3	0.0088 **
Group: CAL + OAL + NTL	Mean annual temperature	MAT	0.0001 ***
	Maximum annual temperature of the warmest month	Tmax	0.0001 ***

https://doi.org/10.5194/egusphere-2025-4114
Preprint. Discussion started: 5 September 2025
© Author(s) 2025. CC BY 4.0 License.

	Oxygen stable isotope	$\delta^{18}O$	0.0001 ***
	Hydrogen stable isotope	δD	0.0001 ***
	Precipitation of driest month	Pdry	0.0001 ***
	Power of hydrogen	pH	0.0001 ***
	Barium ion with two positive charges	Ba^{2+}	0.0001 ***
	Specific electrical conductivity	EC	0.0003 ***
	Negatively charged bicarbonate ions	HCO_3^-	0.0001 ***
	Total dissolved solids	TDS	0.0003 ***
	Magnesium ions with two positive charges	Mg^{2+}	0.0005 ***
	Strontium ions with two positive charges	Sr^{2+}	0.0001 ***
	Negatively charged fluoride ions	F^-	0.0001 ***
	Calcium ions with two positive charges	Ca^{2+}	0.0006 ***
	Dissolved organic carbon	DOC	0.0032 **
	Positively charged potassium ions	K^+	0.0168 *

Multi-level pattern analysis of 43 combined hydrochemical and environmental variables identified 35 variables with strong associations with specific lake types and groups of lake types (Table 2). Only two lake types (old alaas lakes and mountain lakes) were distinctly separated. Old alaas lakes are primarily associated with the hydrochemical major ions of Cluster 2, while mountain lakes are associated with more physical variables, such as elevation, climate (precipitation of wettest months, min temperature of coldest month), and land cover/vegetation variables such as the presence of shrubs and tundra, which dominate the area around the mountain lakes, as well as the aquatic group of sub-emergent macrophytes in the lakes. The connected alaas lakes and mountain lakes are connected with the freshwater lakes. In contrast, new thermokarst lakes and old alaas lakes are associated with brackish waters as well Na^+ and Cl^- enriched waters. SedDNA-derived trees and satellite-derived forest land cover are associated with mountain lakes and new thermokarst lakes, while old alaas lakes and connected alaas lakes are associated with sedDNA-derived grass and satellite-derived grassland land cover.

4 Discussion

4.1 Environmental drivers of physico-chemical lake characteristics

In this study, we provide a comprehensive baseline assessment of the hydrochemistry and associated terrestrial vegetation as well as satellite-derived and sedDNA-derived land cover, and sedDNA-derived aquatic plant diversity of 66 lakes. The lakes span a broad gradient of environmental conditions across a 700-km wide longitudinal transect from the lake-rich thermokarst landscape of Central Yakutia to the under-sampled Verkhoyansk mountain region close to the “cold pole of the Earth”. Using this unique dataset, we assess how the hydrochemical lake status is influenced by climate, geomorphology, elevation, land cover, and land use.

In general, the cover of forest and wetland, and soil carbon density, influence the chemical composition in lakes due to considerable input from surface runoff (Xenopoulos et al. 2003; Sobek et al. 2007). We assume that surface runoff serves as the main source of both dissolved and particulate contributions into our sampled lakes, as high-latitude lake hydrochemistry is typically governed by surface runoff (Fedorov and Konstantinov, 2003, Walvoord and Kurylyk, 2016). We assume for the lowland lakes, that the surface runoff primarily occurs from spring meltwater and strong summer precipitation events, as the majority of the studied lowland lakes have no active inlets or outlets. The limited role of groundwater for contributing dissolved and particulate input from the surrounding sediments and rocks is characteristic of lakes in permafrost landscapes (Pienitz et al. 1997; Pienitz and Smol, 1993), in contrast to groundwater as a dominating source in non-permafrost areas (Wetzel, 2001). Groundwater and intermediate flows in sediment and rocky sublayers are strongly limited due to permafrost acting as a barrier

https://doi.org/10.5194/egusphere-2025-4114
Preprint. Discussion started: 5 September 2025
© Author(s) 2025. CC BY 4.0 License.

to downward and upward water movements, although suprapermafrost flow is possible through the thawed active layer in summer and perennially unfrozen ground (talik) that forms beneath deeper surface water bodies due to the high heat capacity of water (Pienitz et al. 1997; Pavlova et al. 2016; Strauss et al. 2017). Thus, the thawed active layer in the late summer months and sub-lake and sub-river taliks can function as aquifers enabling temporary to steady-state isotope and ionic transport (Walvoord and Kurylyk, 2016). Several of the sampled new thermokarst lakes show a depleted isotopic composition that could indicate lateral input from meltwater of permafrost ground-ice such as described in Popp et al. (2006). The Pleistocene Yedoma sedimentary deposits in which the sampled new thermokarst lakes with depleted isotopic composition are located, are characterised by significantly higher ice content, and therefore, high potential for permafrost degradation due to ground-ice melt. This is in contrast to the considerably reworked and ground-ice depleted Holocene alaas deposits (e.g., Windirsch et al., 2020, for Central Yakutia). As the old alaas lakes and connected alaas lakes are all located in subsided and thoroughly degraded topographic depressions, the major ground-ice thawing processes have occurred several centuries to millennia earlier. Therefore, we can safely assume that no major ground-ice contribution in the form of meltwater input is expected for these two types of alaas lakes, in contrast to the potential meltwater contribution from the ground-ice rich Yedoma sedimentary deposits in the new thermokarst lakes.

Overall, our results indicate that the hydrochemistry of the lowland lakes shows a strong linkage to the lake development stage within the thermokarst chronosequence. In particular, we detect associations between lake type and DOC, pH, hydrogen carbonate, and isotopic composition, as well as the alkali and earth alkali hydrochemical facies types. In agreement with previous studies (Hughes-Allen et al. 2020; Jongejans et al. 2021), we find that the new thermokarst lake type is characterised by the highest DOC concentrations, though with considerable variability. Most of our sampled new thermokarst lakes are surrounded by forest, therefore high organic input into surface waters is to be expected.

All thermokarst lake types in the chronosequence show high DOC, mineral content, and salinity with the exception of the connected alaas lakes. The connected alaas lakes are extensively and regularly flushed during strong precipitation events and the regularly occurring spring floods, resulting in lower water retention times leading to lower levels of minerals, major ions, and DOC despite the high DOC input during snow melt. Similarly, the much lower DOC observed in mountain lakes is likely related to their higher dilution capacity provided by frequent flushing events and their larger water volumes. The surrounding mountain landscapes also contain much thinner organic soils (E. Dietze, personal communication) and less dense forests (Miesner et al. 2022) providing less organic material loading from the surface runoff to the lake. Herzschuh et al. (2013) show that forest land cover contributes to higher HCO_3^- and DOC in the lakes in the forested landscape of Central Yakutia relative to those in tundra and forest-tundra landscapes. Accordingly, within the mountain lake group, lakes with higher forest cover are also characterised by higher DOC.

4.2 Legacy of high salinity in Central Yakutian lakes

Eastern Central Yakutia has a considerably low annual precipitation of only 280 mm and lies within an arid climate zone. The lakes here are subject to strong aridification or even desiccation (Czerniawska and Chlachula, 2020) leading to a negative lake-water balance as described in Kumke et al. (2007). This is evident from our isotopic analyses, with isotopic enrichment in the lowland lakes, and also from the Gibbs-derived assignment into the evaporative sector as water source assessment. The overarching boreal biome setting and the negative water balance due to evaporative processes in summer contributes to generally high lake-water mineral content in the lowland thermokarst lakes in Yakutia (Pestryakova et al., 2012; Herzschuh et al., 2013). Most of our sampled lowland lakes belong to the magnesium-type hydrochemical classification with weak acids predominating over strong acids and alkaline earths exceeding alkali metals. However, some of our sampled lowland lakes in Central Yakutia have exceptionally high salinities with no link to either a specific terrace or the surrounding vegetation or land use. Although Kumke et al. (2007) propose that very high salinity levels in Yakutian lakes could result from anthropogenic influences, their hypothesis is not substantiated by field data or data analyses. On the contrary, our findings indicate that high

https://doi.org/10.5194/egusphere-2025-4114
Preprint. Discussion started: 5 September 2025
© Author(s) 2025. CC BY 4.0 License.

salinity in the lakes we sampled cannot be explained by anthropogenic impacts as they are located far away from settlements and managed lands. In fact, chloride concentrations show high variability across different terraces, land cover, and lake types. For the mountain lakes, the depleting elevation effect can explain the widespread lower isotopic ratio value range. In contrast, for the lowland lakes, the opposite effect of isotopic enrichment due to evaporation effects could lead to a wide range in the higher isotopic ratio. However, the relationship between chloride concentrations and $\delta^{18}O$ exhibits significant scatter suggesting that contemporary evaporation processes are not the primary drivers of the observed $\delta^{18}O$ variability. These sampled highly saline lakes with enriched oxygen isotopic composition despite low chloride concentrations are all specifically characterised by elevated fluoride concentrations. This interesting relationship suggests an influence of local lithology, potentially involving fluoride leaching from Holocene lacustrine sediments or older salt deposits as has been described for other subarid and arid regions (Olago et al., 2009; Wen et al., 2013). Also, an experimental study from Lopez et al. (2007) detected epigenetic salinisation of the active layer in alaas basins, caused by leaching from the surrounding forest soils.

Therefore, in contrast to the conclusions of Kumke et al. (2007), which link elevated lake salinity to anthropogenic factors, our results suggest that high salinity in some of our sampled lakes could be a legacy of highly saline conditions in the past, for example, by leakage from older fluoride-bearing lacustrine sediments of evaporites or some other hydrological link to old or new local salt deposits.

4.3 Specificity of thermokarst lakes and lake hydrochemistry

In our study, we investigated different lake groups in the Central Yakutian lowland and mountain permafrost landscapes. Our sampled mountain lakes in the Verkhoyansk mountain range include a wide range of lake sizes and differ markedly in terms of lake genesis and lake depth. These mountain lakes contain the glacial lake type, which is the most distinctive lake type of this group, and have a wide range of lake settings and morphologies associated with glacial moraines and ancient river floodplains, which are more like thermokarst lakes. Thermokarst lakes include a wide diversity of lake sizes from pond-sized to large lakes. The key difference between our sampled mountain and lowland lakes is related to the influence of climatic factors, such as temperature and precipitation. Several other land surface and lake properties are linked to the harsher climate in the Verkhoyansk mountain range. For example, there is a larger amount of barren land surface, forests are much sparser and contain less biomass and only have thin soils, providing reduced input of minerogenic-organic material into the lakes. As the surface runoff of the surrounding landscapes has a major impact on lake hydrochemistry this may play out differently in comparison to hydrochemistry lakes in non-permafrost catchments (Kokelj and Jorgenson, 2013; Holden et al., 2018; Arsenault et al., 2019).

Arsenault et al. (2022) show how thermokarst lakes seem to combine the morphological and chemical characteristics of lakes as well as peatland ponds. The shallow lake-water level strongly influences the circulation and lake temperature regimes, with the most shallow lake types experiencing intense summer mixing in wind-exposed landscapes, such as in non-forested catchments, and thereby subsequent effects on pH and organic matter recycling (Gavrilova, 1962; Wetterich et al., 2008). In contrast, deeper thermokarst lakes with higher water levels, such as the new thermokarst lake type, stratify during the warm summer months, especially if they are located in forests that will limit the wind and thus circulation. This combination of lake-internal cycling as well as the dominance of land surface runoff is specific to thermokarst lakes in permafrost landscapes (e.g., Arsenault et al., 2022).

There is need for more data on lake hydrochemistry to improve predictions of future trajectories and the hydrochemical responses of mountain and thermokarst lakes as they might differ even with a similar climate forcing. Future cryogenic processes will have a dominant influence on future thermokarst lake hydrochemistry. Here, we provide a conceptual framework for the trajectories of lake hydrochemistry in Central Yakutian thermokarst lakes under future climate warming (Fig. 8). Specifically, old alaas lakes, as residual lakes in alaas depressions, represent the lowland thermokarst lake endmember of this continuum with highest salinities. Mountain lakes with low mineralization and DOC represent the opposite endmember. Under

https://doi.org/10.5194/egusphere-2025-4114
Preprint. Discussion started: 5 September 2025
© Author(s) 2025. CC BY 4.0 License.

future climate warming, old alaas lakes will be endangered as their trajectory will encompass enhanced evaporation with the lake hydrochemistry becoming further enriched in salinity. However, the connected alaas lakes, which are characterised by lower DOC and minerals, will represent a more diluted lake hydrochemistry. Future permafrost degradation, which on one hand, increases hydrological conductivity leading to the formation of more connected alaas lakes, and on the other hand, allows the formation of new thermokarst lakes with lower salinities, could therefore increase the relative share of surface water bodies with lower mineralisation, potentially enriching their usability as resources in Yakutia (Fig. 8).

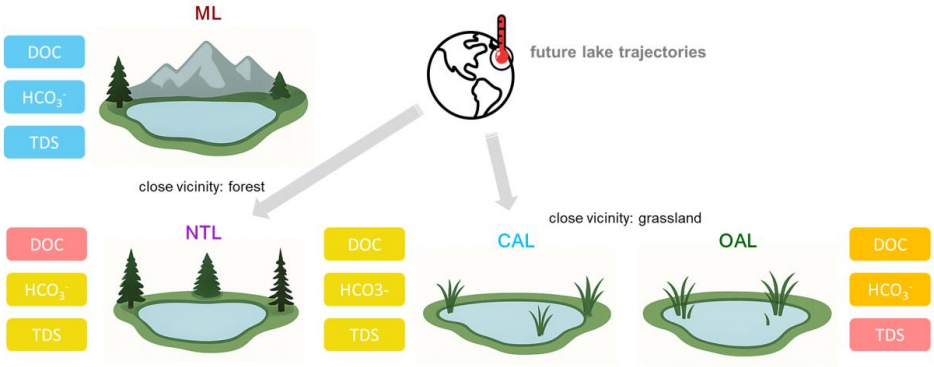

Figure 8: Schematic diagram displaying the main summer-season hydrochemical characteristics of thermokarst lowland lakes in the thermokarst lake chronosequence and of mountain lakes, highlighting the direction of future lake-type development. In the upper row, mountain lakes (ML) are characterised by least dissolved organic carbon (DOC), HCO_3^-, and total dissolved solids (TDS) (blue colours) in contrast to the thermokarst lakes in the lower row (yellow to red colours, yellow indicating medium concentrations, orange high concentrations up to red, highest concentrations). Connected alaas lakes (CAL) are most diluted with the lowest DOC, HCO_3^-, and TDS (yellow colours) in the thermokarst lake sequence. New thermokarst lakes (NTL), typically located in the forests, have moderate DOC and HCO_3^- (orange colour) but also lower TDS (in yellow). In contrast, old alaas lakes (OAL) are characterised by highest TDS (red colour) and by moderate DOC and HCO_3^- (orange colour). We predict that future lake trajectories will result in the formation and higher abundance of CAL and NTL lake types. The lake types in this figure were generated using Perplexity AI.

4.4 Plant diversity derived from sedDNA

Mountain lake surface-sediments generally have a lower median richness of 9 ASVs (compared to lowland lakes with more than 17 ASVs), following trends reported in previous studies where macrophyte richness tends to decrease along latitudinal and elevational gradients due to decreasing temperature and nutrient availability (Squires and Lesack, 2009; Stoof-Leichsenring et al., 2022). Higher variability in macrophyte richness is shown within the lowland lake types, with the highest macrophyte median richness of 20 taxa occurring in connected alaas lakes. Previous studies from lakes in northern and Central Yakutia show that summer temperature and lake-water mineral levels are the main drivers of aquatic plant diversity (Stoof-Leichsenring et al., 2022). This supports the observed pattern in our study, where connected alaas lakes, with their freshwater and the presence of both inflow and outflow, likely have more favourable conditions for greater macrophyte richness.

We can see that there are distinctions between a few taxa which have clear preferences, such as sub-emergent *Hippuris* genera occurring mainly in mountain lakes, or *Myriophyllum* and *Myriophyllum verticulatum* submerged macrophytes that need freshwater and hence only occur in the freshwater lakes in the lowland and mountain regions. In contrast, the cosmopolitan submerged macrophytes *Stuckenia pectinata* and *Potamogeton* sp. can live in highly mineralised water, which explains their abundance across all lakes. The Potamogetonaceae are typical submerged macrophyte taxa of highly mineralised lake water, whereas *Stuckenia pectinata*, which can live in brackish waters, is the only macrophyte species occurring in the highly saline EN21440 lake. This generalist species has a high capability of acclimation and adaptation to environmental changes (Malea et al., 2021).

Submerged macrophytes can completely disappear with lake eutrophication (Bennion et al., 2000, 2018), specifically due to low water transparencies. Despite our observed low water transparencies in old alaas and connected alaas lakes, the observed

https://doi.org/10.5194/egusphere-2025-4114
Preprint. Discussion started: 5 September 2025
© Author(s) 2025. CC BY 4.0 License.

submerged macrophyte abundance in our study does not appear to be limited. This is likely because these lakes provide extensive areas of very shallow water, where light can still penetrate despite poor transparency. These shallow zones offer suitable habitats for submerged and emergent macrophytes, which often form dense surface mats and extensive emergent macrophyte belts. Macrophytes can promote water clarity as well, creating suitable habitats for aquatic organisms (Burks et al., 2006). This extensive vegetation provides habitats for species like the muskrat and Siberian weasel (Zakharov et al., 2022), which were introduced during the Soviet era for fur production (Zakharov et al., 2023), or for birds.

Although this extensive vegetation likely contributes to the higher abundance of emergent and submergent macrophytes in sedDNA and their greater preservation in lake sediments, another important factor is the lack of inflow and outflow, which often leads to alkaline conditions in alaas lakes. Such conditions are unfavourable for a rich diversity of macrophytes and also for the preservation of sedDNA (Jia et al., 2022). A study by Li et al. (2021) highlights that vegetation signals from sedDNA are extremely localised from a small catchment area of lowland lakes due to limited inflow and outflow. High mineral levels can result in low preservation of sedDNA and/or the absence of macrophytes, as seen by the absence of terrestrial plant reads in two lakes, including the complete absence of any preserved sedDNA.

SedDNA-derived vegetation groups match well with the satellite-derived dominant land cover in the 50-m buffer zone around our study lakes for forest and grassland, but less so for the sedDNA-derived emergent macrophyte abundance corresponding to the satellite-derived wetland. Extensive wetland occurs only around some old alaas lakes and connected alaas lakes, whereas sedDNA-derived emergent macrophyte abundance occurs in all lake types. The discrepancy could be due to the spatial resolution mismatch between the coarser scale of the satellite-derived wetland classification compared to the more localised information provided by sedDNA, which captures contributions from submersed, floating, and emergent macrophytes, as well as lake shore environments.

4.5 Yakutian lakes as resource

Lakes in the most densely populated region of Central Yakutia have served as primary sources of drinking water for humans, as well as for herded cattle and wild animals (Vladimirtseva and Germogenov, 2013; Zakharova et al., 2018) since the first settlements of the Sakha people in the 12th century (Alekseev et al., 2020). Traditionally, families resided in their winter settlement (called *kystyk* in the Sakha language) in their alaases, while in spring, they would relocate with their cattle to their summer settlements (called *sayilyk* in the Sakha language) closer to freshwater sources by the river banks (Alekseev et al., 2020). This seasonal migration could help prevent overgrazing and soil degradation in the alaases, as the vegetation diversity of meadows directly depends on grazing and trampling by cattle and horses (Danilova et al., 2013).

During the Soviet era half a century before, this traditional management system was largely replaced by a centralised hydro-territorial order and enforced by a state-driven top-down management approach. This included the consolidation of large-scale subsidiary agricultural and livestock farms (referred to as collective farms - *kolkhozes*, in Russian) and the promotion of industrialisation, which led to the intensive use of surface waters (Crate et al., 2017). Towns and villages were preferentially and strategically established near rivers or, when unavailable, in alaases with large lakes (Zakharova et al., 2018), predominantly of the connected alaas lake type. As a result, bigger settlements such as Churapcha, Tungulu, and Maya integrate several lakes of the connected alaas lake type which experienced increased anthropogenic pressure due to higher population densities and intensified land use.

To this day, most of the communities continue to rely on these lakes, often sharing the same water bodies for both human and livestock consumption. In many cases, cattle have unrestricted access to the lakes, which raises concerns about water quality. While monitoring programmes have been initiated—such as the inclusion of Tungulu Lake in the official water quality monitoring programme of the Republic of Sakha (Ministry of Nature Protection, 1994)—not all lakes in inhabited areas are subject to regular assessments. Many smaller lakes, which are still actively used by local populations, may lack formal monitoring or protective management.

https://doi.org/10.5194/egusphere-2025-4114
Preprint. Discussion started: 5 September 2025
© Author(s) 2025. CC BY 4.0 License.

In our study, most alaas lakes are brackish, rendering them unsuitable for drinking water during the ice-free season due to high salinity, algal blooms, or proliferating macrophytes. In response, the Sakha people developed an adaptive strategy that involves harvesting low-salinity ice from brackish lakes during winter (Zakharova et al., 2018). This practice likely originated as a pragmatic way to store ice blocks outdoors through the long cold season. In spring, as temperatures begin to rise, the harvested lake ice is transferred to permafrost cellars, where it serves as a critical freshwater resource throughout the year (S.A. Fedorova, personal communication, Sakha, Aryylakh, Sakha Republic).

These sustainable water management practices are deeply rooted in centuries of traditional ecological knowledge, and still in use today. However, climate change poses a growing threat to their viability. Ongoing permafrost degradation and warming temperatures increasingly hinder the use of ice cellars, prompting some communities to relocate them or abandon them altogether (Lytkin et al., 2021). Local communities are concerned about wetter alaases and more degraded, softer soils (Popova, 2024).

The traditional, yet still dominant lifestyle of the Sakha people is closely linked to the seasonal use of natural resources (Isaev et al., 2024). Lakes are communal resources, used not only for sustenance but also for recreation and collective wellness. For instance, saline lakes are traditionally valued for their medicinal properties (Alekseev et al., 2020). The lakes also support fishing activities, both during the summer months and under ice in winter (Popova et al., 2020), although autumn to winter fishing is preferred because of easy cold storage during winter, as well as more fat supply to locals, in terms of high-calorie food products (Platonov et., 2020). Use of these resources is traditionally governed by sustainable practices, such as ceasing fishing when overexploitation of a lake is observed (A. Baishev and T. Struchkov, personal communication, Sakha, Tungulu, Sakha Republic).

We see in our study that the different chronological stages of thermokarst lake development offer various resource potentials. We find that new thermokarst lakes, which formed in recent decades typically from human land use or fire disturbance (Fedorov et al., 2014), exhibit good drinking water quality. These lakes could support traditional land uses such as fishing and drinking water resources for humans and forest wildlife. In contrast, old alaas lakes have not expanded or deepened significantly in recent decades (Fedorov et al., 2014). However, alaas rims display evidence of thermokarst activity, including the development of thaw slumps (Séjourné et al. 2015), which may increase turbidity and impact water quality in the future.

Indigenous Peoples commonly view water not as a resource, but as a good to be respected (Martinez-Cruz et al., 2024). Nowadays, there seem to exist fewer top-down social and political barriers in Yakutia as the Soviet-era large-scale agriculture has been drastically reduced. Traditional land use is returning, and with this, good governance of water resources is becoming common practice. A key question for future research is whether intensified thermokarst processes will lead to the formation of more complex fluvial landscapes with an increasing number of interconnected water bodies. Recent studies suggest a potential shift in hydrological dynamics, for example, Shpakova et al. (2021) who documented a rise in river discharge in Central Yakutia coinciding with significant temperature increases observed at meteorological stations. Enhanced river discharges and enhanced connectivity in lake systems may mitigate some of the adverse effects of climate change by improving water circulation, reducing concentrations of nutrients, pollutants, and salts, and potentially compensating for increased evaporation rates under a warming climate.

5. Conclusions

Our study provides a new comprehensive assessment of the limnological state of 66 lakes in the Central Yakutian alaas landscapes and the data-deficient Oymyakon high mountain plateau of the Verkhoyansk mountain range. We classified the lakes in Central Yakutia according to the thermokarst lake development sequence into new thermokarst, old alaas, and connected alaas lakes. Our analyses suggest that specific lake-type properties within the thermokarst lake sequence seem to drive inorganic, organic, and isotopic lake hydrochemistry. New thermokarst lakes are characterised by high DOC, while

https://doi.org/10.5194/egusphere-2025-4114
Preprint. Discussion started: 5 September 2025
© Author(s) 2025. CC BY 4.0 License.

connected alaas lakes, where settlements are typically located, show lower DOC and mineral content due to hydrological connection. Based on their hydrochemical characteristics, the connected alaas lakes together with mountain lakes, represent a major group of freshwater lakes, whereas old alaas lakes are mostly brackish to saline. For highly saline lowland lakes, there seems to be no connection to specific land cover or land use.

Specifically, the highly saline lowland lakes that we sampled were characterised by high fluoride and low chloride levels together with isotopic enrichment. Low chloride concentration implies that contemporary evaporation processes in these lakes are not responsible for the observed high salinities and maximum isotopic enrichment. Instead, there could exist a legacy of lacustrine sediments or leakage from fluoride-bearing salt deposits.

Future warming and prolonged exposure to evaporation may lead to more extreme conditions, and therefore, less diversification within lake macrophyte assemblages in old alaas lakes. On the other hand, enhanced permafrost degradation and rising surface water discharge as it is already observed in Eastern Siberia may also lead to higher hydrological connectivity and an increase of connected alaas lakes, this case providing more freshwater to the region. New thermokarst lakes also provide good water quality supporting traditional land uses such as fishing and drinking water resources for humans and forest wildlife.

6 Acknowledgements

All data were collected and processed by scientists from the Alfred Wegener Institute, Helmholtz Centre for Polar and Marine Research (AWI), Germany, the University of Potsdam, Germany, and the North-Eastern Federal University of Yakutsk (NEFU), Russia. Our sincere gratitude goes to Iris Eder, Boris K. Biskaborn, Phillip Meister, Jan Kahl, Igor Syrovatsky, Aleksey N. Pestryakov for supporting the field work and handling of the expedition samples. We acknowledge the help of Sarah Olischläger and Holly Blevins with sedDNA extractions, Mikaela Weiner for assistance in ISOLAB, and Bennet Juhls for the support in the Hydrochemistry Laboratory and optical measurements. We also thank Thomas Böhmer for helpful discussion of geodata processing. We are grateful to Cathy Jenks for English proofreading.

7 Funding

The author(s) declare financial support was received for the research, authorship, and/or publication of this article. This study was supported through the ERC consolidator grant no. 772852 to UH (PI) and partially by FSRG-2023-0027. IB was supported by the DAAD Scholarship No.91775743, the AWI Graduate School (POLMAR), and a PhD Completion Scholarship provided by University of Potsdam, Germany.

8 Data availability

The hydrochemical data, the isotopic composition of the lakes and the drone-derived lake data presented in this study are published in the PANGAEA repository (Baisheva et al. 2022) and (Stieg et al. 2023a,b, 2022), respectively. SedDNA data are available in the European Nucleotide Archive (ENA) at EMBL-EBI under accession number PRJEB89990.

9 Author contributions

IB, BH and UH and LAP designed this study. IB and BH led the data collection and synthesis. LAP, UH, PVD, SNL, RMG and LAP organized the Yakutia 2021 expedition in Central Yakutia. IB, BH, AS, RG, ESZ, AVE, PVD, LAU, RJ, SK, LAP and UH participated in fieldwork. IB and KRS conducted the sedDNA analyses. AS and HM conducted the isotopic analyses. AO and PPO processed the hydrochemical samples and provided guidance. AS, SK and RJ provided and processed the drone

https://doi.org/10.5194/egusphere-2025-4114
Preprint. Discussion started: 5 September 2025
© Author(s) 2025. CC BY 4.0 License.

image data, IB, BH and JGM undertook the satellite-derived land cover analyses. IB and AS created the data publications. IB performed statistical analyses and created figures with input from BH, JGM and UH. IB and BH led the writing of the first draft of manuscript, supported by JGM and UH. All coauthors contributed to the revision of the draft.

10 Disclaimer

This study presents results previously included as a chapter in a doctoral thesis (Baisheva, 2025).

11 References

Alekseev, A., Bravina, R., Romanova, E., Alekseeva, E., Argunov, V., Arkhipov, N., Barashkov, N., Bashkirov, M., Vasiliev, V., Gogolev, A., Golovnev, A., Danilova, N., Desyatkin, R., Dyakonov, V., Ignatieva, V., Missonova, L., Okhlopkov, I., Pavlinskaya, L., Pevnov, A., and Shadrin, V.: History of Yakutia, 2020.

Directive 2000/60 EN Water Framework Directive, EUR-Lex: https://eur-lex.europa.eu/eli/dir/2000/60/oj/eng, last access: 29 July 2025.

Arsenault, J., Talbot, J., Moore, T. R., Beauvais, M.-P., Franssen, J., and Roulet, N. T.: The Spatial Heterogeneity of Vegetation, Hydrology and Water Chemistry in a Peatland with Open-Water Pools, Ecosystems, 22, 1352–1367, https://doi.org/10.1007/s10021-019-00342-4, 2019.

Arsenault, J., Talbot, J., Brown, L. E., Holden, J., Martinez-Cruz, K., Sepulveda-Jauregui, A., Swindles, G. T., Wauthy, M., and Lapierre, J.-F.: Biogeochemical Distinctiveness of Peatland Ponds, Thermokarst Waterbodies, and Lakes, Geophysical Research Letters, 49, e2021GL097492, https://doi.org/10.1029/2021GL097492, 2022.

Baisheva, I.: Past and present environmental conditions in Yakutia - a (palaeo)ecological study using lake sediments, Universität Potsdam, https://doi.org/10.25932/publishup-67056, 2025.

Baisheva, I., Biskaborn, B. K., Stoof-Leichsenring, K. R., Andreev, A., Heim, B., Meucci, S., Ushnitskaya, L. A., Zakharov, E. S., Dietze, E., Glückler, R., Pestryakova, L. A., and Herzschuh, U.: Late Glacial and Holocene vegetation and lake changes in SW Yakutia, Siberia, inferred from sedaDNA, pollen, and XRF data, Front. Earth Sci., 12, https://doi.org/10.3389/feart.2024.1354284, 2024.

Baisheva, I., Pestryakova, L., Levina, S., Glückler, R., Biskaborn, B. K., Vyse, S. A., Heim, B., Herzschuh, U., and Stoof-Leichsenring, K. R.: Permafrost-thaw lake development in Central Yakutia: sedimentary ancient DNA and element analyses from a Holocene sediment record, J Paleolimnol, 70, 95–112, https://doi.org/10.1007/s10933-023-00285-w, 2023.

Baisheva, I., Pestryakova, L., Ushnitskaya, L., Davydova, P., Levina, S., Egorov, A., Zakharov, E., Gorodnichev, R., Glückler, R., Stieg, A., Eder, I., Kahl, J., Meister, P., Wieczorek, M., Overduin, P., Eulenburg, A., Stoof-Leichsenring, K., Biskaborn, B., Herzschuh, U. and Heim, B.: Summer anorganic hydrochemistry (cations and anions) of thermokarst lakes in the Central Yakutian Lowland and mountain lakes in the Verkhoyansk Mountain Range in Eastern Yakutia [dataset]. PANGAEA, https://doi.org/10.1594/PANGAEA.959459, 2022.

Becker, R. A., Wilks, A. R., Brownrigg, R., Minka, T. P., and Deckmyn, A.: maps: Draw Geographical Maps, 2025.

Bekryaev, R. V., Polyakov, I. V., and Alexeev, V. A.: Role of Polar Amplification in Long-Term Surface Air Temperature Variations and Modern Arctic Warming, Journal of Climate, 23, 3888–3906, https://doi.org/10.1175/2010JCLI3297.1, 2010.

Bennion, H., Appleby, P. G., Boyle, J. J., Carvalho, L., Luckes, S. J., and Henderson, A. C. G.: Water quality investigation of Loweswater, Cumbria, (ECRC Research Report 68). Environmental Change Research Centre: London., Environmental Change Research Centre, London, 80 pp., 2000.

Bennion, H., Sayer, C. D., Clarke, S. J., Davidson, T. A., Rose, N. L., Goldsmith, B., Rawcliffe, R., Burgess, A., Clarke, G., Turner, S., and Wiik, E.: Sedimentary macrofossil records reveal ecological change in English lakes: implications for conservation, J Paleolimnol, 60, 329–348, https://doi.org/10.1007/s10933-017-9941-7, 2018.

https://doi.org/10.5194/egusphere-2025-4114
Preprint. Discussion started: 5 September 2025
© Author(s) 2025. CC BY 4.0 License.

Biskaborn, B. K., Herzschuh, U., Bolshiyanov, D., Savelieva, L., and Diekmann, B.: Environmental variability in northeastern Siberia during the last ~13,300 yr inferred from lake diatoms and sediment–geochemical parameters, Palaeogeography, Palaeoclimatology, Palaeoecology, 329–330, 22–36, https://doi.org/10.1016/j.palaeo.2012.02.003, 2012.

Biskaborn, B. K., Smith, S. L., Noetzli, J., Matthes, H., Vieira, G., Streletskiy, D. A., Schoeneich, P., Romanovsky, V. E., Lewkowicz, A. G., Abramov, A., Allard, M., Boike, J., Cable, W. L., Christiansen, H. H., Delaloye, R., Diekmann, B., Drozdov, D., Etzelmüller, B., Grosse, G., Guglielmin, M., Ingeman-Nielsen, T., Isaksen, K., Ishikawa, M., Johansson, M., Johannsson, H., Joo, A., Kaverin, D., Kholodov, A., Konstantinov, P., Kröger, T., Lambiel, C., Lanckman, J.-P., Luo, D., Malkova, G., Meiklejohn, I., Moskalenko, N., Oliva, M., Phillips, M., Ramos, M., Sannel, A. B. K., Sergeev, D., Seybold, C., Skryabin, P., Vasiliev, A., Wu, Q., Yoshikawa, K., Zheleznyak, M., and Lantuit, H.: Permafrost is warming at a global scale, Nat Commun, 10, 264, https://doi.org/10.1038/s41467-018-08240-4, 2019.

Bosikov, N.P.: Evolution of alas of Central Yakutia (in russian), USSR Academy of Sciences, Siberian Branch, Institute of Permafrost Science, Yakutsk, 136 pp., 1991.

Boyer, F., Mercier, C., Bonin, A., Le Bras, Y., Taberlet, P., and Coissac, E.: obitools: a unix-inspired software package for DNA metabarcoding, Molecular Ecology Resources, 16, 176–182, https://doi.org/10.1111/1755-0998.12428, 2016.

Burks, R. L., Mulderij, G., Gross, E., Jones, I., Jacobsen, L., Jeppesen, E., and Van Donk, E.: Center Stage: The Crucial Role of Macrophytes in Regulating Trophic Interactions in Shallow Lake Wetlands, in: Wetlands: Functioning, Biodiversity Conservation, and Restoration, vol. 191, edited by: Bobbink, R., Beltman, B., Verhoeven, J. T. A., and Whigham, D. F., Springer Berlin Heidelberg, Berlin, Heidelberg, 37–59, https://doi.org/10.1007/978-3-540-33189-6_3, 2006.

Craig, H.: Isotopic Variations in Meteoric Waters, Science, 133, 1702–1703, https://doi.org/10.1126/science.133.3465.1702, 1961.

Crate, S., Ulrich, M., Habeck, J. O., Desyatkin, A. R., Desyatkin, R. V., Fedorov, A. N., Hiyama, T., Iijima, Y., Ksenofontov, S., Mészáros, C., and Takakura, H.: Permafrost livelihoods: a transdisciplinary review and analysis of thermokarst-based systems of indigenous land use, Anthropocene, 18, https://doi.org/10.1016/j.ancene.2017.06.001, 2017.

Czerniawska, J. and Chlachula, J.: Climate-Change Induced Permafrost Degradation in Yakutia, East Siberia, ARCTIC, 73, 509–528, https://doi.org/10.14430/arctic71674, 2020.

Danilova, A. A., Danilov, P. P., Savvinov, G. N., Gavrilyeva, L. D., Petrov, A. A., and Alekseev, G. A.: Changes in properties of alas soils in Central Yakutia caused by pasture degradation, Arid Ecosyst, 3, 205–211, https://doi.org/10.1134/S2079096113040057, 2013.

Dansgaard, W.: Stable isotopes in precipitation, 16, 436, https://doi.org/10.3402/tellusa.v16i4.8993, 1964.

De Cáceres Miquel: Indicator species analysis, 2025.

Desyatkin, R. and Desyatkin, A.: Thermokarst transformation of soil cover on cryolithozone flat territories, Symptom Environ. Chang. Sib. Permafr. Reg. 213–224. 2006.

Desyatkin, A. R., Takakai, F., Fedorov, P. P., Nikolaeva, M. C., Desyatkin, R. V., and Hatano, R.: CH4 emission from different stages of thermokarst formation in Central Yakutia, East Siberia, Soil Science and Plant Nutrition, 55, 558–570, https://doi.org/10.1111/j.1747-0765.2009.00389.x, 2009.

Desyatkin, R., Filippov, N., Desyatkin, A., Konyushkov, D., and Goryachkin, S.: Degradation of Arable Soils in Central Yakutia: Negative Consequences of Global Warming for Yedoma Landscapes, Front. Earth Sci., 9, 683730, https://doi.org/10.3389/feart.2021.683730, 2021.

Desyatkin, R. V.: Soil Formation in Thermokarst Depressions - Alases of Cryolithozone (in Russian), Nauka, Novosibirsk, 324 p. pp., 2008.

Du, Y., Chen, F., Zhang, Y., He, H., Wen, S., Huang, X., Song, C., Li, K., Wang, J., Keellings, D., and Lu, Y.: Human Activity Coupled With Climate Change Strengthens the Role of Lakes as an Active Pipe of Dissolved Organic Matter, Earth's Future, 11, e2022EF003412, https://doi.org/10.1029/2022EF003412, 2023.

https://doi.org/10.5194/egusphere-2025-4114
Preprint. Discussion started: 5 September 2025
© Author(s) 2025. CC BY 4.0 License.

Dudarev, A. A.: Public Health Practice Report: water supply and sanitation in Chukotka and Yakutia, Russian Arctic, International Journal of Circumpolar Health, 77, 1423826, https://doi.org/10.1080/22423982.2018.1423826, 2018.

Epp, L. S., Zimmermann, H. H., and Stoof-Leichsenring, K. R.: Sampling and Extraction of Ancient DNA from Sediments, in: Ancient DNA, vol. 1963, edited by: Shapiro, B., Barlow, A., Heintzman, P. D., Hofreiter, M., Paijmans, J. L. A., and Soares, A. E. R., Springer New York, New York, NY, 31–44, https://doi.org/10.1007/978-1-4939-9176-1_5, 2019.

Fedorov, A. and Konstantinov, P.: Observations of surface dynamics with thermokarst initiation, Yukechi site, Central Yakutia, 2003.

Fedorov, A. N., Ivanova, R. N., Park, H., Hiyama, T., and Iijima, Y.: Recent air temperature changes in the permafrost landscapes of northeastern Eurasia, Polar Science, 8, 114–128, https://doi.org/10.1016/j.polar.2014.02.001, 2014.

Gavrilova, M.K.: Climate of Central Yakutia (in Russian), Yakutsk Publishing House, Yakutsk, 63 p. pp., 1962.

Geng, R., Andreev, A., Kruse, S., Heim, B., van Geffen, F., Pestryakova, L., Zakharov, E., Troeva, E., Shevtsova, I., Li, F., Zhao, Y., and Herzschuh, U.: Modern Pollen Assemblages From Lake Sediments and Soil in East Siberia and Relative Pollen Productivity Estimates for Major Taxa, Front. Ecol. Evol., 10, 837857, https://doi.org/10.3389/fevo.2022.837857, 2022.

Gu, Z.: circlize: Circular Visualization, 2024.

Piper and Stiff–A workbook for creating Piper plots and Stiff diagrams, version 9,: https://halfordhydrology.com/piper-and-stiff/, last access: 9 July 2024.

Herzschuh, U., Pestryakova, L. A., Savelieva, L. A., Heinecke, L., Böhmer, T., Biskaborn, B. K., Andreev, A., Ramisch, A., Shinneman, A. L. C., and Birks, H. J. B.: Siberian larch forests and the ion content of thaw lakes form a geochemically functional entity, Nat Commun, 4, 2408, https://doi.org/10.1038/ncomms3408, 2013.

Herzschuh, U., Liu, Y., Liu, S., Stoof-Leichsenring, K. R., Porada, P., Courtin, J., Farkas, L. Z., Böhmer, T., Biskaborn, B. K., Diekmann, B., Huang, Y., Kaufman, D., Melles, M., Meyer, H., Pestryakova, L. A., Russell, J. M., and Wagner, B.: Arctic-Boreal Bryophyte Dynamics Since the Last Glacial Inferred From Ancient DNA Metabarcoding, Journal of Biogeography, n/a, e70015, https://doi.org/10.1111/jbi.70015, 2025.

Hijmans, R. J., Etten, J. van, Sumner, M., Cheng, J., Baston, D., Bevan, A., Bivand, R., Busetto, L., Canty, M., Fasoli, B., Forrest, D., Ghosh, A., Golicher, D., Gray, J., Greenberg, J. A., Hiemstra, P., Hingee, K., Ilich, A., Geosciences, I. for M. A., Karney, C., Mattiuzzi, M., Mosher, S., Naimi, B., Nowosad, J., Pebesma, E., Lamigueiro, O. P., Racine, E. B., Rowlingson, B., Shortridge, A., Venables, B., and Wueest, R.: raster: Geographic Data Analysis and Modeling, 2025.

Holden, J., Moody, C. S., Edward Turner, T., McKenzie, R., Baird, A. J., Billett, M. F., Chapman, P. J., Dinsmore, K. J., Grayson, R. P., Andersen, R., Gee, C., and Dooling, G.: Water-level dynamics in natural and artificial pools in blanket peatlands, Hydrological Processes, 32, 550–561, https://doi.org/10.1002/hyp.11438, 2018.

Hu, J., Long, Y., Zhou, W., Zhu, C., Yang, Q., Zhou, S., and Wu, P.: Influence of different land use types on hydrochemistry and heavy metals in surface water in the lakeshore zone of the Caohai wetland, China, Environmental Pollution, 267, 115454, https://doi.org/10.1016/j.envpol.2020.115454, 2020.

Hughes-Allen, L., Bouchard, F., Laurion, I., Séjourné, A., Marlin, C., Hatté, C., Costard, F., Fedorov, A., and Desyatkin, A.: Seasonal patterns in greenhouse gas emissions from thermokarst lakes in Central Yakutia (Eastern Siberia), Limnology and Oceanography, 66, S98–S116, https://doi.org/10.1002/lno.11665, 2021.

Hughes-Allen, L., Bouchard, F., Séjourné, A., Fougeron, G., and Léger, E.: Automated Identification of Thermokarst Lakes Using Machine Learning in the Ice-Rich Permafrost Landscape of Central Yakutia (Eastern Siberia), Remote Sensing, 15, 1226, https://doi.org/10.3390/rs15051226, 2023.

Huser, B. J., Futter, M. N., Bogan, D., Brittain, J. E., Culp, J. M., Goedkoop, W., Gribovskaya, I., Karlsson, J., Lau, D. C. P., Rühland, K. M., Schartau, A. K., Shaftel, R., Smol, J. P., Vrede, T., and Lento, J.: Spatial and temporal variation in Arctic freshwater chemistry—Reflecting climate-induced landscape alterations and a changing template for biodiversity, Freshwater Biology, 67, 14–29, https://doi.org/10.1111/fwb.13645, 2022.

© Author(s) 2025. CC BY 4.0 License.

IPCC: Climate Change 2022 – Impacts, Adaptation and Vulnerability: Working Group II Contribution to the Sixth Assessment Report of the Intergovernmental Panel on Climate Change, 1st ed., Cambridge University Press, https://doi.org/10.1017/9781009325844, 2022.

Isaev, A. P., Gavrilyeva, T. N., Mikhaleva, L. G., and Chikidov, I. I.: Forest food resources in the Sakha Republic (Yakutia), Siberian Journal of Life Sciences and Agriculture, 16, 474–503, https://doi.org/10.12731/2658-6649-2024-16-3-847, 2024.

Jia, W., Liu, X., Stoof-Leichsenring, K. R., Liu, S., Li, K., and Herzschuh, U.: Preservation of sedimentary plant DNA is related to lake water chemistry, Environmental DNA, 4, 425–439, https://doi.org/10.1002/edn3.259, 2022.

Juggins, S.: rioja: Analysis of Quaternary Science Data, 2022.

Karger, D. N., Conrad, O., Böhner, J., Kawohl, T., Kreft, H., Soria-Auza, R. W., Zimmermann, N. E., Linder, H. P., and Kessler, M.: Climatologies at high resolution for the earth's land surface areas, Sci Data, 4, 170122, https://doi.org/10.1038/sdata.2017.122, 2017.

Karger, D. N., Nobis, M. P., Normand, S., Graham, C. H., and Zimmermann, N. E.: CHELSA-TraCE21k – high-resolution (1 km) downscaled transient temperature and precipitation data since the Last Glacial Maximum, Climate of the Past, 19, 439–456, https://doi.org/10.5194/cp-19-439-2023, 2023.

Kassambara, A.: ggpubr: "ggplot2" Based Publication Ready Plots, 2025.

Kassambara, A. and Mundt, F.: factoextra: Extract and Visualize the Results of Multivariate Data Analyses, 2020.

Katamura, F., Fukuda, M., Bosikov, N. P., Desyatkin, R. V., Nakamura, T., and Moriizumi, J.: Thermokarst Formation and Vegetation Dynamics Inferred from A Palynological Study in Central Yakutia, Eastern Siberia, Russia, Arctic, Antarctic, and Alpine Research, 38, 561–570, https://doi.org/10.1657/1523-0430(2006)38[561:TFAVDI]2.0.CO;2, 2006.

Khudoley, A. and Prokopiev, A.: Defining the eastern boundary of the North Asian craton from structural and subsidence history studies of the Verkhoyansk fold-and-thrust belt, Special Paper of the Geological Society of America, 433, 391–410, https://doi.org/10.1130/2007.2433(19), 2007.

Kloss, A. L.: Water isotope geochemistry of recent precipitation in Central and North Siberia as a proxy for the local and regional climate system, Diplom, Leibniz Universität Hannover, 95 pp., 2008.

Kokelj, S. V. and Jorgenson, M. T.: Advances in Thermokarst Research: Recent Advances in Research Investigating Thermokarst Processes, Permafrost and Periglac. Process., 24, 108–119, https://doi.org/10.1002/ppp.1779, 2013.

Kumke, T., Ksenofontova, M., Pestryakova, L., Nazarova, L., and Hubberten, H.-W.: Limnological characteristics of lakes in the lowlands of Central Yakutia, Russia, J Limnol, 66, 40, https://doi.org/10.4081/jlimnol.2007.40, 2007.

Lento, J., Culp, J. M., Levenstein, B., Aroviita, J., Baturina, M. A., Bogan, D., Brittain, J. E., Chin, K., Christoffersen, K. S., Docherty, C., Friberg, N., Ingimarsson, F., Jacobsen, D., Lau, D. C. P., Loskutova, O. A., Milner, A., Mykrä, H., Novichkova, A. A., Ólafsson, J. S., Schartau, A. K., Shaftel, R., and Goedkoop, W.: Temperature and spatial connectivity drive patterns in freshwater macroinvertebrate diversity across the Arctic, Freshwater Biology, 67, 159–175, https://doi.org/10.1111/fwb.13805, 2022.

Li, K., Stoof-Leichsenring, K. R., Liu, S., Jia, W., Liao, M., Liu, X., Ni, J., and Herzschuh, U.: Plant sedimentary DNA as a proxy for vegetation reconstruction in eastern and northern Asia, Ecological Indicators, 132, 108303, https://doi.org/10.1016/j.ecolind.2021.108303, 2021.

Li, W., Cao, X., Stoof-Leichsenring, K., Hou, X., Yu, S.-Y., Tian, F., and Herzschuh, U.: Holocene lake response to glacier and catchment changes on the eastern Tibetan Plateau from quantitative conductivity reconstructions based on sedaDNA-derived macrophyte records, Quaternary Science Reviews, 338, 108806, https://doi.org/10.1016/j.quascirev.2024.108806, 2024.

Lopez, C. M. L., Brouchkov, A., Nakayama, H., Takakai, F., Fedorov, A. N., and Fukuda, M.: Epigenetic salt accumulation and water movement in the active layer of central Yakutia in eastern Siberia, Hydrological Processes, 21, 103–109, https://doi.org/10.1002/hyp.6224, 2007.

https://doi.org/10.5194/egusphere-2025-4114
Preprint. Discussion started: 5 September 2025
© Author(s) 2025. CC BY 4.0 License.

Lytkin, V., Suleymanov, A., Vinokurova, L., Grigorev, S., Golomareva, V., Fedorov, S., Kuzmina, A., and Syromyatnikov, I.: Influence of Permafrost Landscapes Degradation on Livelihoods of Sakha Republic (Yakutia) Rural Communities, 21, 2021a.

Lytkin, V., Suleymanov, A., Vinokurova, L., Grigorev, S., Golomareva, V., Fedorov, S., Kuzmina, A., and Syromyatnikov, I.: Influence of Permafrost Landscapes Degradation on Livelihoods of Sakha Republic (Yakutia) Rural Communities, Land, 10, 101, https://doi.org/10.3390/land10020101, 2021b.

Malea, L., Nakou, K., Papadimitriou, A., Exadactylos, A., and Orfanidis, S.: Physiological Responses of the Submerged Macrophyte Stuckenia pectinata to High Salinity and Irradiance Stress to Assess Eutrophication Management and Climatic Effects: An Integrative Approach, Water, 13, 1706, https://doi.org/10.3390/w13121706, 2021.

Meyer, H., Schönicke, L., Wand, U., Hubberten, H. W., and Friedrichsen, H.: Isotope Studies of Hydrogen and Oxygen in Ground Ice - Experiences with the Equilibration Technique, Isotopes in Environmental and Health Studies, 36, 133–149, https://doi.org/10.1080/10256010008032939, 2000.

Miesner, T., Herzschuh, U., Pestryakova, L. A., Wieczorek, M., Zakharov, S., Kolmogorov, A. I., Davydova, P. V., and Kruse, S.: Forest structure and individual tree inventories of north-eastern Siberia along climatic gradients, Open Access, 30, 2022.

Miner, K. R., Turetsky, M. R., Malina, E., Bartsch, A., Tamminen, J., McGuire, A. D., Fix, A., Sweeney, C., Elder, C. D., and Miller, C. E.: Permafrost carbon emissions in a changing Arctic, Nat Rev Earth Environ, 3, 55–67, https://doi.org/10.1038/s43017-021-00230-3, 2022.

Morgenstern, A., Heim, B., Pestryakova, L., Bolshiyanov, D., Grigoriev, M., Ayunov, D., and Dill, A.: Russian-German Cooperation: Expeditions to Siberia in 2021, 2023.

Naumov, A., Akimova, V., Sidorova, D., and Topnikov, M.: Agriculture and land use in the North of Russia: Case study of Karelia and Yakutia, Open Geosciences, 12, 1497–1511, https://doi.org/10.1515/geo-2020-0210, 2020.

Nitzbon, J., Westermann, S., Langer, M., Martin, L. C. P., Strauss, J., Laboor, S., and Boike, J.: Fast response of cold ice-rich permafrost in northeast Siberia to a warming climate, Nat Commun, 11, 2201, https://doi.org/10.1038/s41467-020-15725-8, 2020.

Nitze, I., Grosse, G., Jones, B. M., Romanovsky, V. E., and Boike, J.: Remote sensing quantifies widespread abundance of permafrost region disturbances across the Arctic and Subarctic, Nat Commun, 9, 5423, https://doi.org/10.1038/s41467-018-07663-3, 2018.

Olago, D., Opere, A., and Barongo, J.: Holocene palaeohydrology, groundwater and climate change in the lake basins of the Central Kenya Rift, Hydrological Sciences Journal, 54, 765–780, https://doi.org/10.1623/hysj.54.4.765, 2009.

Pavlova, N. A., Kolesnikov, A. B., Efremov, V. S., and Shepelev, V. V.: Groundwater chemistry in intrapermafrost taliks in Central Yakutia, Water Resour, 43, 353–363, https://doi.org/10.1134/S0097807816020135, 2016.

Pestryakova, L. A., Herzschuh, U., Wetterich, S., and Ulrich, M.: Present-day variability and Holocene dynamics of permafrost-affected lakes in central Yakutia (Eastern Siberia) inferred from diatom records, Quaternary Science Reviews, 51, 56–70, https://doi.org/10.1016/j.quascirev.2012.06.020, 2012.

Pienitz, R. and Smol, J. P.: Diatom assemblages and their relationship to environmental variables in lakes from the boreal forest-tundra ecotone near Yellowknife, Northwest Territories, Canada, Hydrobiol, 269, https://doi.org/10.1007/BF00028037R, 1993.

Pienitz, R., Smol, J. P., and Lean, D. R.: Physical and chemical limnology of 59 lakes located between the southern Yukon and the Tuktoyaktuk Peninsula, Northwest Territories (Canada), Can. J. Fish. Aquat. Sci., 54, 330–346, https://doi.org/10.1139/f96-274, 1997.

A graphic procedure in the geochemical interpretation of water-analyses: https://agupubs.onlinelibrary.wiley.com/doi/10.1029/TR025i006p00914, last access: 9 July 2024.

© Author(s) 2025. CC BY 4.0 License.

Platonov, T., Stepanov, K., Nyukkanov, A., Kuzmina, N., and Gorokhova, A.: Food value and basic parasitosis of fish used in food by indigenous populations of Yakutia, BIO Web Conf., 17, 00242, https://doi.org/10.1051/bioconf/20201700242, 2020.

Popova, L.: Indigenous Subsistence Practices of the Sakha Horse Herders under Changing Climate in the Arctic, Climate, 12, 134, https://doi.org/10.3390/cli12090134, 2024.

Popova, N. V., Abramov, A. F., and Markova, L. N.: Fishing as an important source of food in the Arctic and subarctic zones of Yakutia, Open Agriculture, 5, 213–218, https://doi.org/10.1515/opag-2020-0022, 2020.

Popp, S., Diekmann, B., Meyer, H., Siegert, C., Syromyatnikov, I., and Hubberten, H.-W.: Palaeoclimate signals as inferred from stable-isotope composition of ground ice in the Verkhoyansk foreland, Central Yakutia, Permafrost and Periglacial Processes, 17, 119–132, https://doi.org/10.1002/ppp.556, 2006.

Rantanen, M., Karpechko, A. Y., Lipponen, A., Nordling, K., Hyvärinen, O., Ruosteenoja, K., Vihma, T., and Laaksonen, A.: The Arctic has warmed nearly four times faster than the globe since 1979, Commun Earth Environ, 3, 1–10, https://doi.org/10.1038/s43247-022-00498-3, 2022.

Revéret, A., Alsos, I., and Heintzman, P.: Aquatic Vegetation DNA from Lake Sediments, 235–253, https://doi.org/10.1007/978-3-031-43799-1_8, 2023a.

R Core Team. (2025) R A Language and Environment for Statistical Computing. R Foundation for Statistical Computing. Scientific Research Publishing: https://www.scirp.org/reference/referencespapers?referenceid=3967248, last access: 29 July 2025.

Revéret, A., Rijal, D. P., Heintzman, P. D., Brown, A. G., Stoof-Leichsenring, K. R., and Alsos, I. G.: Environmental DNA of aquatic macrophytes: The potential for reconstructing past and present vegetation and environments, Freshwater Biology, 68, 1929–1950, https://doi.org/10.1111/fwb.14158, 2023b.

Rockström, J., Kotzé, L., Milutinović, S., Biermann, F., Brovkin, V., Donges, J., Ebbesson, J., French, D., Gupta, J., Kim, R., Lenton, T., Lenzi, D., Nakicenovic, N., Neumann, B., Schuppert, F., Winkelmann, R., Bosselmann, K., Folke, C., Lucht, W., Schlosberg, D., Richardson, K., and Steffen, W.: The planetary commons: A new paradigm for safeguarding Earth-regulating systems in the Anthropocene, Proceedings of the National Academy of Sciences, 121, e2301531121, https://doi.org/10.1073/pnas.2301531121, 2024.

Romanovsky, V. E., Drozdov, D. S., Oberman, N. G., Malkova, G. V., Kholodov, A. L., Marchenko, S. S., Moskalenko, N. G., Sergeev, D. O., Ukraintseva, N. G., Abramov, A. A., Gilichinsky, D. A., and Vasiliev, A. A.: Thermal state of permafrost in Russia, Permafrost and Periglacial Processes, 21, 136–155, https://doi.org/10.1002/ppp.683, 2010.

Różańska-Boczula, M. and Sender, J.: Exploring the relationships between macrophyte groups and environmental conditions in lake ecosystems, Sci Rep, 15, 11162, https://doi.org/10.1038/s41598-024-80553-5, 2025.

Rumyantsev, V. A., Kondratyev, S. A., and Izmaylova, A. V.: Russian Lakes, Geographical Classification, in: Encyclopedia of Lakes and Reservoirs, edited by: Bengtsson, L., Herschy, R. W., and Fairbridge, R. W., Springer Netherlands, Dordrecht, 679–691, https://doi.org/10.1007/978-1-4020-4410-6_242, 2012.

Serreze, M. C. and Barry, R. G.: Processes and impacts of Arctic amplification: A research synthesis, Global and Planetary Change, 77, 85–96, https://doi.org/10.1016/j.gloplacha.2011.03.004, 2011.

Shahgedanova, M.: The Physical Geography of Northern Eurasia, Oxford University Press, 597 pp., 2003.

Shpakova, R. N.: Changes in the Behavior of Long-Term Waterflow Variations in the Middle Part of Yakutia under the Global Warming Conditions, IOP Conf. Ser.: Earth Environ. Sci., 666, 042010, https://doi.org/10.1088/1755-1315/666/4/042010, 2021.

Slowikowski, K., Schep, A., Hughes, S., Dang, T. K., Lukauskas, S., Irisson, J.-O., Kamvar, Z. N., Ryan, T., Christophe, D., Hiroaki, Y., Gramme, P., Abdol, A. M., Barrett, M., Cannoodt, R., Krassowski, M., Chirico, M., Aphalo, P., and Barton, F.: ggrepel: Automatically Position Non-Overlapping Text Labels with "ggplot2," 2024.

https://doi.org/10.5194/egusphere-2025-4114
Preprint. Discussion started: 5 September 2025
© Author(s) 2025. CC BY 4.0 License.

Smith, S. L., O'Neill, H. B., Isaksen, K., Noetzli, J., and Romanovsky, V. E.: The changing thermal state of permafrost, Nat Rev Earth Environ, 3, 10–23, https://doi.org/10.1038/s43017-021-00240-1, 2022.

Spatial Data Science: https://r-spatial.org/book/, last access: 31 May 2024.

Sobek, S., Tranvik, L. J., Prairie, Y. T., Kortelainen, P., and Cole, J. J.: Patterns and regulation of dissolved organic carbon: An analysis of 7,500 widely distributed lakes, Limnology and Oceanography, 52, 1208–1219, https://doi.org/10.4319/lo.2007.52.3.1208, 2007.

Soloviev, P.A.: The permafrost zone of the northern part of the Lena-Amga interfluve (in Russian), Academy of Sciences of the USSR, V. A. Obruchev Institute of Permafrost Studies, Northeastern Branch, Moscow, 143 pp., 1959.

Squires, M. and Lesack, L.: The relation between sediment nutrient content and macrophyte biomass and community structure along a water transparency gradient among lakes of the Mackenzie Delta, Canadian Journal of Fisheries and Aquatic Sciences, 60, 333–343, https://doi.org/10.1139/f03-027, 2011.

Stauch, G. and Lehmkuhl, F.: Quaternary glaciations in the Verkhoyansk Mountains, Northeast Siberia, Quaternary Research, 74, 145–155, https://doi.org/10.1016/j.yqres.2010.04.003, 2010.

Stieg, A., Kruse, S., Jackisch, R., Farkas, L., Büchner, J., Baisheva, I., Glückler, R., Zakharov, E. S., Heim, B., Wieczorek, M., Pestryakova, L. A., and Herzschuh, U.: 53 orthomosaics processed from Unoccupied Aerial Vehicle (UAV) image data of lake shorelines sampled during a field campaign in Central and Eastern Yakutia, Siberia in 2021 (RU-Land_2021_Yakutia), https://doi.org/10.1594/PANGAEA.956223, 2023a.

Stieg, A., Kruse, S., Jackisch, R., Farkas, L., Büchner, J., Baisheva, I., Glückler, R., Zakharov, E. S., Heim, B., Wieczorek, M., Pestryakova, L. A., and Herzschuh, U.: Lake information on orthomosaics created from lake image data sampled during a field campaign in Central and Eastern Yakutia, Siberia in 2021 (RU-Land_2021_Yakutia) [dataset]. https://doi.org/10.1594/PANGAEA.955723, 2023b.

Stieg, A., Herzschuh, U., Baisheva, I., Glückler, R., Eder, I., Zakharov, E.S., Biskaborn, B.K., Meister, P., Davydova, P.V.; Kahl, J., Weiner, M., Marent, A., Heim, B., Wieczorek, M. and Meyer, H.: Stable water isotope data of 66 lakes from a summer field campaign in Central and Eastern Yakutia, Siberia in 2021 (RU-Land_2021_Yakutia) [dataset]. PANGAEA, https://doi.org/10.1594/PANGAEA.950688, 2022.

Stoof-Leichsenring, K. R., Huang, S., Liu, S., Jia, W., Li, K., Liu, X., Pestryakova, L. A., and Herzschuh, U.: Sedimentary DNA identifies modern and past macrophyte diversity and its environmental drivers in high-latitude and high-elevation lakes in Siberia and China, Limnology and Oceanography, 67, 1126–1141, https://doi.org/10.1002/lno.12061, 2022.

Strauss, J., Schirrmeister, L., Grosse, G., Fortier, D., Hugelius, G., Knoblauch, C., Romanovsky, V., Schädel, C., Schneider Von Deimling, T., Schuur, E. A. G., Shmelev, D., Ulrich, M., and Veremeeva, A.: Deep Yedoma permafrost: A synthesis of depositional characteristics and carbon vulnerability, Earth-Science Reviews, 172, 75–86, https://doi.org/10.1016/j.earscirev.2017.07.007, 2017.

Sukneva, S. A.: Migration processes in the Sakha Republic (Yakutia), Espace populations sociétés. Space populations societies, https://doi.org/10.4000/eps.10352, 2021.

Suleymanov, A. A., Lytkin, V. M., Vinokurova, L. I., Grigoryev, S. A., Fedorov, S. I., Golomareva, V. Yu., Basharin, N. I., and Aprosimov, D. A.: Rural Communities of Yakutia in Conditions of Permafrost Degradation: Key Risks, Social Consequences, and Adaptation Mechanisms, AaN, 199–231, https://doi.org/10.37482/issn2221-2698.2023.52.199, 2023.

Taberlet, P., Coissac, E., Pompanon, F., Gielly, L., Miquel, C., Valentini, A., Vermat, T., Corthier, G., Brochmann, C., and Willerslev, E.: Power and limitations of the chloroplast trnL (UAA) intron for plant DNA barcoding, Nucleic Acids Research, 35, e14–e14, https://doi.org/10.1093/nar/gkl938, 2007.

Troeva, E. I. (Ed.): The far North: plant biodiversity and ecology of Yakutia, Springer, Dordrecht ; New York, 390 pp., 2010.

Ulrich, M.: Holocene thermokarst dynamics in Central Yakutia - A multi-core and robust grain-size endmember modeling approach, Quaternary Science Reviews, 24, 2019.

© Author(s) 2025. CC BY 4.0 License.

Ulrich, M., Matthes, H., Schirrmeister, L., Schütze, J., Park, H., Iijima, Y., and Fedorov, A. N.: Differences in behavior and distribution of permafrost-related lakes in Central Yakutia and their response to climatic drivers, Water Resources Research, 53, 1167–1188, https://doi.org/10.1002/2016WR019267, 2017a.

Ulrich, M., Wetterich, S., Rudaya, N., Frolova, L., Schmidt, J., Siegert, C., Fedorov, A. N., and Zielhofer, C.: Rapid thermokarst evolution during the mid-Holocene in Central Yakutia, Russia, The Holocene, 27, 1899–1913, https://doi.org/10.1177/0959683617708454, 2017b.

Vladimirtseva, M. V. and Germogenov, N. I.: Birds of Yakutia: Fauna Diversity, Ecology, Role in Ecosystems and Human Life, J Biodivers Endanger Species, 01, https://doi.org/10.4172/2332-2543.1000114, 2013.

Walsh, J. E.: Intensified warming of the Arctic: Causes and impacts on middle latitudes, Global and Planetary Change, 117, 52–63, https://doi.org/10.1016/j.gloplacha.2014.03.003, 2014.

Walvoord, M. A. and Kurylyk, B. L.: Hydrologic Impacts of Thawing Permafrost—A Review, Vadose Zone Journal, 15, vzj2016.01.0010, https://doi.org/10.2136/vzj2016.01.0010, 2016.

Wang, W., Jin, H., Zhang, Z., Zhelezniak, M. N., Spektor, V. V., Șerban, R.-D., Li, A., Tumskoy, V., Jin, X., Yang, S., Zhang, S., Li, X., Șerban, M., Wu, Q., and Wen, Y.: Monitoring Ground Surface Deformation of Ice-Wedge Polygon Areas in Saskylakh, NW Yakutia, Using Interferometric Synthetic Aperture Radar (InSAR) and Google Earth Engine (GEE), Remote Sensing, 15, 1335, https://doi.org/10.3390/rs15051335, 2023.

Wei, T., Simko, V., Levy, M., Xie, Y., Jin, Y., Zemla, J., Freidank, M., Cai, J., and Protivinsky, T.: corrplot: Visualization of a Correlation Matrix, 2024.

Wen, D., Zhang, F., Zhang, E., Wang, C., Han, S., and Zheng, Y.: Arsenic, fluoride and iodine in groundwater of China, Journal of Geochemical Exploration, 135, 1–21, https://doi.org/10.1016/j.gexplo.2013.10.012, 2013.

Wetterich, S., Herzschuh, U., Meyer, H., Pestryakova, L., Plessen, B., Lopez, C. M. L., and Schirrmeister, L.: Evaporation effects as reflected in freshwaters and ostracod calcite from modern environments in Central and Northeast Yakutia (East Siberia, Russia), Hydrobiologia, 614, 171–195, https://doi.org/10.1007/s10750-008-9505-y, 2008.

Wetzel, R. G.: Limnology: Lake and River Ecosystems, Gulf Professional Publishing, 1023 pp., 2001.

Wickham, H., Hester, J., Chang, W., Bryan, J., and RStudio: devtools: Tools to Make Developing R Packages Easier, 2022.

Wickham, H., François, R., Henry, L., Müller, K., Vaughan, D., Software, P., and PBC: dplyr: A Grammar of Data Manipulation, 2023.

Wickham, H., Chang, W., Henry, L., Pedersen, T. L., Takahashi, K., Wilke, C., Woo, K., Yutani, H., Dunnington, D., Brand, T. van den, Posit, and PBC: ggplot2: Create Elegant Data Visualisations Using the Grammar of Graphics, 2025.

Windirsch, T., Grosse, G., Ulrich, M., Schirrmeister, L., Fedorov, A. N., Konstantinov, P. Ya., Fuchs, M., Jongejans, L. L., Wolter, J., and Strauss, J.: Organic Carbon Characteristics in Ice-rich Permafrost in Alas and Yedoma Deposits, Central Yakutia, Siberia, Biogeochemistry: Sediment, https://doi.org/10.5194/bg-2019-470, 2020.

Xenopoulos, M., Lodge, D., Frentress, J., Kreps, T., Bridgham, S., Grossman, E., and Jackson, C.: Regional Comparisons of Watershed Determinants of Dissolved Organic Carbon in Temperate Lakes from the Upper Great Lakes Region and Selected Regions Globally, Limnology and oceanography, 48, 2321–2334, https://doi.org/10.4319/lo.2003.48.6.2321, 2003.

Zakharov, E., Smetanin, N., Sidorov, I., Zakharova, O., Filippova, V., and Zakharova, N.: Distribution of the Muskrat (Ondatra zibethicus L.) and the American Mink (Neovison vison Schreber) in Yakutia (Northeast Asia, Russia), Russian Journal of Biological Invasions, 14, 329–337, https://doi.org/10.1134/S2075111723030219, 2023.

Zakharov, E. S., Safronov, V. M., Zakharova, N. N., Petrov, R. E., Filippova, V. V., Koryakina, L. P., and Kruse, S.: Abundance dynamics of the Siberian weasel (Mustela sibirica) and their determinants on the northeastern periphery of its geographic range (Yakutia, Russia), Rus. J. Theriol., 21, 153–161, https://doi.org/10.15298/rusjtheriol.21.2.06, 2022.

https://doi.org/10.5194/egusphere-2025-4114
Preprint. Discussion started: 5 September 2025
© Author(s) 2025. CC BY 4.0 License.

Zanaga, D., Van De Kerchove, R., Daems, D., De Keersmaecker, W., Brockmann, C., Kirches, G., Wevers, J., Cartus, O., Santoro, M., Fritz, S., Lesiv, M., Herold, M., Tsendbazar, N.-E., Xu, P., Ramoino, F., and Arino, O.: ESA WorldCover 10 m 2021 v200 (v200), https://doi.org/10.5281/zenodo.7254221, 2022.

Zhirkov, A., Sivtsev, M., Lytkin, V., Kirillin, A., Séjourné, A., and Wen, Z.: An Assessment of the Possibility of Restoration and Protection of Territories Disturbed by Thermokarst in Central Yakutia, Eastern Siberia, Land, 12, 197, https://doi.org/10.3390/land12010197, 2023.

Zimmermann, H. H., Raschke, E., Epp, L. S., Stoof-Leichsenring, K. R., Schwamborn, G., Schirrmeister, L., Overduin, P. P., and Herzschuh, U.: Sedimentary ancient DNA and pollen reveal the composition of plant organic matter in Late Quaternary permafrost sediments of the Buor Khaya Peninsula (north-eastern Siberia), Biogeosciences, 14, 575–596, https://doi.org/10.5194/bg-14-575-2017, 2017.

https://doi.org/10.5194/egusphere-2025-4114
Preprint. Discussion started: 5 September 2025
© Author(s) 2025. CC BY 4.0 License.

12 Appendix

Table A1: Overview of lake location and the administrative and topographic settings of the 66 sampled lakes per lake type sorted according to the lake type (mountain lakes, connected alaas lakes, old alaas lakes, new thermokarst lakes. In addition, we code the group of new thermokarst lakes even more specifically related to their stage of thermokarst lake development (*dyede, §tyympy, #shallowing, see chapter introduction for details on the lake genesis).

Lake code EN21	District	Latitude N	Longitude E	Topographic setting
Mountain lakes (ML)				
401	Verkhoyansky	63.33302	141.06282	Verkhoyansk mountains
402	Verkhoyansky	63.32696	141.0843	Verkhoyansk mountains
403	Verkhoyansky	63.32012	141.07993	Verkhoyansk mountains
404	Verkhoyansky	63.32943	141.1181	Verkhoyansk mountains
405	Verkhoyansky	63.43886	140.3983	Verkhoyansk mountains
406	Verkhoyansky	63.30998	141.072	Verkhoyansk mountains
407	Verkhoyansky	63.31018	141.0634	Verkhoyansk mountains
408	Verkhoyansky	63.38775	140.5752	Verkhoyansk mountains
409	Verkhoyansky	63.39182	140.5811	Verkhoyansk mountains
410	Verkhoyansky	63.23035	142.9573	Verkhoyansk mountains
411	Verkhoyansky	63.22168	142.8945	Verkhoyansk mountains
412	Tomponsky	63.21885	139.5503	Verkhoyansk mountains
413	Tomponsky	63.22801	139.5759	Verkhoyansk mountains
414	Verkhoyansky	63.32861	141.1654	Verkhoyansk mountains
415	Verkhoyansky	63.33238	141.1591	Verkhoyansk mountains
Connected alaas lake (CAL)				
417	Churapchinsky	62.07997	132.3637	Abalakh terrace
419	Churapchinsky	62.08767	132.3534	Abalakh terrace
421	Churapchinsky	62.01409	132.4127	Abalakh terrace
422	Churapchinsky	62.035	132.3634	Abalakh terrace
427	Megino-Kangalassky	62.14336	130.93548	Magan terrace
435	Megino-Kangalassky	62.35747	130.61391	Tyungyulu terrace
439	Megino-Kangalassky	62.16978	130.67147	Tyungyulu terrace
441	Megino-Kangalassky	62.20703	130.71456	Tyungyulu terrace
Old alaas lake (OAL)				
420	Churapchinsky	62.03883	132.3943	Abalakh terrace
425	Megino-Kangalassky	62.16929	130.9102	Magan terrace
426	Megino-Kangalassky	62.18077	130.8822	Magan terrace
426-2	Megino-Kangalassky	62.17728	130.87956	Magan terrace
430	Megino-Kangalassky	62.31045	130.33331	Bestyakh terrace
431	Megino-Kangalassky	62.12932	130.86965	Magan terrace
433	Megino-Kangalassky	62.13806	130.87054	Magan terrace
436	Megino-Kangalassky	62.35076	130.35281	Bestyakh terrace
437	Megino-Kangalassky	62.3447	130.37543	Tyungyulu terrace
438	Megino-Kangalassky	62.15538	130.63903	Tyungyulu terrace
440	Megino-Kangalassky	62.20035	130.65014	Tyungyulu terrace
442	Megino-Kangalassky	61.78578	130.50197	Abalakh terrace
443	Megino-Kangalassky	61.78637	130.48923	Abalakh terrace
444	Megino-Kangalassky	61.7799	130.49321	Abalakh terrace
446	Megino-Kangalassky	61.76476	130.45989	Abalakh terrace
447	Megino-Kangalassky	61.7655	130.46841	Abalakh terrace
449	Megino-Kangalassky	61.7471	130.5389	Abalakh terrace
452	Megino-Kangalassky	61.76038	130.55066	Abalakh terrace
453	Megino-Kangalassky	61.89956	130.49017	Tyungyulu terrace
454	Megino-Kangalassky	61.89654	130.42726	Tyungyulu terrace
455	Megino-Kangalassky	61.90249	130.41174	Tyungyulu terrace
456	Megino-Kangalassky	61.88556	130.44829	Tyungyulu terrace
457	Megino-Kangalassky	61.73336	130.2533	Tyungyulu terrace
459	Megino-Kangalassky	61.77814	130.37526	Abalakh terrace
463	Megino-Kangalassky	61.74491	130.50345	Abalakh terrace
464	Megino-Kangalassky	61.7558	130.49233	Abalakh terrace
465	Megino-Kangalassky	61.75424	130.4924	Abalakh terrace
466	Megino-Kangalassky	61.75357	130.49204	Abalakh terrace

https://doi.org/10.5194/egusphere-2025-4114
Preprint. Discussion started: 5 September 2025
© Author(s) 2025. CC BY 4.0 License.

New thermokarst lake (NTL)				
416*	Churapchinsky	62.08455	132.3706	Abalakh terrace
418§	Churapchinsky	62.08219	132.3473	Abalakh terrace
423*	Tattinsky	62.38716	133.7447	Abalakh terrace
424*	Tattinsky	62.3299	133.6651	Abalakh terrace
428*	Megino-Kangalassky	62.28146	130.3724	Bestyakh terrace
429*	Megino-Kangalassky	62.26311	130.33965	Bestyakh terrace
432*	Megino-Kangalassky	62.13574	130.88602	Magan terrace
434§	Megino-Kangalassky	62.14543	130.8669	Magan terrace
445*	Megino-Kangalassky	61.7676	130.49493	Abalakh terrace
448#	Megino-Kangalassky	61.74609	130.53302	Abalakh terrace
450§	Megino-Kangalassky	61.73757	130.52488	Abalakh terrace
451§	Megino-Kangalassky	61.73978	130.52555	Abalakh terrace
458#	Megino-Kangalassky	61.73217	130.26011	Tyungyulu terrace
462*	Megino-Kangalassky	61.71745	130.48135	Tyungyulu terrace
467§	Megino-Kangalassky	61.76225	130.48483	Abalakh terrace

1182

https://doi.org/10.5194/egusphere-2025-4114
Preprint. Discussion started: 5 September 2025
© Author(s) 2025. CC BY 4.0 License.

Table A2: Overview of temperature- and precipitation-related CHELSA bioclimatic variables (CHELSA V2.1, Karger et al. 2017) used in this study.

Abbreviation	CHELSA short name	Description	Unit
Temperature-related variables			
MAT	bio_1	Mean annual air temperature	°C
Tmax	bio_5	Mean maximum daily air temperature of the warmest month	°C
Tmin	bio_6	Mean minimum daily air temperature of the coldest month	°C
Precipitation-related variables			
TAP	bio_12	Total annual precipitation	kg m^{-2} $year^{-1}$
Pwet	bio_13	Precipitation amount of the wettest month	kg m^{-2} $month^{-1}$
Pdry	bio_14	Precipitation amount of the driest month	kg m^{-2} $month^{-1}$

Table A3: Physico-chemical properties of surface water samples collected from the central part of the lakes (n = number of lakes, SD = standard deviation (±) and CV = coefficient of variation (%)).

Variable	n	Mean	Median	SD	Skew	n	Mean	Median	SD	Skew	n	401	405
	Lowland lakes					Mountain lakes					Deep mountain lakes		
Lake depth (m)	**44**	3.1	2.1	3.02	3.77	**13**	8.2	7.4	3.6	0.5	**2**	33.8	43
Secchi depth (m)	**33**	0.8	0.6	0.54	0.69	**13**	2.8	2.6	1.2	0.9	**2**	4.14	5.39
Elevation (m asl)	**51**	190	174	51	0.60	**13**	1069	1036	169	-0.1	**2**	1260	946
Lake area (km^2)	**50**	1.4	0.57	1.4	3.14	**13**	0.11	0.54	0.1	1.49	**2**	4.7	0.5
pH	**51**	8.7	8.8	0.55	-1.04	**13**	7.6	7.6	0.5	0.1	**2**	7.69	7.91
EC (µS cm^{-1})	**51**	1520.4	1228	1048.1	1.87	**13**	93.7	83.2	55.4	0.4	**2**	66.1	70.9
DOC (mg L^{-1})	**51**	97.80	75.90	73.06	2.45	**13**	14.8	14.0	5.0	0.1	**2**	125	64.9
TDS	**51**	1415	1200.5	981.7	1.75	**13**	55.5	61.0	29.2	0.1	**2**	46	49
Ca^{2+} (mg L^{-1})	**51**	25.24	25.91	13.81	0.49	**13**	9.4	10.6	4.9	0.0	**2**	8.7	7.62
Mg^{2+} (mg L^{-1})	**51**	120.2	111.6	73.87	1.26	**13**	3.8	4.2	2.0	0.3	**2**	2.12	3
Na^{+} (mg L^{-1})	**51**	191.3	124.1	209.73	2.82	**13**	1.0	0.9	0.5	0.2	**2**	0.82	2.38
K^{+} (mg L^{-1})	**51**	16.9	10.1	21.22	2.92	**13**	0.6	0.7	0.2	0.0	**2**	0.51	0.59
Si (mg L^{-1})	**46***	2.57	1.4	2.70	1.63	**12[a]**	0.7	0.6	0.3	0.2	**2**	0.55	0.39
PO_4^{3-} (mg L^{-1})	**19[§]**	1.73	0.98	1.87	1.83	**0[b]**	-	-	-	-	**0[%]**	-	-
HCO_3^{-} (mg L^{-1})	**50**	904.4	709.3	600.86	1.43	**13**	36.6	32.6	21.1	0.5	**2**	30.4	31.3
Cl^{-} (mg L^{-1})	**51**	86.7	42.3	111.95	3.44	**0[b]**	-	-	-	-	**0[%]**	-	-
SO_4^{2-} (mg L^{-1})	**40[+]**	82.7	8.1	191.57	3.26	**11[c]**	4.6	1.7	5.9	2.1	**2**	2.8	4.43
F^{-} (µg L^{-1})	**49[^]**	0.4	0.4	0.28	2.08	**3[d]**	0.1	0.1	0.0	-0.8	**0[%]**	-	-
NO_3^{-} (mg L^{-1})	**2[°]**	0.4	0.4	0.33	-	**1[e]**	0.2	0.2	0.0	-	**1[@]**	-	0.26
Fe (µg L^{-1})	**9[&]**	373.5	238.8	300.22	1.32	**6[f]**	323.6	239.6	217.0	1.7	**0[~]**	-	-
Al (µg L^{-1})	**3[#]**	165.6	177.5	87.69	-0.49	**2[g]**	101.4	101.4	43.6	-	**0[$]**	-	-
Sr^{2+} (µg L^{-1})	**51**	217.2	207.9	98.25	0.33	**12[h]**	97.3	108.1	41.5	-0.3	**2**	81	79
Ba^{2+} (µg L^{-1})	**39[ü]**	39.2	37.3	12.66	1.37	**12[h]**	21.9	21.9	0.0	-	**0[‘]**	-	-
Mn (µg L^{-1})	**18[ß]**	111.2	41.5	132.11	1.98	**4[i]**	42.7	33.2	22.9	1.5	**0[’]**	-	-
Br (µg L^{-1})	**47[ö]**	2.8	1.5	4.70	4.70	**0[b]**	-	-	-	-	**0[%]**	-	-
P (mg L^{-1})	**24[ä]**	0.6	0.47	0.64	1.68	**0[b]**	-	-	-	-	**0[%]**	-	-
Below detection limit	*****(n=5 < 0.10) **§** (n=32 < 0.10) **+** (n=11 < 0.10) **^** (n=2 < 0.10) **°** (n=49 < 0.10) **&** (n=42 < 100) **#** (n=48 < 50) **Ü** (n=12 < 20) **ß** (n=33 < 20) **ö** (n=4 < 0.10) **ä** (n=27 < 0.10)					**a** (n=1 < 0.10) **b** (n=13 < 0.10) **c** (n=2 < 0.10) **d** (n=10 < 0.10) **e** (n=12 < 0.10) **f** (n=7 < 100) **g** (n=11 < 50) **h** (n=1 < 20) **I** (n=9 < 20)					**%** (n=2 < 0.10) **@** (n=1 < 0.10) **~** (n=2 < 100) **$** (n=2 < 50) **‘** (n=2 < 20)		

https://doi.org/10.5194/egusphere-2025-4114
Preprint. Discussion started: 5 September 2025
© Author(s) 2025. CC BY 4.0 License.

Table A4: **Taxonomic richness of macrophyte amplicon sequence variants (median in bold, range, and counts (in brackets)) from sedDNA functional groups for the four lake types: connected alaas lakes (CAL), old alaas lakes (OAL), mountain lakes (ML), and new thermokarst lakes (NTL).**

Functional groups	CAL **median** min-max (counts)	OAL **median** min-max (counts)	ML **median** min-max) (counts)	NTL **median** min-max (counts)	Total richness (Total counts)
Floating	**3** 0-5 (75,679)	**2** 0-6 (192,048)	**0** 0-3 (34,847)	**1** 0-6 (39,177)	7 (341,751)
Submerged	**8** 4-10 (1,090,540)	**6.5** 2-11 (2,506,335)	**6** 1-10 (456,279)	**6** 1-9 (927,318)	13 (4,980,472)
Sub-emergent	-	**0** 0-1 (10,183)	**1** 0-1 (219,152)	**0** 0-1 (20,476)	2 (249,811)
Emergent	**8.5** 1-16 (75,058)	**8** 0-18 (801,663)	**5.5** 1-17 (85,692)	**7** 1-22 (194,950)	65 (1,157,363)
Total richness **median** min-max (total counts)	42 **20** 6-28 (1,241,277)	66 **17** 3-31 (3,510,229)	49 **9** 2-40 (795,970)	61 **17** 8-35 (1,181,921)	87 (6,729,397)

Table A5: Counts and taxonomic richness* of terrestrial plant amplicon sequence variants (ASVs) derived from sedDNA grouped by vegetation type for the four lake types: connected alaas lakes (CAL), old alaas lakes (OAL), mountain lakes (ML), and new thermokarst lakes (NTL).

Functional groups	CAL **median** min-max (counts)	OAL **median** min-max (counts)	ML **median** min-max) (counts)	NTL **median** min-max (counts)	Total richness (Total counts)
Trees	**2** 1-4 (39,077)	**2** 0-6 (152,642)	**4** 1-4 (564,065)	**3.5** 1-6 (243,701)	9 (999,485)
Shrubs	**0** 1-3 (75)	**0** 0-9 (10,622)	**3** 1-12 (123,766)	**0.5** 0-12 (15,827)	16 (150,290)
Grasses and herbs	**9** 3-25 (115,480)	**9.5** 1-29 (463,231)	**3.5** 0-30 (58,558)	**9.5** 0-23 (88,695)	83 (725,964)
Bryophyta	**0** 0-1 (11)	**0** 0-1 (861)	**0** 0-3 (323)	**0** 0-2 (705)	8 (1,900)
Total richness **median** min-max (total counts)	43 **14** 4-26 (154,643)	69 **12** 3-33 (627,356)	68 **11** 2-40 (746,712)	81 **17** 2-29 (348,928)	116 (1,877,639)

https://doi.org/10.5194/egusphere-2025-4114
Preprint. Discussion started: 5 September 2025
© Author(s) 2025. CC BY 4.0 License.

Table A6: Overview of abbreviations and details of variable groups in this study.

Group	Short name	Detailed description
Lake Types	ML	mountain lakes
	CAL	connected alaas lakes
	NTL	new thermokarst lakes
	OAL	old alaas lakes
Lake salinity	freshwater	freshwater lakes TDS < 1000 mg L^{-1} (mg L^{-1})
	brackish	brackish lakes TDS > 1000 mg L^{-1} (mg L^{-1})
Lake clusters	C1	Cluster 1 (*Fig. A3*)
	C2	Cluster 2 (*Fig. A3*)
	C3	Cluster 3 (*Fig. A3*)
SedDNA-derived macrophyte functional groups	DNA_fm	prop. of sedDNA-derived floating macrophyte functional group (%)
	DNA_sm	prop. of sedDNA-derived submerged macrophyte functional group (%)
	DNA_sem	prop. of sedDNA-derived submerged-emergent macrophyte functional group (%)
	DNA_em	prop. of sedDNA-derived emergent macrophyte functional group (%)
SedDNA-derived terrestrial plants functional groups	trees	prop. of sedDNA-derived tree terrestrial plant functional groups (%)
	shrubs	prop. of sedDNA-derived shrubs terrestrial plant functional groups (%)
	grasses	prop. of sedDNA-derived grasses and forbs terrestrial plant functional groups (%)
	bryophyta	prop. of sedDNA-derived bryophyte terrestrial plant functional groups (%)
Satellite-derived land cover*	FOREST	prop. of satellite-derived forest land cover (%)
	GRASS	prop. of satellite-derived grassland land cover (%)
	WETLAND	prop. of satellite-derived wetland land cover (%)
	BARE	prop. of satellite-derived barren land cover (%)
	TUNDRA	prop. of satellite-derived tundra land cover (%)
Topography**	Elev	elevation (m a.s.l)
Climate data***	MAT	mean annual air temperature (C°)
	Tmax	mean maximum daily air temperature of the warmest month (C°)
	Tmin	mean minimum daily air temperature of the coldest month (C°)
	TAP	total annual precipitation (kg m^{-2} $year^{-1}$)
	Pwet	precipitation amount of the wettest month (kg m^{-2} $month^{-1}$)
	Pdry	precipitation amount of the driest month (kg m^{-2} $month^{-1}$)

* source for elevation was obtained during fieldwork
** Land cover was obtained from ESA World Cover 2021 (© ESA WorldCover project / Contains modified Copernicus Sentinel data (2021) processed by ESA WorldCover consortium; Zanaga et al. 2022. ESA WorldCover 10 m 2021 v200. https://doi.org/10.5281/zenodo.7254221, last accesses on May 2024)
*** Climate data is derived from CHELSA V2.1 (Karger et al. 2017, last accessed on May 2024)

https://doi.org/10.5194/egusphere-2025-4114
Preprint. Discussion started: 5 September 2025
© Author(s) 2025. CC BY 4.0 License.

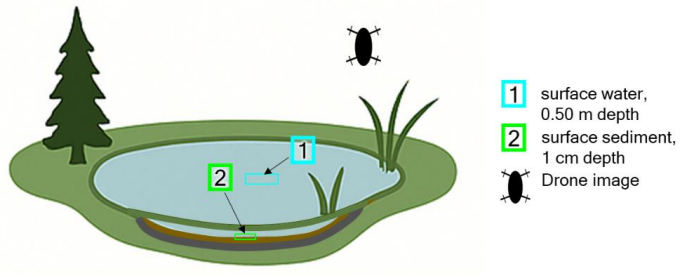

Figure A1: Scheme for lake sampling during the 2021 Yakutia expedition. The sampling categories included surface water sampling [1] for in situ physico-chemical measurements and taking water samples, and lake surface-sediment sampling [2] for sedDNA. In addition, we mapped the lake shore area with multispectral drone-based imaging. The figure was generated using Perplexity AI.

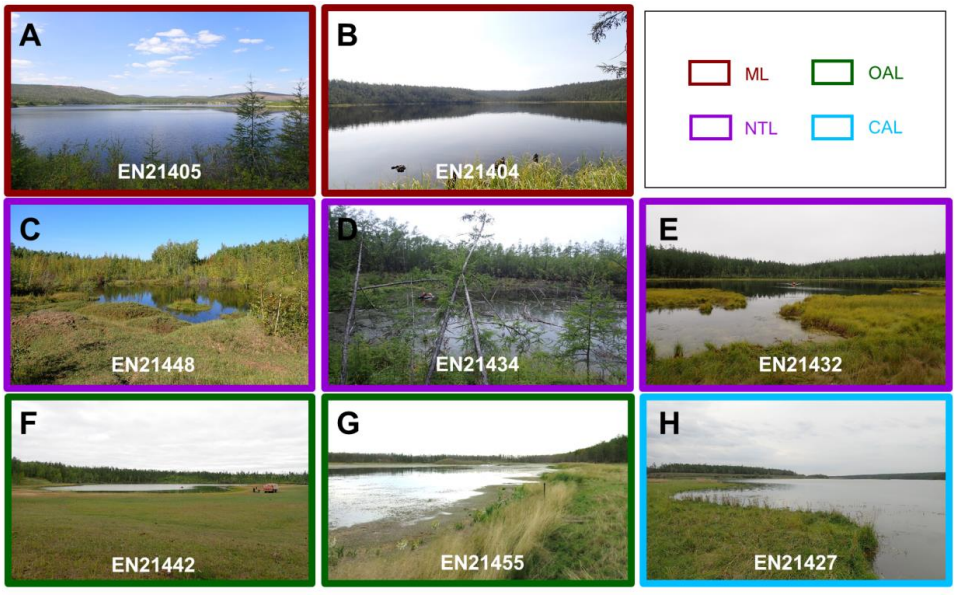

Figure A2: (A-H) Photos of examples of the different lake types sampled: A and B show mountain lakes (ML) of the Verkhoyansk Mountains (A-deep lake, B-shallow lake) and C–H show thermokarst lakes in Central Yakutia (NTL-new thermokarst lakes, OAL-old alaas lakes, and CAL-connected alaas lakes). The thermokarst lakes are sorted according to the thermokarst lake sequence (C-dyede lake stage, D-tympy lake stage, E-shallowing lake stage, F-old alaas lake, G-old alaas lake with pingo, H-connected alaas lake).

https://doi.org/10.5194/egusphere-2025-4114
Preprint. Discussion started: 5 September 2025
© Author(s) 2025. CC BY 4.0 License.

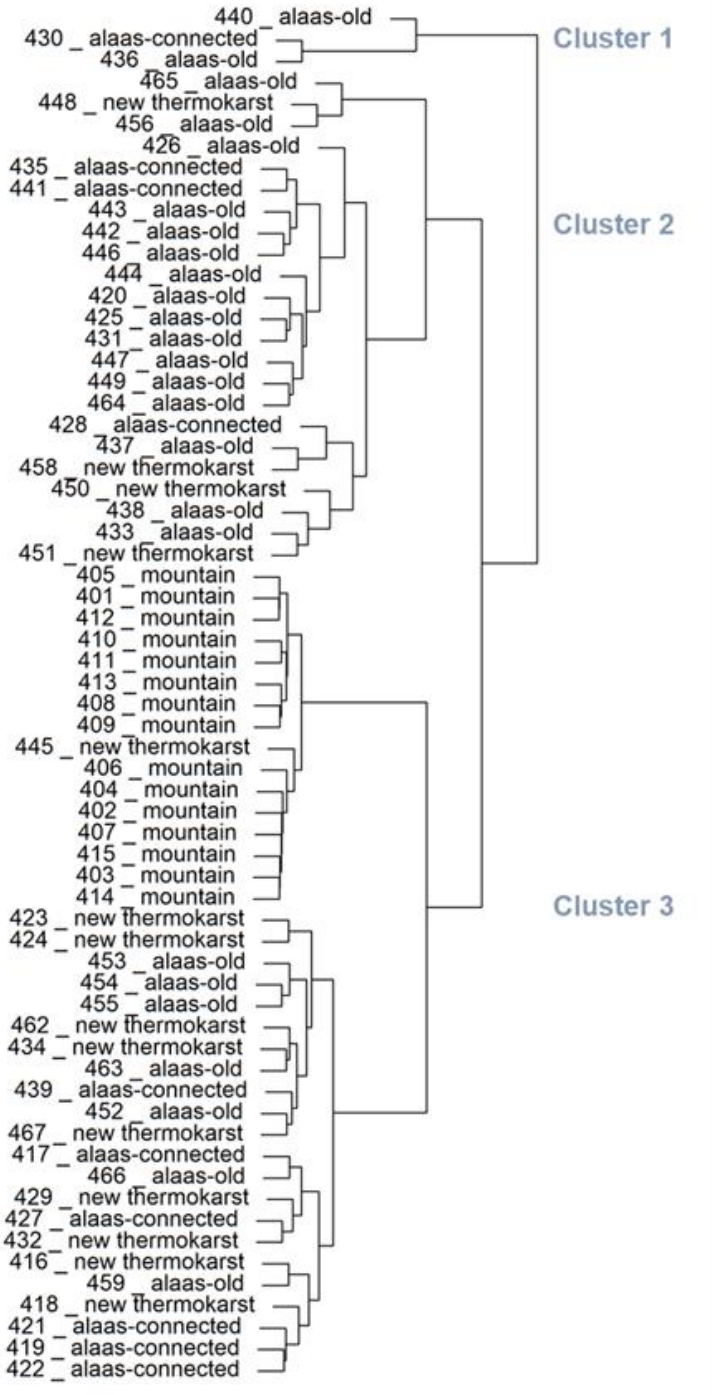

Figure A3: Hierarchical clustering of the lakes by major ion hydrochemistry.

https://doi.org/10.5194/egusphere-2025-4114
Preprint. Discussion started: 5 September 2025
© Author(s) 2025. CC BY 4.0 License.

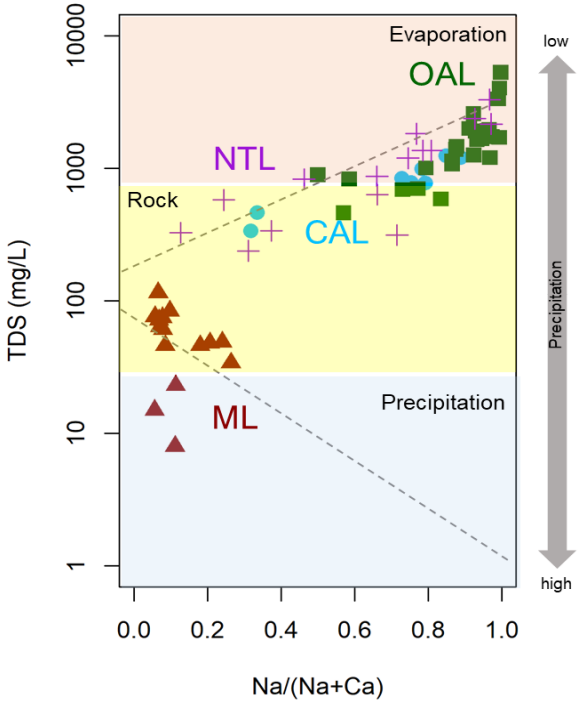

Figure A4: Gibbs diagram of Na^+ / (Na^+ + Ca^{2+}) vs. log-normalised total dissolved solids (TDS: mg L^{-1}). Mountain lakes (ML) are displayed as brown triangles, connected alaas lakes (CAL) as blue circles, old alaas lakes (OAL) as green squares, new thermokarst lakes (NTL) as purple crosses.

https://doi.org/10.5194/egusphere-2025-4114
Preprint. Discussion started: 5 September 2025
© Author(s) 2025. CC BY 4.0 License.

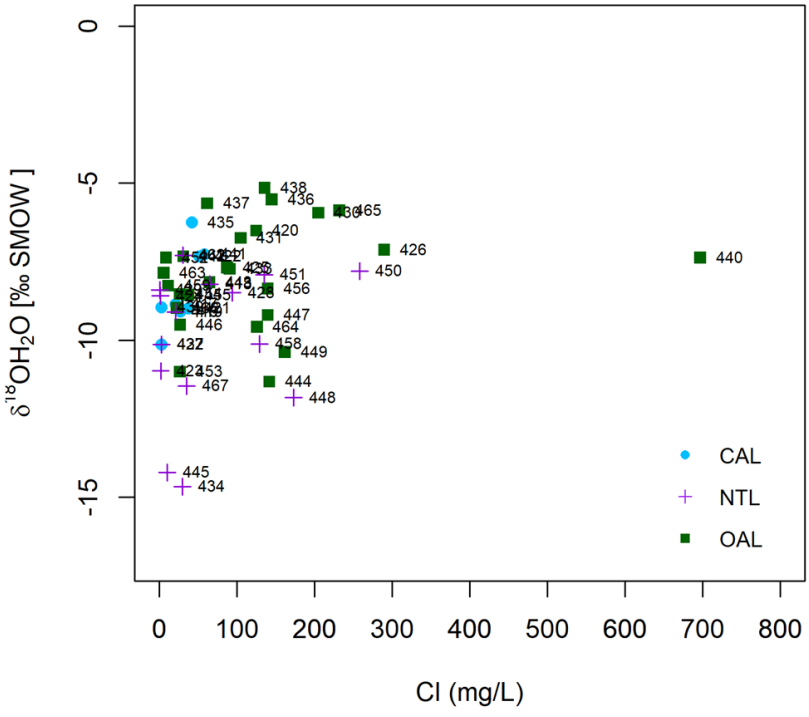

Figure A5: Scattergram of the stable $\delta^{18}O$ water isotope versus chloride concentration (mg L^{-1}), for the group of lowland lakes only: old alaas lakes (OAL; green squares), connected alaas lakes (CAL; blue circles), and new thermokarst lakes (NTL; purple crosses).

https://doi.org/10.5194/egusphere-2025-4114
Preprint. Discussion started: 5 September 2025
© Author(s) 2025. CC BY 4.0 License.

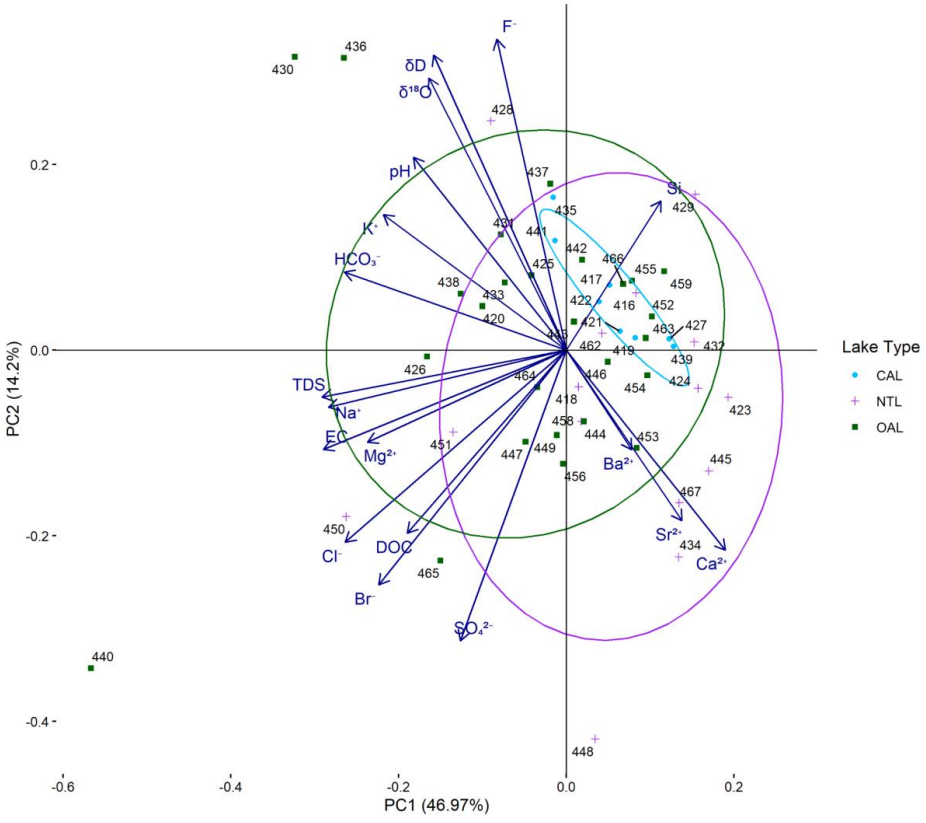

Figure A6: PC1-PC2 biplot of hydrochemical variables (minor and major ions, hydrophysics, isotopes) from the group of lowland lakes only, with ellipses outlining the lake types: new thermokarst lakes (NTL; purple crosses), old alaas lakes (OAL; green squares), and connected alaas lakes (CAL; blue circles). The length of the vectors expresses the loadings of the hydrochemical variables in the PC1-PC2 space.

https://doi.org/10.5194/egusphere-2025-4114
Preprint. Discussion started: 5 September 2025
© Author(s) 2025. CC BY 4.0 License.

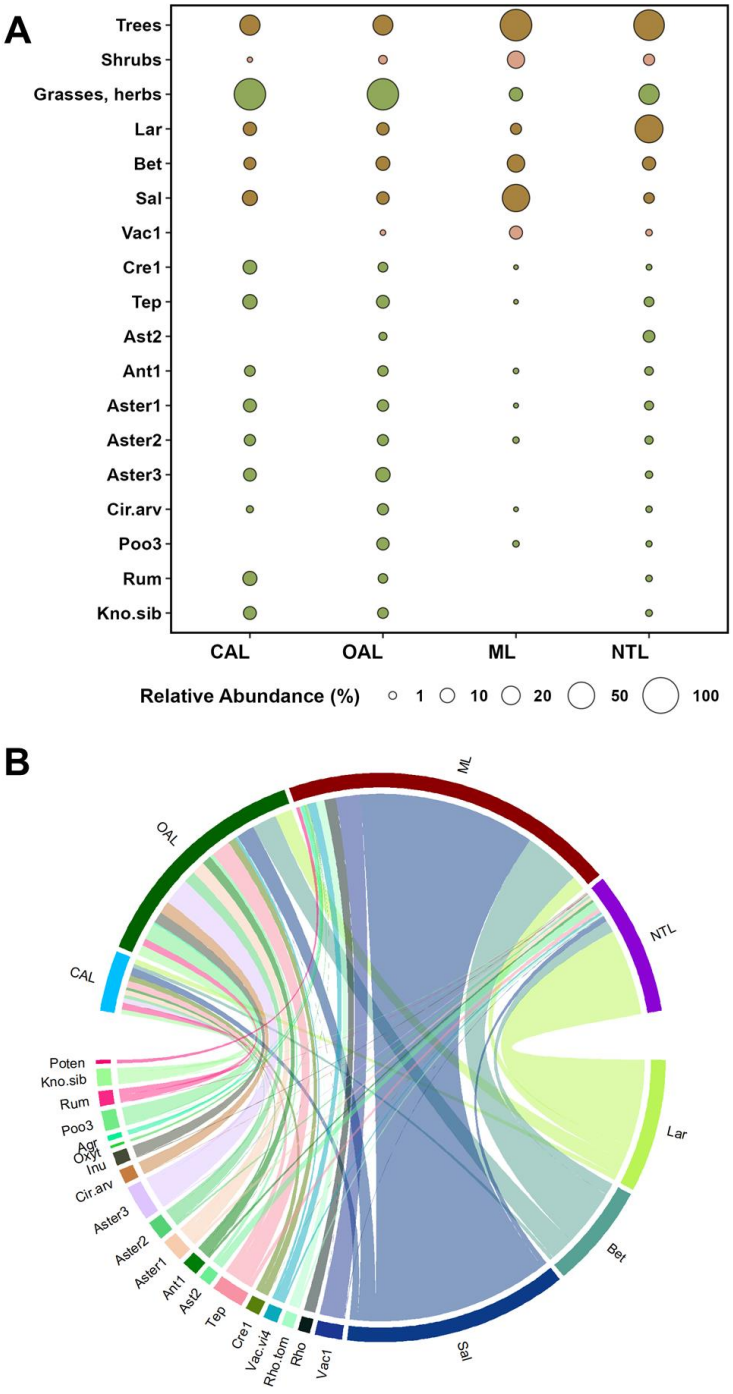

Figure A7: (A) Bubble-chart illustrating the relative abundance of terrestrial vegetation by lake type: mountain lakes (ML), old alaas lakes (OAL), connected alaas lakes (CAL), and new thermokarst lakes (NTL). Relative abundance of plant types is displayed as total share by lake type, and a subset of plants with >5% occurrence is also shown. (B) Chord-diagram showing the most abundant taxa within the four lake types and their relationship to lake type. Short names of taxa refer as follows: Poten-Potentilleae, Kno.sib-*Knorringia sibirica*, Rum-*Rumex*, Poo3-Pooideae3, Inu-*Inulinae*, Cir.arv-*Cirsium arvense*, Aster3-Asteraceae3, Aster2-Asteraceae2, Aster1-Asteraceae1, Ant1-Anthemideae1, Ast2-Asteroideae2, Tep-*Tephroseris*, Cre2-Crepidinae2, Vac.vi4-*Vaccinium vitis-idaea4*, Rho.tom-*Rhodondendron tomentosum*, Rho-*Rhodondendron*, Vac1-*Vaccinium1*, Sal-Salicaceae, Bet-*Betula*, Lar-*Larix*.

https://doi.org/10.5194/egusphere-2025-4114
Preprint. Discussion started: 5 September 2025
© Author(s) 2025. CC BY 4.0 License.

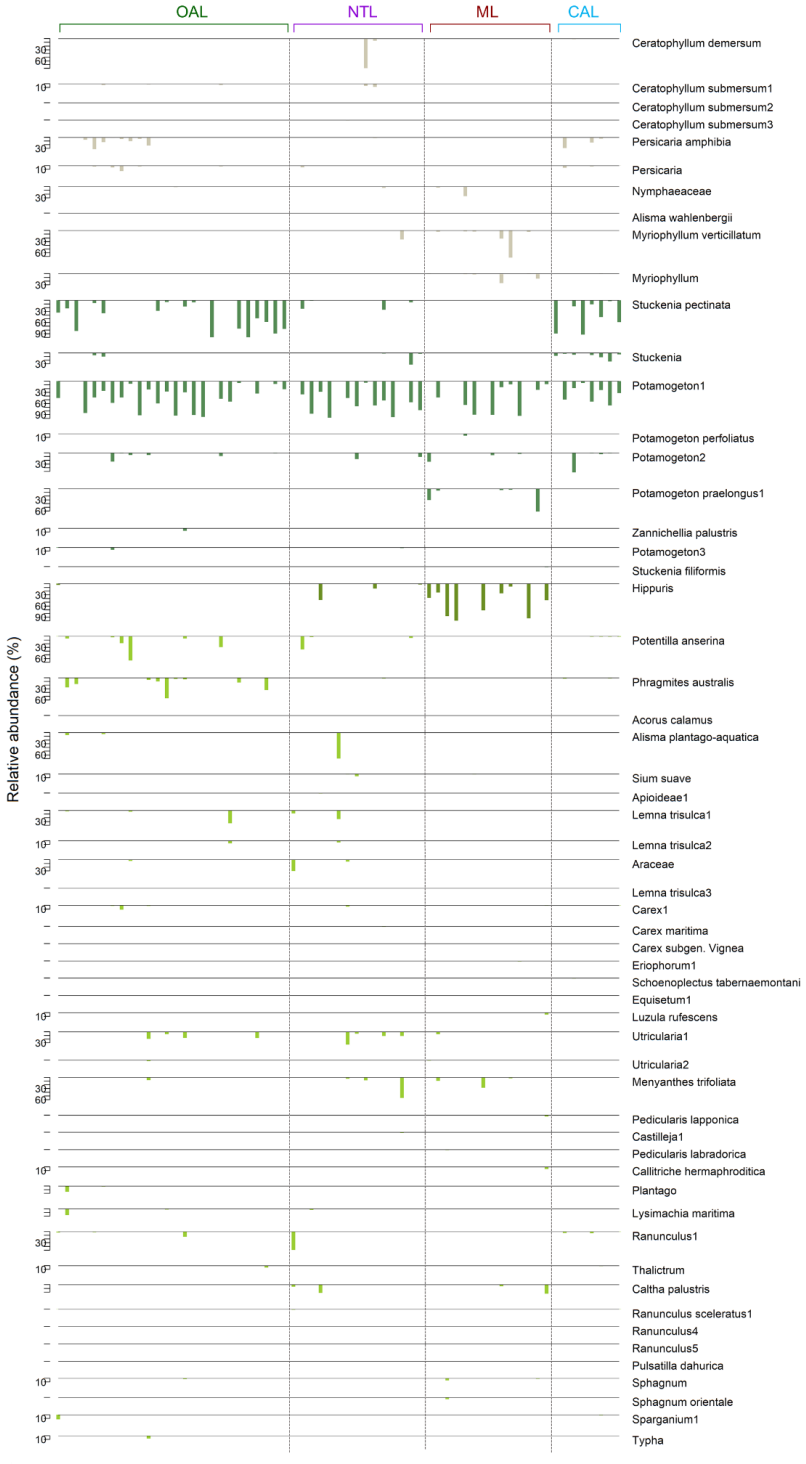

Figure A8: Relative abundance of sedDNA-derived macrophytes. Relative proportion is shown with a subset higher than 5%. Lake types are connected alaas lakes (CAL), old alaas lakes (OAL), mountain lakes (ML), new thermokarst lakes (NTL).

https://doi.org/10.5194/egusphere-2025-4114
Preprint. Discussion started: 5 September 2025
© Author(s) 2025. CC BY 4.0 License.

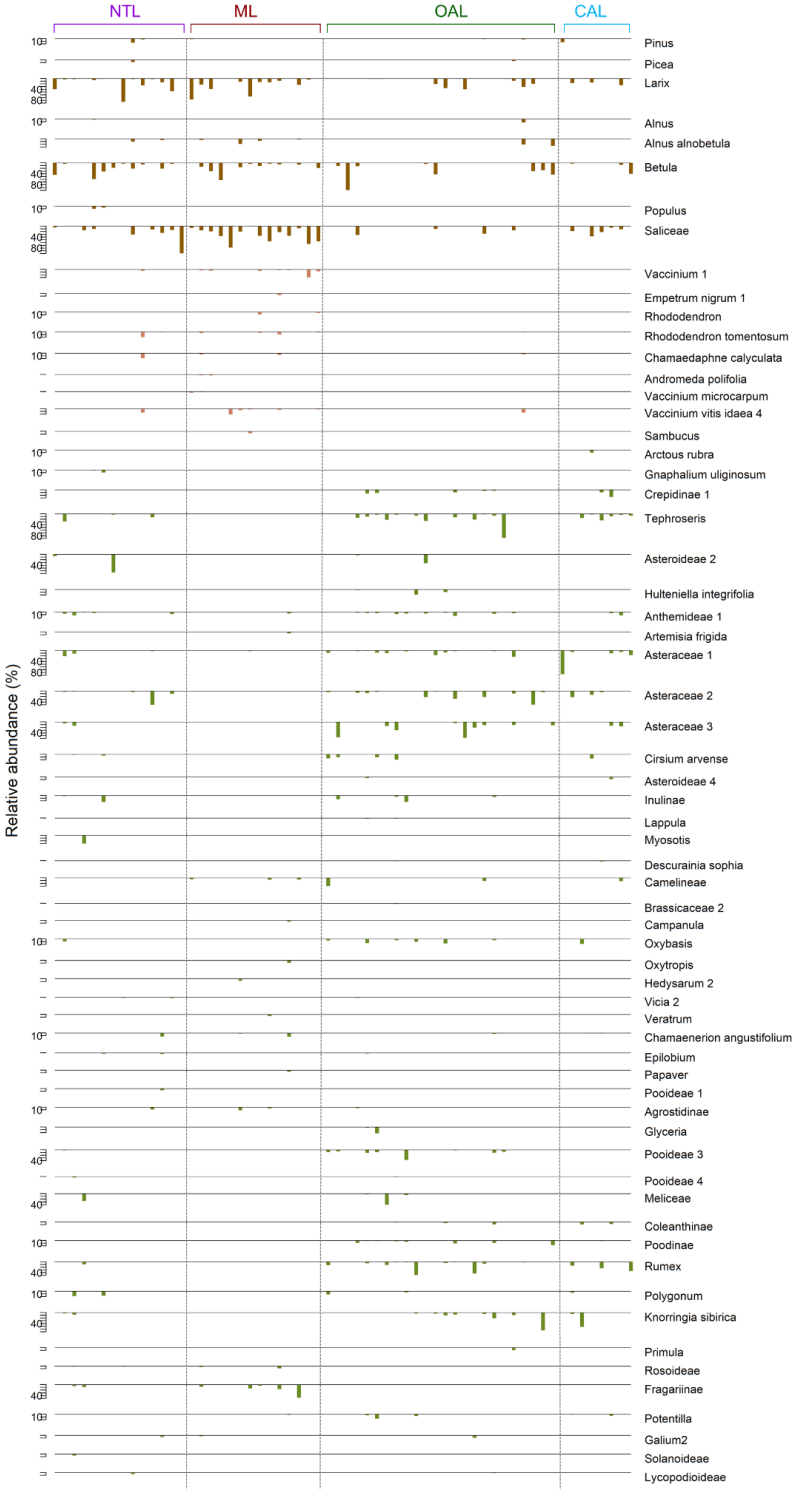

Figure A9: Relative abundance of sedDNA-derived terrestrial plants. Relative proportion is shown with a subset higher than 5%. Lake types are connected alaas lakes (CAL), old alaas lakes (OAL), mountain lakes (ML), new thermokarst lakes (NTL).

https://doi.org/10.5194/egusphere-2025-4114
Preprint. Discussion started: 5 September 2025
© Author(s) 2025. CC BY 4.0 License.

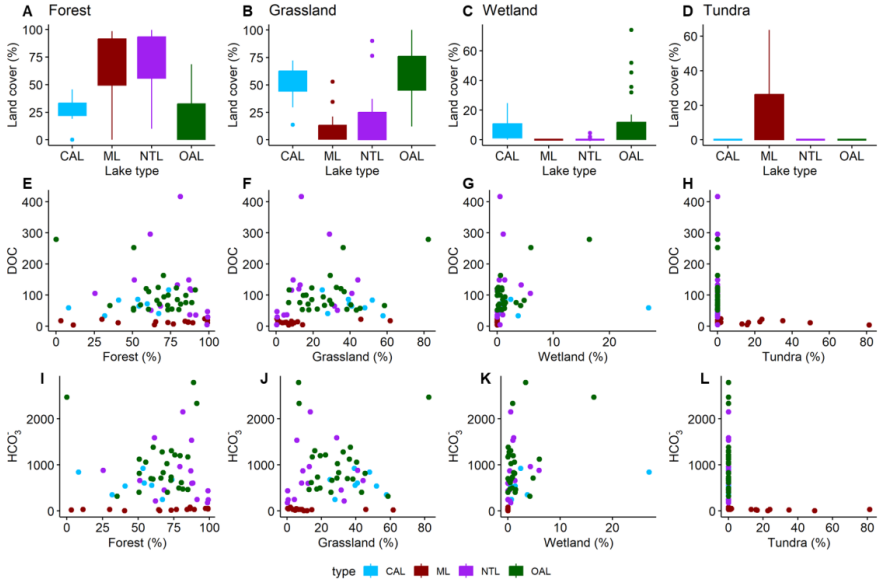

Figure A10. Percentage of satellite-derived land cover (50 m buffer zone) per lake type by land-cover category, shown as boxpots (A-D). Scatterplots display the relationship (E-H) between forest land cover and DOC, and (I-L) between forest land cover and HCO_3^-. DOC and HCO_3^- values are given in mg L^{-1}. Mountain lakes (ML) in brown, new thermokarst lakes (NTL) in purple, connected alaas lakes (CAL) in blue, and old alaas lakes (OAL) in green.

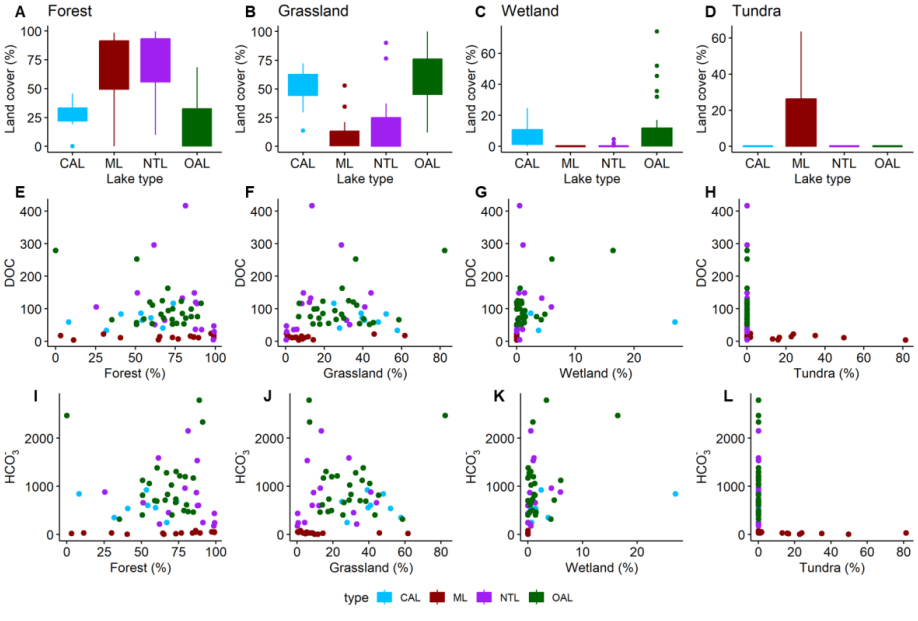

Figure A11: Percentage of satellite-derived land cover (360 m buffer zone) per lake type by land-cover category, shown as boxpots (A-D). Scatterplots display the relationship (E-H) between forest land cover and DOC, and (I-L) between forest land cover and HCO_3^-. DOC and HCO_3^- values are given in mg L^{-1}. Mountain lakes (ML) in brown, new thermokarst lakes (NTL) in purple, connected alaas lakes (CAL) in blue, and old alaas lakes (OAL) in green.

https://doi.org/10.5194/egusphere-2025-4114
Preprint. Discussion started: 5 September 2025
© Author(s) 2025. CC BY 4.0 License.

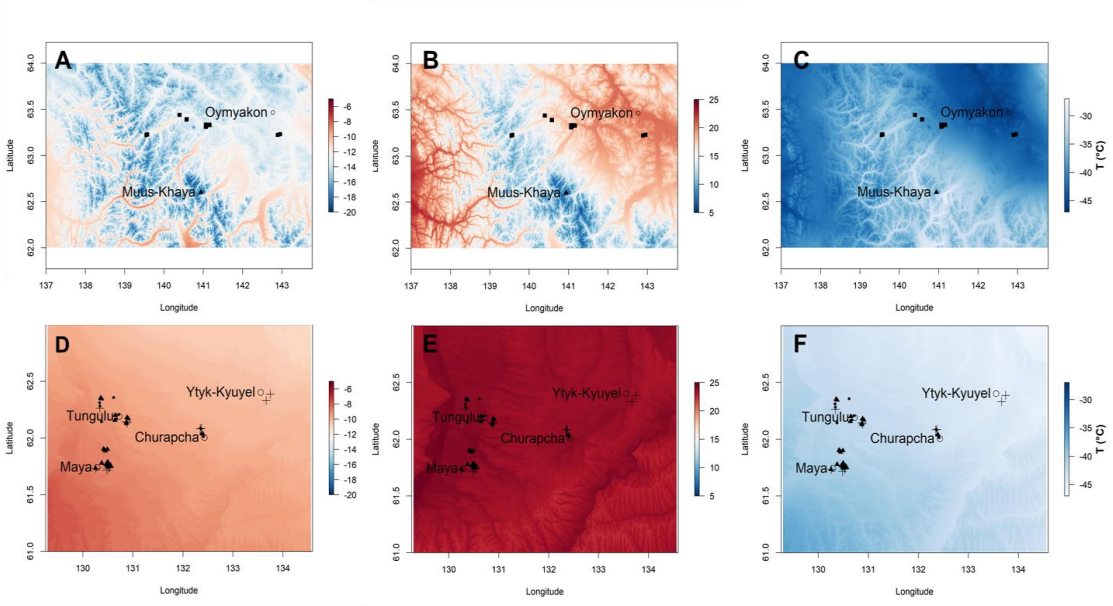

Figure A12: Temperature gradient extracted from CHELSA for two regions: mountain region (upper row panels A-C) and lowland region (lower row panels D-F). Left panel columns (A, D) display the mean annual temperature (MAT). Mid panel columns (B, E) display the maximum temperature of warmest month (Tmax). Right panel columns (C, F) display the minimum temperature of the coldest month (Tmin). Lake types are shown by different symbols: connected alaas lakes (filled circles), old alaas lakes (cubes), mountain lakes (triangles), new thermokarst lakes (crosses). Nearby settlements are given in circles, Muus Khaya is marked as a filled triangle.

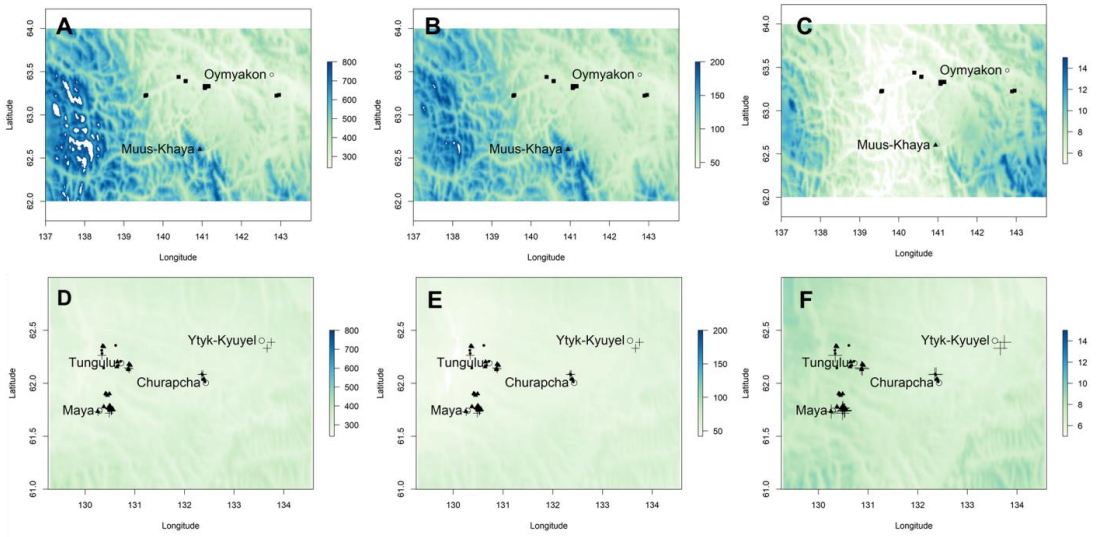

Figure A13: Precipitation gradient extracted from CHELSA for two regions: mountain region (upper row panels A-C) and lowland region (lower row panels D-F). Left panel columns (A, D) display the total annual precipitation (TAP, shown in kg m^{-2} $year^{-1}$ (=mm)). Mid panel columns (B, E) display the precipitation of the wettest month (Pwet, shown in kg m^{-2} (=mm) $month^{-1}$). Right panel columns (C, F) display the precipitation of the driest month (Pdry, shown in kg m^{-2} (=mm) $month^{-1}$). Lake types are shown by different symbols: connected alaas lakes (filled circles), old alaas lakes (cubes), mountain lakes (triangles), new thermokarst lakes (crosses). Nearby settlements are given in circles, Muus Khaya is marked as a filled triangle.

https://doi.org/10.5194/egusphere-2025-4114
Preprint. Discussion started: 5 September 2025
© Author(s) 2025. CC BY 4.0 License.

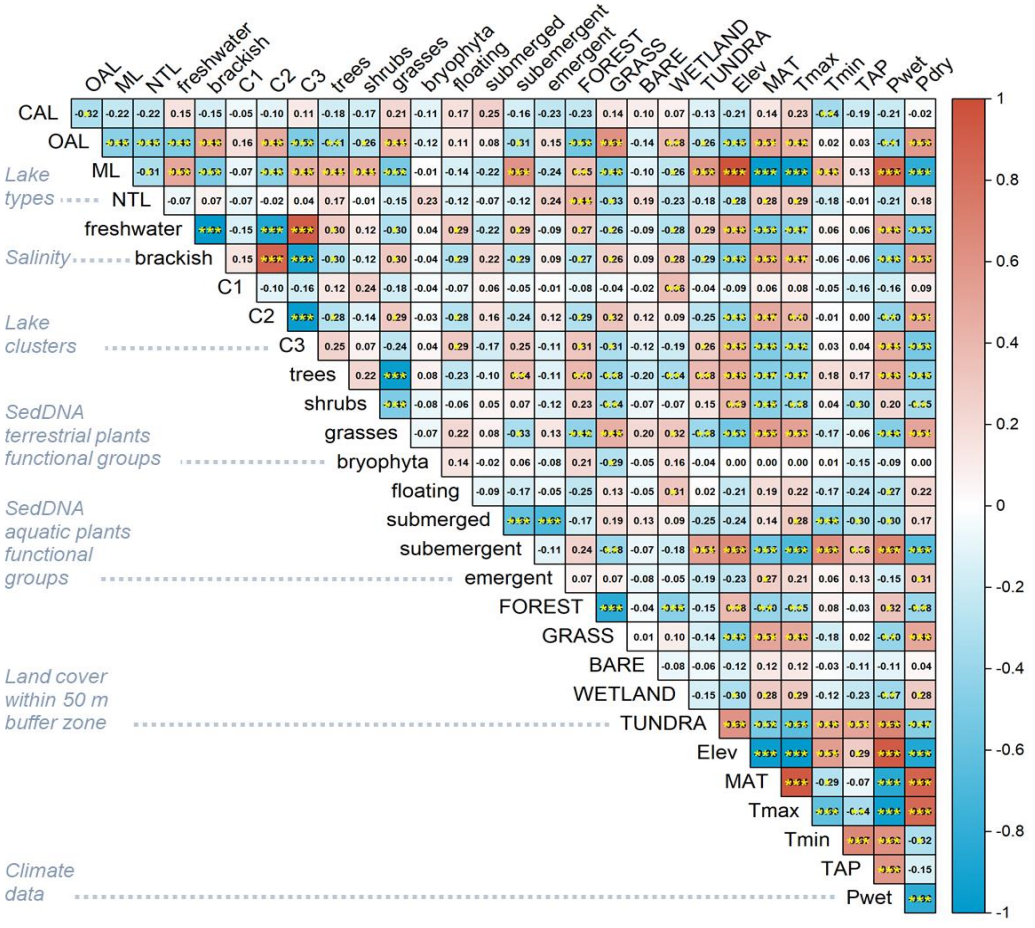

Figure A14: Correlation matrix for the main environmental variables (see Table A6).

https://doi.org/10.5194/egusphere-2025-4114
Preprint. Discussion started: 5 September 2025
© Author(s) 2025. CC BY 4.0 License.

1306

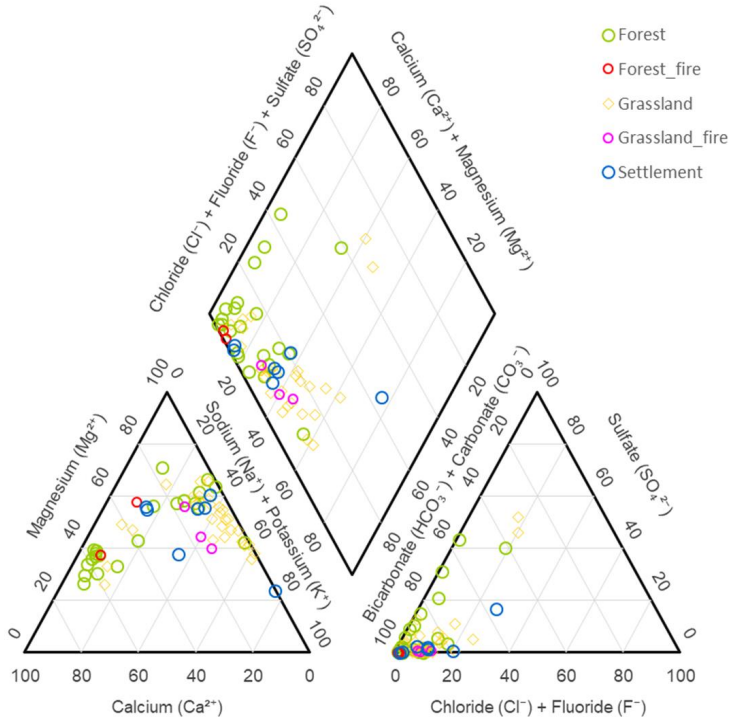

1307
1308 **Figure A15: Hydrochemical facies of lakes linked to the dominant different land-cover type in a Piper diagram showing forest**
1309 **(green), forest fire-scars (red), grasslands (yellow), grasslands with fire-scars (pink), and settlements (blue).**

https://doi.org/10.5194/egusphere-2025-4114
Preprint. Discussion started: 5 September 2025
© Author(s) 2025. CC BY 4.0 License.

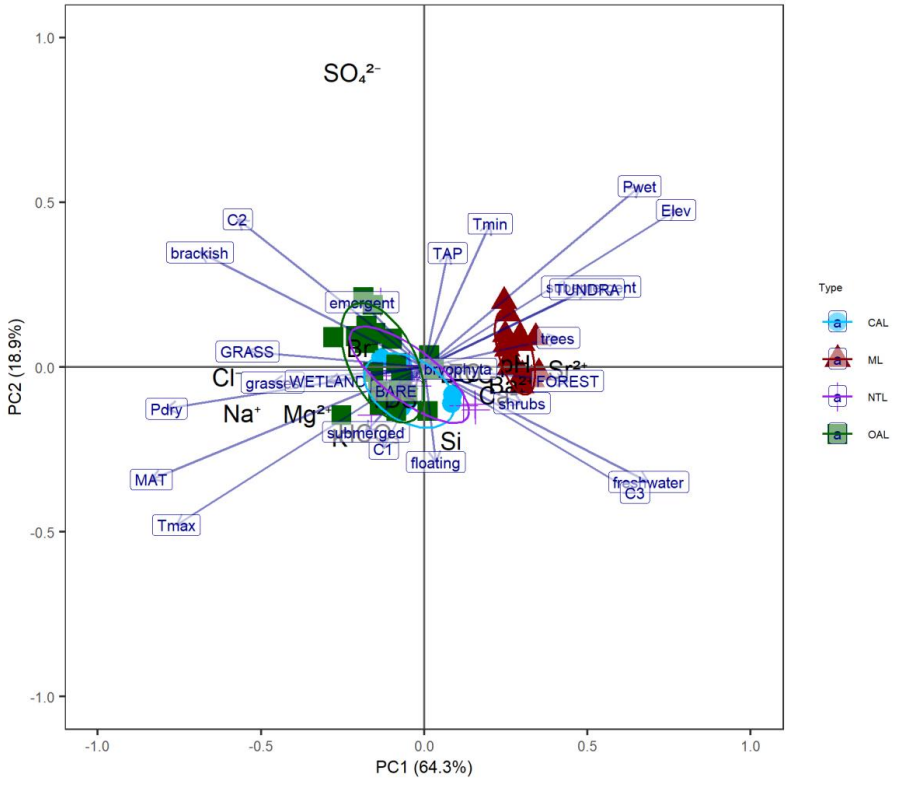

Figure A16: Principal component analysis (PCA) performed on all hydrochemical and environmental variables related to all lakes. Arrows indicate the loadings of the different environmental variables. The color legend shows the lake types: connected alaas lakes (CAL), old alaas lakes (OAL), new thermokarst lakes (NTL), mountain lakes (ML). For better visibility variable names have been abbreviated, please see Table A6.

https://doi.org/10.5194/egusphere-2025-4114
Preprint. Discussion started: 5 September 2025
© Author(s) 2025. CC BY 4.0 License.

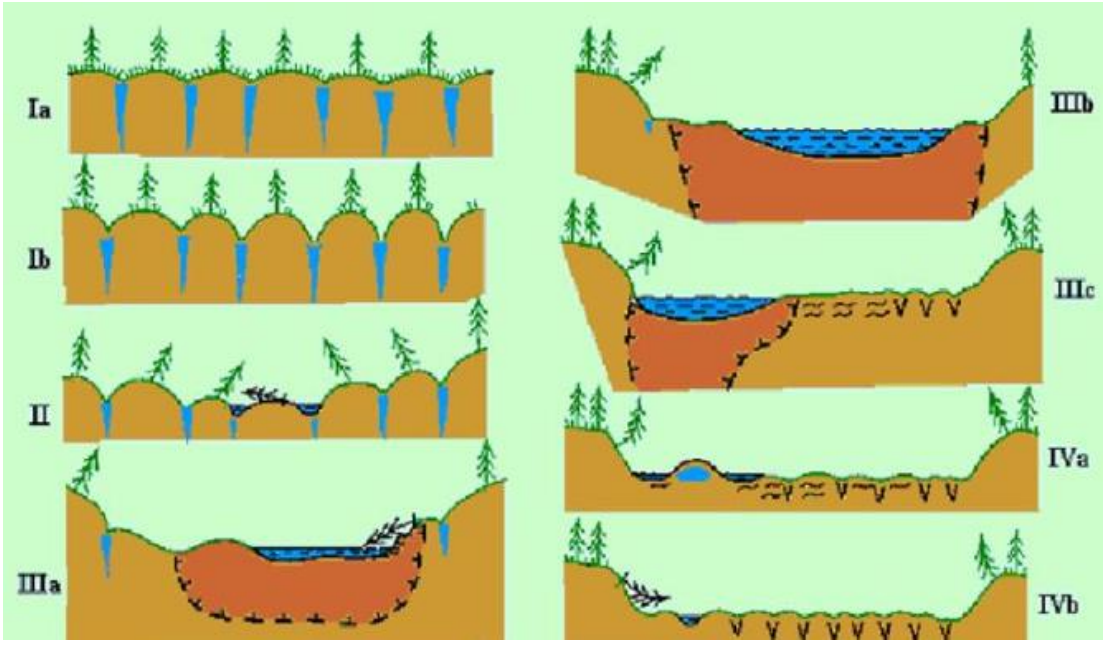

Figure A17: Scheme of the thermokarst lake stage development by Soloviev (1959) from Desyatkin and Desyatkin, 2006. Ia-forested lowland landscape with ground-ice rich (frozen pore water and Pleistocene ice wedges) subground (Pleistocene ice wedges filled with ground ice visualised in blue), such as the Yedoma sedimentary deposits; Ib-Byllar stage; II-Dyede lake stage; IIIa-Tyympy lake stage with unfrozen sediment (talik, visualised in orange) framing the water body and beneath; IIIb-alaas lake stage with unfrozen talik framing the water body and beneath; IIIc-mature alaas with a residual lake, a reduced talik beneath the water body and refreezing and formation and degradation of Holocene ice wedges on the alaas ground; IVa-old alaas with a pingo (ice hill with ice core visualised in blue) froming in the shallow residual alaas lake; IVb-old alaas with a very reduced residual alaas lake, degraded ice wedge geomorphology within the alaas and forest only on the upland.